INL/EXT-18-45226
Revision 0

AGC-5 Graphite Pre-irradiation Data Analysis Report

David Rohrbaugh
W. David Swank

June 2018

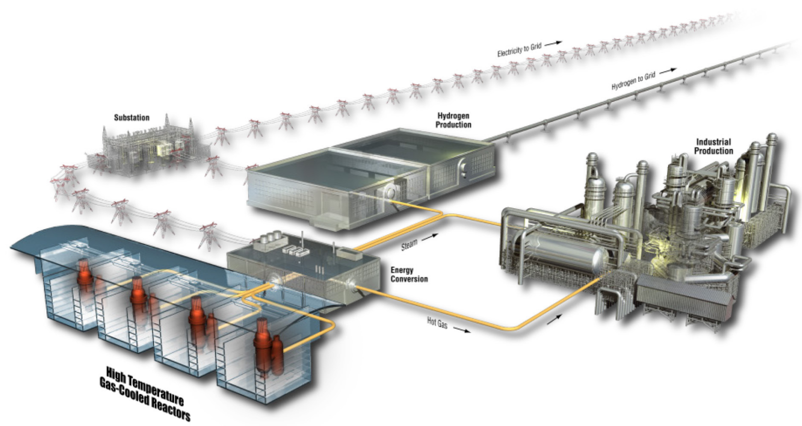

The INL is a
U.S. Department of Energy
National Laboratory
operated by
Battelle Energy Alliance

Idaho National Laboratory

INL/EXT-18-45226
Revision 0

AGC-5 Graphite
Pre-irradiation Data Analysis Report

David Rohrbaugh
W. David Swank

June 2018

Idaho National Laboratory

Idaho Falls, Idaho 83415
http://www.inl.gov

Prepared for the
U.S. Department of Energy
Office of Nuclear Energy
Under DOE Idaho Operations Office
Contract DE-AC07-05ID14517

ART Program

AGC-5 Graphite Pre-irradiation Data Analysis Report

INL/EXT-18-45226
Revision 0

June 2018

Approved by:

William E. Windes
Graphite Technical Peer Reviewer

6/1/2018
Date

Michelle T. Sharp
INL Quality Assurance

6/5/18
Date

James R. Wolf for

Hans. D. Gougar
INL ART Director

6/5/18
Date

SUMMARY

This report documents all pre-irradiation examination material-property measurement data for graphite specimens that were to be used within the fifth advanced graphite capsule (AGC) -5 irradiation capsule. The AGC-5 capsule was to be the fifth in six planned irradiation capsules comprising the AGC test series that was designed to irradiate graphite specimens in a temperature range of 600–1100°C and medium dose levels to 7 dpa (displacements per atom). This would provide quantitative data necessary for predicting the irradiation behavior and operating performance of new nuclear graphite grades for use within very-high-temperature reactor designs.

However, due to the lack of commercial interest in building a very-high-temperature reactor design within the United States, the graphite irradiation program was redirected by the Department of Energy Advanced Reactor Technology to re-irradiate the existing specimens from AGC-1 through AGC-4 in the remaining AGC capsules to achieve higher dose levels (15 dpa) at a lower irradiation temperature range (600–800°C). These new irradiation capsules have been designated as the high-dose graphite (HDG) capsules. This new low-temperature, high-dose irradiation program favors the current high-temperature reactor design of interest to the United States commercial nuclear community.

This report summarizes measurements from material property tests on the designated AGC-5 specimens. Similar to past AGC runs, the specimens were categorized as major graphite grades (IG-110, NBG-17, NBG-18, PCEA, and 2114) and smaller experimental samples (thermal-diffusivity-sized specimens of major grades). It is anticipated that some AGC-5 specimens may be required for use within the new HDG-1 capsule. Any specimens from this pre-irradiation testing campaign will be identified in the future HDG-1 pre-irradiation data report. AGC-5 specimen testing was conducted at Idaho National Laboratory from December 2015 to February 2018.

CONTENTS

FIGURES

TABLES

ACRONYMS

AGC	advanced graphite creep
AG	against grain
ART	Advanced Reactor Technology
ASTM	American Society for Testing and Materials
ATR	Advanced Test Reactor
COV	coefficient of variation
CTE	coefficient of thermal expansion
dpa	displacements per atom
HDG	high-dose graphite
HTR	high-temperature reactor
INL	Idaho National Laboratory
IQR	interquartile range
LFA	laser flash apparatus
ORNL	Oak Ridge National Laboratory
PIE	Post-irradiation examination
Pre-IE	Preirradiation Examination
R&D	Research and development
VHTR	very-high-temperature reactor
WG	with grain

AGC-5 Graphite Pre-irradiation Data Analysis Report

1. INTRODUCTION

The Advanced Reactor Technology (ART) Graphite Research and Development program is conducting an extensive graphite irradiation program to provide data for licensing of a high-temperature reactor (HTR) design. In past applications, graphite has been used effectively as a structural and moderator material in both research and commercial high-temperature gas-cooled reactor designs (Burchell, Bratton, and Windes 2007). Nuclear graphite H-451, used previously in the United States for nuclear reactor graphite components, is no longer available. New nuclear graphite grades have been developed and are considered suitable candidates for new HTR designs. To support the design and licensing of new HTR core components within a commercial reactor, a complete properties database must be developed for these current grades of graphite. Quantitative data on in-service material performance is required for the physical, mechanical, and thermal properties of each major graphite grade with a specific emphasis on data accounting for the life-limiting effects of irradiation creep on key physical properties of the HTR-candidate graphite grades. Further details on the research and development activities and associated rationale required to qualify nuclear-grade graphite for use within the HTR are documented in the graphite technology development plan and graphite specimen selection strategy (Windes, Burchell, and Bratton 2010, Bratton, Burchell 2005).

Based on experience with previous graphite-core components, the phenomenon of irradiation-induced creep within graphite has been shown to be critical to the total useful lifetime of graphite components. Irradiation-induced creep occurs under the simultaneous application of high temperatures, neutron irradiation, *and* applied stresses within the graphite components. Significant internal stresses within the graphite components can result from a second phenomenon—irradiation-induced dimensional change—where the graphite physically changes (i.e., first shrinking and then expanding with increasing neutron dose). This disparity in material-volume change can produce significant internal stresses within graphite components. Irradiation-induced creep relaxes these large internal stresses, thus reducing the risk of crack formation and component failure. Obviously, higher irradiation creep levels tend to relieve more internal stress, thus allowing the components longer useful lifetimes within the core. Determining the irradiation creep rates of nuclear-grade graphite is critical for determining the useful lifetime of graphite components and is a major component of the Advanced Graphite Creep (AGC) experiment.

The AGC experiment is currently underway to determine the in-service behavior of these new graphite grades for HTR and molten-salt reactor designs. This experiment will examine properties and behavior of several nuclear graphite grades at two irradiation temperatures, a spectrum of irradiation fluences, and three applied stress levels that are expected to cause irradiation creep strains within an HTR graphite component. Irradiation data are provided through the AGC test series, which comprises six planned capsules irradiated in the Advanced Test Reactor (ATR) in a large flux trap located at Idaho National Laboratory (INL). Each irradiation capsule consists of over 400 graphite specimens that are characterized before and after irradiation to determine the irradiation-induced material-properties changes and life-limiting irradiation creep rate for each graphite grade.

In 2018, a significant change to the AGC irradiation experiment was initiated by the Department of Energy's ART Program. From 2005 to 2017, the AGC irradiation experiment was focused on very-high-temperature, low-dose irradiations in support of the original very-high-temperature reactor (VHTR) design with an anticipated outlet temperature of 1000°C. However, current interest for graphite-core component reactors lies with HTR designs with anticipated outlet temperature of only 750°C, but with much higher received dose levels for the graphite components. To support this new reactor design direction the AGC experiment was changed to eliminate the very-high-temperature irradiations in place of a higher-dose irradiation. Details of this change will be presented in the following sections.

2. AGC EXPERIMENT DESCRIPTION

The AGC experiment is designed to establish the data necessary to determine the safe operating envelope of graphite-core components for an HTR by measuring the irradiated material property changes and behavior of several new nuclear graphite grades over a range of temperatures, neutron fluence levels, and mechanical compressive loads. The experiment consists of three interrelated stages: pre-irradiation characterization of the graphite specimens, the irradiation test series (designated as six separate irradiation test train capsules), and post-irradiation examination (PIE) and analysis of the graphite specimens after irradiation. Separate reports for each distinct stage are prepared after each individual activity is completed.

The pre-irradiation examination reports detail the total number of graphite types and specimens, specimen loading configuration to expose all specimens to the entire range of irradiation conditions, and pre-irradiation material property testing results. The test series as-run irradiation reports detail the irradiation history of each capsule while in the reactor, noting any changes from the technical and function specifications for each specific test series capsule, and identifying the possible improvements to the next test series capsule design. The PIE reports detail the changes in the specimen material-property measurements, compare the results to the pre-irradiation examination material-property measurements, and analyze the data to assist in determining credible safe operating limits for graphite-core components in an HTR design and licensing application.

Due to changes in the AGC irradiation experiment, this specific pre-irradiation report on AGC-5 specimens will only record the total number of graphite types, specimens, and the corresponding pre-irradiation material property testing results.

2.1 Background Information for the AGC Experiment

The AGC experiment will provide irradiated material-property data for current graphite types available for used within an HTR design. Due to volume limitations within typical material test reactors (i.e., ATR), only a limited number of specimens can be irradiated—far fewer than can be used in an accurate statistical specimen population analysis. Therefore, the AGC only measures the irradiated material-property changes and behavior of relatively few specimens of new nuclear graphite grades over the anticipated operating-temperature range, neutron fluences, and mechanical loads. The experiment does generate quantitative material-property change data (and limited irradiation-creep data) that will be used in conjunction with the as-fabricated material-property measurement program (baseline program) to predict the in-service behavior and operating performance of these new nuclear graphite grades for pebble bed and prismatic reactor designs. Changes to key thermal, physical, and mechanical material properties are determined by comparing the material properties of each specimen before and after irradiation. Differences measured from the irradiation conditions will provide irradiation behavior data in graphite with a specific emphasis on data accounting for the life-limiting effects of irradiation creep on key physical properties of several candidate graphite grades for an HTR.

The critical component of the AGC experiment is the irradiation test series, which irradiates the graphite specimens after pre-irradiation examination characterization has been completed. The AGC test series comprises six planned capsules that are irradiated in ATR in a large flux trap, as described in the graphite technology development plan (Windes, Burchell, and Bratton 2010). Originally, the test series planned to expose graphite specimens of selected nuclear grades to temperatures and a range of doses that are expected within a VHTR design (Figure 1). However, beginning in 2018, the AGC experiment was changed to better reflect the direction of new advanced reactor designs with anticipated outlet temperature of only 750°C and with much higher received dose levels for the graphite components. The very-high-temperature irradiations (1100°C) were eliminated, and the irradiation capsules were repurposed to provide higher-dose irradiations. These new high-dose graphite (HDG) capsules will be used to re-irradiate previous specimens irradiated in the AGC-2, AGC-3, and AGC-4 capsules to provide a total fast neutron (E >0.1 MeV) dose range of 0.5–15 dpa, (see Figure 2).

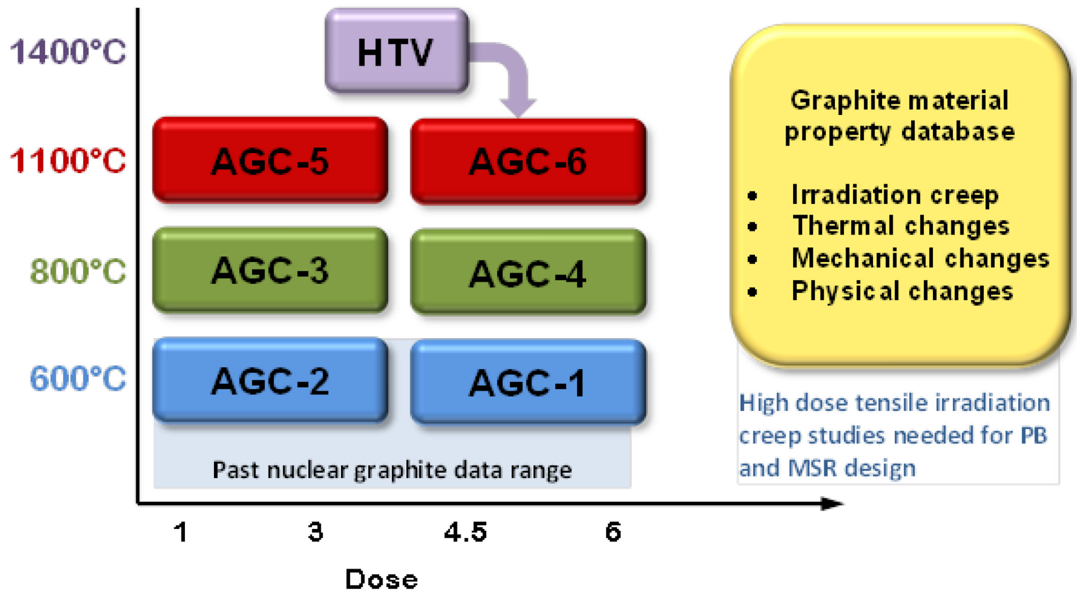

Figure 1. Original (2005–2017) design of AGC experiment illustrating planned dose levels and irradiation temperatures for all six test irradiation capsules in support of a VHTR design (1100°C outlet temperature).

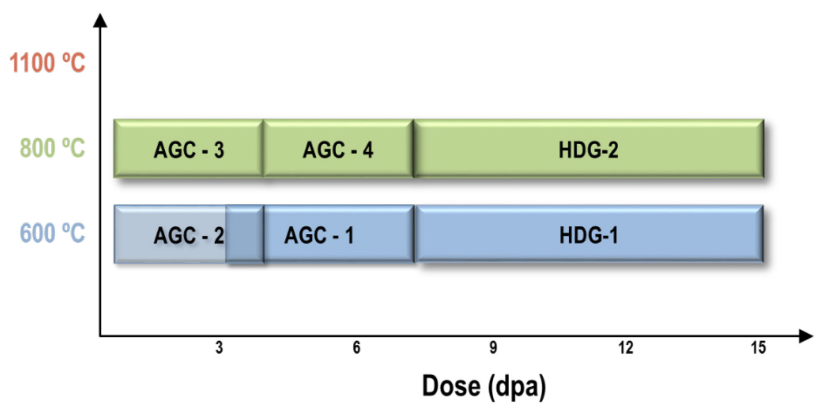

Figure 2. New graphite irradiation plan with high-dose graphite irradiations illustrating a lower-temperature, higher-dose irradiation plan.

The higher irradiation dose, HDG, capsules, will be irradiated up to dose levels of 10 dpa at temperatures of 600 and 800°C to correspond to the previous irradiation temperatures of the AGC-2, AGC-3, and AGC-4 capsules. Unfortunately, all AGC-1 specimens were destructively tested before the new direction to re-irradiated was made, and they are no longer available. By re-irradiating the previous AGC specimens, a combined total maximum received dose of ~15 dpa is anticipated; this should exceed turnaround dose levels for the AGC graphite grades. As illustrated in Figure 2, AGC-2 specimens will be re-irradiated in the HDG-1 capsule while AGC-3 and AGC-4 specimens will be re-irradiated in the HDG-2 capsule.

Because of this new direction, AGC-5 and AGC-6 unirradiated specimens will no longer be required for the AGC irradiation experiment. The repurposed capsules, HDG-1 and HDG-2, will use previously irradiated specimens. Therefore, this specific pre-irradiation report on AGC-5 specimens will only record the total number of graphite types, specimens, and the corresponding pre-irradiation material-property testing results in the event that they may be used within the new HDG capsules or with another graphite-irradiation program at some future date.

Similar to previous specimens in the AGC-1 through AGC-4 test series, the AGC-5 specimen inventory contains two primary specimen types: (1) creep specimens providing irradiation-creep rate values as well as mechanical properties, and (2) piggyback specimens providing thermal material-property changes to the graphite. The creep specimens are 25.4 mm tall by 12.5 mm in diameter and are irradiated in the mechanically loaded outer stack positions of the capsule body where an applied load can be imposed upon half of the specimens. Piggyback specimens are short (6 mm tall by 12.5 mm in diameter) button specimens that reside in the axial spine of the capsule, receive no applied load, and are subjected only to neutron irradiation to assess the effects of a reactor environment on the specific graphite grade. Together, both specimen types provide material-property changes for stressed and unstressed graphite types. The physical dimensions for both creep and piggyback specimens are shown in INL Dwg. 780577, "ATR Advanced Graphite Capsule (AGC) AGC-5 Graphite Specimen Cutout Diagrams."

The larger creep specimens are best suited for physical and mechanical testing techniques, such as dimensional change, irradiation creep, elastic modulus, density, and thermal expansion. The smaller piggyback specimens are best suited for thermal and physical testing, such as thermal diffusivity, mass measurements, and density.

2.2 Description of AGC-5 Test Specimens

The five major grades of graphite that were used in AGC-3/AGC-4 were also to be used in AGC-5. These major grades are PCEA, NBG-17, NBG-18, IG-110, and 2114. These are also the grades that will be used within the new HDG capsules (HDG-1 and HDG-2).

The piggyback specimens in the AGC-5 capsule are smaller, button-size specimens that are approximately 12.5 mm (1/2 in.) diameter by 6.3 mm (1/4 in.) tall. They are made of all of the major grades of graphite. A list of all major graphite grades is provided in Table 1.

Table 1. Graphite grades and grain orientations within AGC-5 capsule.

Grade	Specimen Type	Dimension	With Grain (WG)/ Against Grain (AG)
2114	Creep	Ø12.5 × 25.4 mm	51 WG / 0 AG
NBG-17	Creep	Ø12.5 × 25.4 mm	24 WG / 21 AG
NBG-18	Creep	Ø12.5 × 25.4 mm	30 WG / 27 AG
IG-110	Creep	Ø12.5 × 25.4 mm	33 WG / 15 AG
PCEA	Creep	Ø12.5 × 25.4 mm	39 WG / 15 AG
2114	Piggyback	Ø12.5 × 6.3 mm	22 WG / 15 AG
NBG-17	Piggyback	Ø12.5 × 6.3 mm	21 WG / 14 AG
NBG-18	Piggyback	Ø12.5 × 6.3 mm	20 WG / 16 AG
IG-110	Piggyback	Ø12.5 × 6.3 mm	19 WG / 13 AG
PCEA	Piggyback	Ø12.5 × 6.3 mm	16 WG / 13 AG

3. PRE-IRRADIATION MATERIAL PROPERTY MEASUREMENTS

The objective of the AGC experiment is to determine the material-property changes induced in nuclear-grade graphite during exposure to a high-temperature neutron environment. The approach is to perform extensive pre-irradiation characterization testing on each specimen before exposing the graphite specimens to various neutron doses. After irradiation, the same characterization tests will be performed on each irradiated specimen to quantify changes to the material properties of the graphite. As previously mentioned, the AGC-5 and AGC-6 irradiation capsules are being replaced with the HDG, HDG-1 and HDG-2 capsules. However, it is anticipated that the HDG capsules will utilize some fraction of the characterized AGC-5 specimens described in this report and, therefore, the material properties of the specimens will be recorded in anticipation of this future use.

A brief summary of the material testing is provided in Table 2. These measurements include dimensional and non-destructive characterization of the physical properties. The properties measured were bulk density, electrical resistivity, thermal diffusivity (room temperature to 1000°C), thermal expansion (100–1000°C), and elastic constants using two methods. The resonant fundamental frequency method is used to measure flexural dynamic Young's modulus, and a sonic velocity method is used for obtaining both the Young's and shear modulus.

Table 2. Graphite measurement and test equipment.

Measurement	Standard	Instrumentation	Calibration Method	Result
Physical dimensions and mass	ASTM C559-90 (reapproved 2010)	Mitutoyo micrometer 121-155 INL ID: 725884 INL ID: 727312 Mitutoyo caliper CD-6-in. CSX INL ID: 725813 INL ID: 726607 INL ID: 727194 Sartorius scale ME235P INL ID: 412642 INL ID: 415907	INL Standards and Calibration Laboratory	Bulk density

Table 2. (continued).

Measurement	Standard	Instrumentation	Calibration Method	Result
Fundamental frequency	ASTM C747-16	J. W. Lemmens GrindoSonic INL ID: 412850	No calibration required per instrument manufacturer	Elastic modulus (flexural mode)
Sonic velocity	ASTM C769-98 (re-approved 2005)	Olympus NDT square wave pulser/receiver 5077PR INL ID: 728024 National Instruments digitizer USB 5133 INL ID: 726725 INL ID: 415868	INL Standards and Calibration Laboratory	Young's modulus, shear modulus, Poisson's ratio
Four-point electrical resistivity	ASTM C611-98 (reapproved 2010)	Keithly 6220 precision current source INL ID: 725865 INL ID: 727290 Keithly 2182A nano voltmeter INL ID: 725866 INL ID: 727289	INL Standards and Calibration Laboratory	Electrical resistivity
Laser flash diffusivity	ASTM E1461-07	Netzsch laser flash apparatus (LFA) 457, two each INL ID: 412855 INL ID: 412864	Calibration by user per manufacturer's instructions	Thermal diffusivity
Push rod dilatometry	ASTM E228-06	Netzsch DIL 402 C, two each INL ID: 412860 INL ID: 412861	Calibration by user per manufacturer's instructions	Coefficient of thermal expansion (CTE)
Environmental monitoring	All	Vaisala pressure, humidity and temperature transmitter PTU301 INL ID: 726912 INL ID: 727884 INL ID: 727502	INL Standards and Calibration Laboratory	Laboratory environmental conditions

The measurements listed in Table 2 are segregated into individual stations that consist of the instrumentation necessary, a computer for automated data acquisition, and a bar-code reader. The bar code of the individual specimen container is read, and the file for that specimen is automatically opened for data input prior to each measurement. Associated with each measurement type is a unique laboratory notebook maintained in accordance with MCP-2875, "Proper Use and Maintenance of Laboratory Notebooks," and PLN-2690, "Idaho National Laboratory Advanced Reactor Technologies Technology Development Office Quality Assurance Program Plan." Accepted data will be stored in the Nuclear Data Management and Analysis System, a satellite file location for ART. Data in a standardized Excel file format will be transmitted to the Nuclear Data Management and Analysis System using Form 250.01, "Data Management and Analysis Transmittal," following PLN-4653, "INL Records Management Plan."

In addition to laboratory notebooks, the individual measurement control computers are networked to a server computer where the measurement data are automatically stored. Control of the measurement computers and data acquisition are accomplished with custom LabVIEW software. This software comprises five main programs: manufacturers data, physical and dimensional measurements, electrical resistivity measurements, sonic resonance (fundamental frequency) measurements, and sonic velocity measurements. These five programs acquire data from instrumentation and user input. The programs then record the results in an Excel spreadsheet located on a server computer. In the case of thermal-expansion and thermal-diffusivity measurements, two other LabVIEW programs have also been written to parse vendor-software-acquired data into Excel spreadsheets. The development, accuracy, and configuration control of this software is governed by LWP-20000-01, "Conduct of Research."

Following is the sequence in which the measurements are made:

1. Wash and dry—all specimens.
2. Mass and dimensional measurements—all specimens.
3. Thermal diffusivity—piggyback specimens.
4. Elastic modulus by sonic resonance—creep specimens.
5. Electrical resistivity—creep specimens.
6. Elastic modulus by measurement of sonic velocity—creep specimens.
7. Wash and dry to remove couplant—creep specimens.
8. CTE—creep specimens.

3.1 General Provisions

The AGC-5 specimens have been characterized per PLN-5580, "AGC-5 Graphite Specimen Pre-irradiation Characterization Plan." This plan describes the thermal, physical, and mechanical measurement techniques that were used to characterize the different graphite types being tested in the AGC-5 experiment. It is intended to meet the requirements of MCP-1380, "Research and Development Test Control," and NQA-1-2008/1a-2009, "Quality Assurance Requirements for Nuclear Facility Applications," Requirement 11, Test Control. Described within the plan are the instruments, fixtures, and methods used for pre-irradiation material-property measurements of bulk density, thermal diffusivity, CTE, elastic modulus, and electrical resistivity.

All work was performed in accordance with LWP-21220, "Work Management." All records designated in implementing documents as quality assurance records were controlled in accordance with PLN-4653.

The data resulting from the pre-irradiation characterization are plotted in Appendix A. Statistical evaluation has been performed using an inner quartile range analysis to identify levels of precision and outliers in the data.

3.2 Specimen Description and Preparation

The major nuclear-grade graphite types to be tested in AGC-5 are NBG-17, NBG-18, PCEA, 2114, and IG-110. All major grades have been characterized fully per PLN-5580. The two primary specimen types in the AGC experiments are creep specimens and piggyback specimens. All specimens are 12.5 mm in diameter, with the creep specimens being 25.4 mm long, and the piggyback specimens being 6.3 mm long. Details specimen geometries and how specimens were cut from the graphite blocks are contained in INL Dwg. 780577.

Immediately after being machined, each specimen is placed in an individual container that is bar-coded with a unique identification number per INL Dwg. 780577. Each graphite specimen is then laser-engraved with that same unique identification number around the circumference at one end. Prior to any material-property measurement, each specimen is identified by its unique identification number, and the data are recorded and stored under this identification number. After the specimens have been laser-engraved, they are ultrasonically cleaned as follows:

1. The specimens are handled only by persons wearing cotton or powder-free nitrile gloves.
2. All dust and debris is removed from the specimens using an aerosol pressurized dust-off product.
3. Specimens are ultrasonically cleaned for 20 minutes in deionized water.
4. Specimens are rinsed in ethyl alcohol to help displace water.
5. Specimens are allowed to air dry.
6. Specimens are placed in a laboratory oven at 130°C for 2 hours.
7. Specimens are allowed to cool in a desiccator and are retained there in storage until resistivity or bulk density measurements are taken.

3.3 Personnel and Training

Personnel who perform measurements identified in this plan are qualified in accordance with LWP-12033, "Personnel Qualification and Certification." Their ability to adequately perform measurements described in this plan is demonstrated by instrument manufacturers' training and certification and/or performance of an instrument or measurement operational validation. Personnel qualifications are reviewed by the Graphite research and development lead and documented in laboratory notebooks.

3.4 Variations, Exceptions, and Discrepancies

Several variations, exceptions, and discrepancies may occur. The first is a known departure from the applicable American Society for Testing and Materials (ASTM) standard. These departures are typically related to geometrical constraints. All currently known departures or exceptions taken to the ASTM standard are described in detail in Section 3 of PLN-5580. Any departure not captured in PLN-5580 will be recorded in laboratory notebooks associated with the measurement. In most cases, the effects of the exception or departure from the ASTM method on the measured value are not well understood. When possible, sensitivity studies will be performed and documented in laboratory notebooks to understand the impact of these exceptions and departures.

It is likely that the ASTM standards and/or test methods will be revised and improved during the more than 10-year-long AGC experiment cycle. Each revision or development will be evaluated for how it could impact future measurements and their consistency with measurements made under previous revisions or techniques. A programmatic determination will be made whether to continue with the current version of the ASTM/method or use the updated version. This determination will be documented in laboratory notebooks associated with the affected measurement.

While measurements are being made, it is possible that something out of the ordinary may occur. Any unusual event that occurs during a measurement will be documented in the laboratory notebook associated with that specific measurement and duly noted within the database associated with the data generated for this program. The principle investigator will be notified of the event and will determine what impact it has on the data. The significance of the result will be documented in the laboratory notebook by the principle investigator.

3.5 Calibration and Functional Validation

The measurement protocol consists of calibration, functional validation, and data acquisition. Functional validations established for each measurement in collaboration with the instrument manufacturer are performed periodically to ensure that accurate and consistent data are acquired. All validations are performed on traceable standards and documented in retrievable laboratory notebooks associated with each measurement. In the event that an instrument's functional validation fails, the reason for the failure is investigated and resolved prior to that measurement being used for further characterization. Upon resolution, a determination is made as to the impact the failure might have had on data taken prior to the failure and back to the last valid measurement. If it is determined the data captured during this interval is suspect, the impacted data will be evaluated for accuracy.

LWP-13455, "Control of Measuring and Test Equipment," is followed for calibration standards, methods, and frequencies that have been established for each measurement. Where it is not possible to use the INL Standards and Calibration Laboratory, user procedures for calibration are established based on ASTM standards and manufacturers' instructions and performed against international standards. These procedures are documented in laboratory notebooks associated with each measurement.

4. TEST METHODS

Before any measurements are made, specimen numbers and basic information about each type of graphite are entered into the manufacturer's data program. Once basic information about the graphite type has been recorded, that information is automatically saved to an Excel spreadsheet file, and the individual specimen numbers are entered using a bar-code reader. Following the initial input of general information, individual material-property measurements are made starting with mass and dimensional measurements for determining bulk density.

4.1 Mass, Dimensions, and Bulk Density

Dimensional change is one of the key parameters affecting the performance of graphite in a neutron environment. Determining volumetric and linear dimension as a function of temperature and radiological dose is necessary to understand critical performance measures such as dimensional-change turnaround, irradiation creep, and internal stresses imposed upon graphite components. Dimensional and mass measurements are performed to ASTM C559-90 (re-approved 2010), which describes in detail the procedure for making dimensional measurements and calculating bulk density.

The accuracy of the dial micrometers used here is stated by the manufacture to be 2 μm. This is a 0.008% accuracy on a 25.4 mm measurement. However, when evaluating the uncertainty of the density determination, other factors must be considered, such as the hardness of the material and the force with which the micrometer blade is engaged with the material, specimen-temperature variation, technician skill, etc. These and other factors were considered in a propagation-of-error analysis to arrive at an uncertainty of 0.08%, with the measurement of the diameter being the largest contributor to the error.

4.2 Electrical Resistivity

Electrical resistivity is used as a rapid, simple means to determine grain orientation, structure and crystallinity of graphite. In conjunction with optical microscopy, it can be used to determine the microstructural texture of graphite components without much specimen preparation. Resistivity is measured following ASTM C 611-98 (re-approved 2010). The measurement technique is commonly referred to as four-point probe. It consists of passing a known current through the specimen and measuring the voltage across the specimen at known locations.

Based on Ohms Law, the resistance is determined, and the resistivity is calculated from:

$$\rho = R \cdot A / L$$

where

R = the measured resistance

A = the cross-sectional area

L = the length over which the voltage is measured.

Figure 3 shows a test fixture fabricated at INL that allows a specimen to be rotated for multiple measurements of voltage around its periphery.

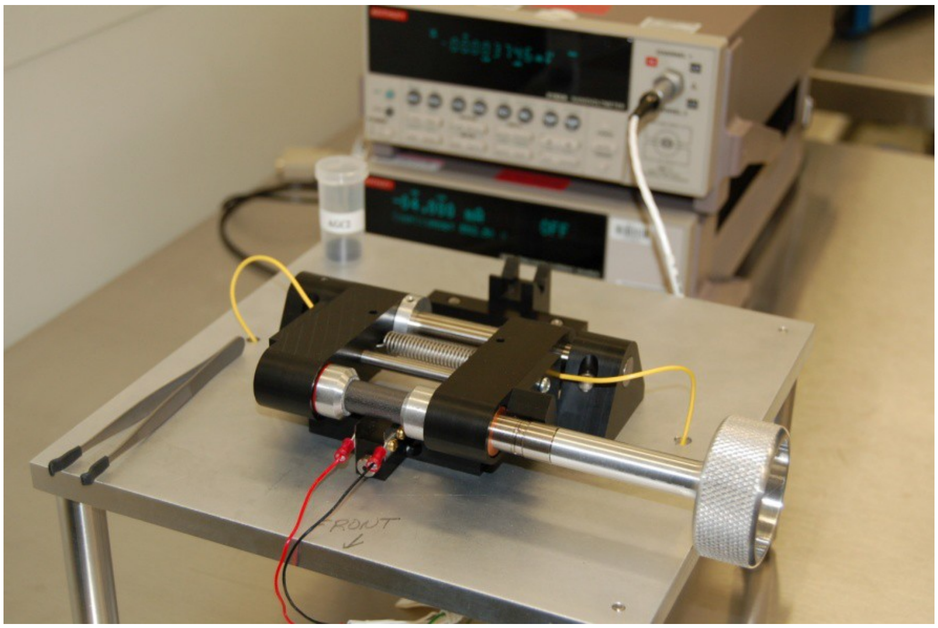

Figure 3. Electrical resistivity measurement station.

Uncertainty in the resistivity measurement is mainly composed of the contact resistance between the specimen and the contacting blades for the voltage measurement. Specimen temperature and the temperature of other bimetal junctions in the voltage-measuring leads are also factors. These effects are minimized by passing the current through the specimen in two directions and averaging the measured voltage for each direction. In this way, any thermoelectric or small differences in junction resistances will cancel. A round-robin test series reported in the precision and bias section of ASTM C 611-98 states a lab-to-lab variability of 2.5%. This kind of round-robin test series would take into account the variables discussed above and is considered a good estimate of the measurement uncertainty.

4.3 Approximation of Elastic Modulus from the Measurement of Sonic Velocity

The mechanical properties of graphite are necessary to determine the structural integrity of graphite components. These properties are vital to determining the viability of the structural strength and integrity of the reactor core. The as-received and irradiated values are needed for whole-core models, which will be used for the graphite design code. This test is carried out in accordance with ASTM C 769-98 (re-approved 2005). In this measurement, the transmitting piezoelectric transducer sends a 2.25-MHz sound wave through the specimen. At the opposite end of the specimen, the acoustic wave is received by another piezoelectric transducer. The sonic velocity of the specimen is the ratio of specimen length to the signal time lapse between transducers.

An approximate value for Young's modulus, E, can be obtained from:

$$E = \rho V^2$$

where

ρ = the specimen density

V = the sonic velocity.

Figure 4 shows the sonic-velocity measurement station. In the foreground are the fixtures for clamping the specimen between the transducer and receiver that were specifically designed and fabricated at INL for this application. They have unique features that improve measurement accuracy, precision, and efficiency. For example, measurement precision is improved because the spring-loaded clamp applies consistent pressure between the transducers and specimen, resulting in repeatable couplant thickness. The specimens are easily and rapidly loaded into the fixture using the cam-operated clamp.

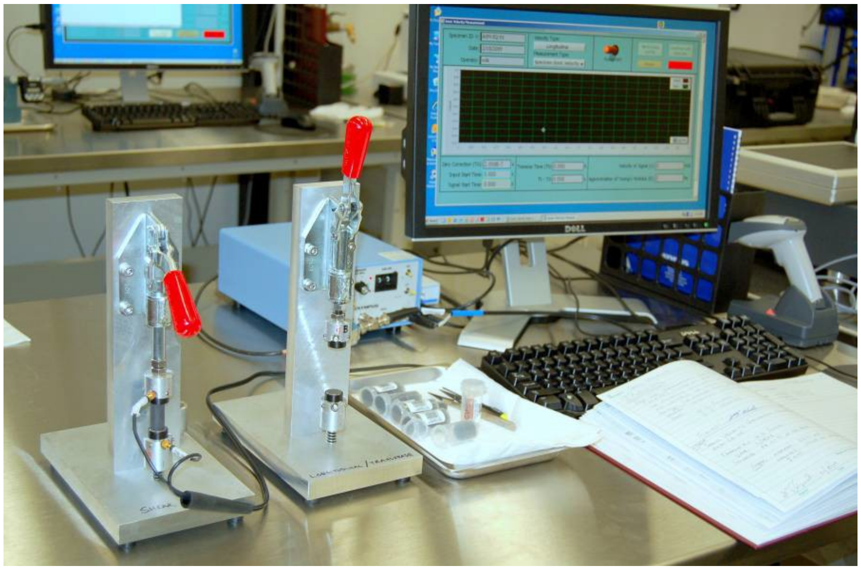

Figure 4. Sonic-velocity measurement station.

As specified in Paragraphs 8.1 and 8.5.1 of ASTM C 769-98, a suitable coupling medium should be used and reported with the data. Here, Shear Gel, manufactured by Sonotech, Inc., is used for a shear wave couplant and Ultragel II, also manufactured by Sonotech, Inc., is used for the transverse wave couplant.

Figure 5 shows the display, including the LabVIEW software user interface for sonic-velocity measurements after scanning the bar code of the specimen to be tested. This screen is used to acquire sonic-velocity measurements of a specimen in both the longitudinal and shear directions. Operating much like an oscilloscope, the cursors automatically mark the time between the transmitted wave and the received wave. Also shown in Figure 6 are two examples of the shear-wave and transverse-wave timing locations for properly coupled specimens. The specimen length, divided by this transit time, is the sonic velocity.

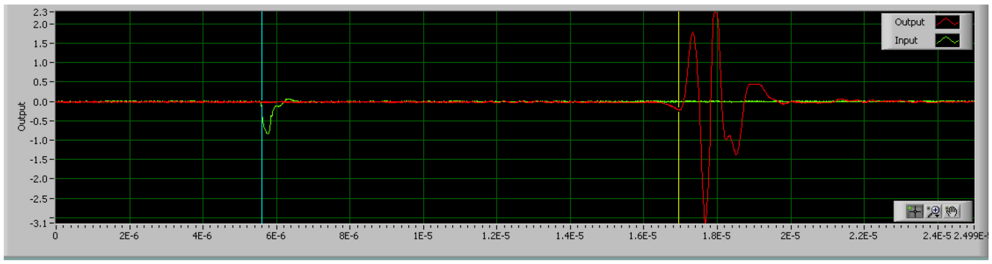

Shear wave timing

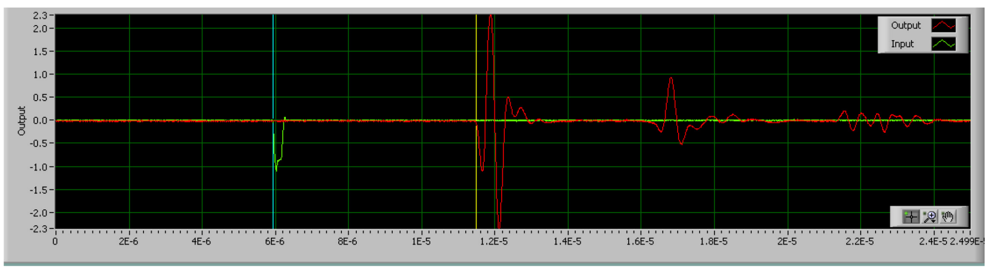

Transverse wave timing

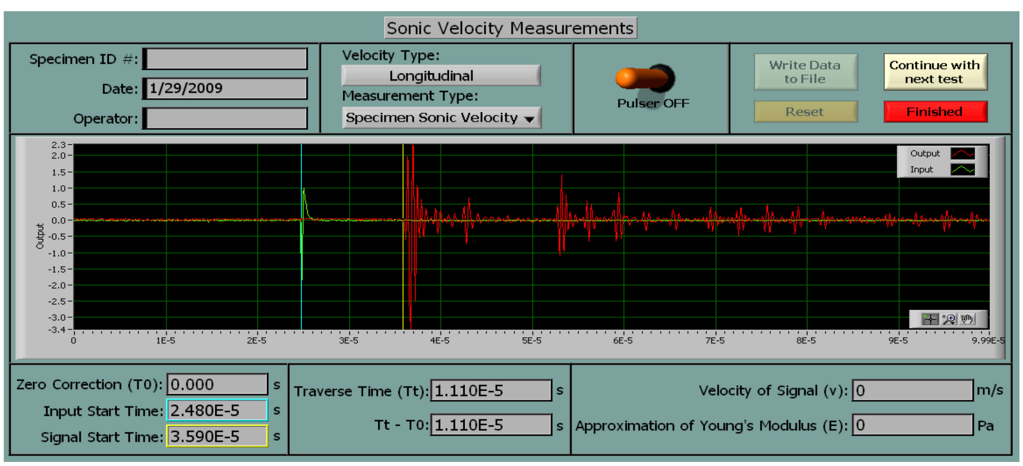

Figure 5. Sonic-velocity measurement user interface.

Figure 6. Commercial push rod dilatometer for measurement of CTE.

The uncertainty in determining elastic moduli from the measurement of sonic velocity comes from several sources. First, there is an effect of material- and geometry-related dispersion of the transmitted wave. ASTM C 769 provides guidance on how to minimize this problem by choosing the correct frequency. This technique also assumes linear elastic behavior, and graphite is not completely linearly elastic. And finally, the operator's judgment on the placement of the timing cursors is somewhat subjective. Clean wave forms to base these judgments on are highly dependent on the quality of the transducer-material coupling. These sources of error are difficult to quantify and, therefore, difficult to combine in a propagation-of-error analysis. However, ASTM C 769 describes in some detail a round-robin test series between different labs. Using round-robin test data to determine a coefficient of variation (COV) is a good means of estimating the measurement uncertainty. With caution, the COV of 3.8% reported in ASTM C 769 is taken here to be representative of the uncertainty of these measurements. When considering a single material and making comparisons between the pre- and post-irradiation values, the precision of these measurements is good enough to consider differences greater than 4% significant. However, one is cautioned to refrain from using the values here as absolute, or better than ±10% accurate.

4.4 Modulus of Elasticity by Measurement of Fundamental Frequency

The mechanical properties of graphite are necessary to determine the structural integrity of graphitic components. These properties are vital to determining the viability of the structural strength and integrity of the reactor core. This test method measures the fundamental resonant frequency of test specimens of suitable geometry by exciting them mechanically with a singular elastic strike. Specimen supports, impulse locations, and signal pickup points are selected to induce and measure specific modes of the transient vibration of the specimen. The transient signals are analyzed, and the fundamental resonant frequency is isolated and measured by the signal analyzer. The measured fundamental resonant frequency, specimen dimensions, and mass are used to calculate the dynamic Young's modulus, shear modulus, and Poisson's ratio per ASTM C747-16. The fundamental frequency measurement station is shown in Figure 7.

Figure 7. Fundamental frequency measurement station.

After placing a specimen in the test fixture, the user excites it by lightly tapping it with a small mechanical impulse. A consistent impulse is achieved by placing the ball hammer onto a lever that rotates out from under the hammer as it is raised. The specimen is supported in such a way that it vibrates at its natural frequency. A microphone placed underneath one end of the specimen in combination with the GrindoSonic electronics measure this frequency, which is recorded and displayed by the computer. The modulus of elasticity is calculated and displayed next to the newly acquired frequency. If the results are satisfactory, the user can press the "Save 1st Frequency" button and go on to the next measurement. Following the recommendations of ASTM C747-16, 10 readings of the fundamental frequency are measured before the results of the test are written to the applicable Excel spreadsheet.

The precision of this test method is based on an inter-laboratory study of ASTM C747-16. Two graphite materials were analyzed by five participating laboratories. Further detail is provided in ASTM Research Report No. ILS - 1259. As described above the measurements are made on cylindrical geometry creep specimens vibrating in the flexural mode. Table 3 shows the precision statistics in units of GPa for dynamic Young's modulus calculated for a circular rod with L/D <10 vibrating in the flexural mode.

Table 3. Precision statistics in units of GPa for dynamic Young's modulus calculated for a circular rod with L/D <10 vibrating in the flexural mode.

Material	Average ($\bar{x}$)	Repeatability Standard Deviation (s_r)	Reproducibility Standard Deviation (s_R)	Repeatability Limit (r)	Reproducibility Limit (R)
IG-110	8.70	0.04	0.10	0.11	0.29
NBG-18	12.24	0.17	0.17	0.46	0.46

Repeatability is the difference between repetitive results obtained by the same operator in a given laboratory applying the same test method with the same apparatus under constant operating conditions on identical test material within short intervals of time. The repeatability limits for IG-110 and NBG-18 were found to be 0.11 and 0.46 GPa, respectively.

Reproducibility is the difference between two single and independent results obtained by different operators applying the same test method in different laboratories using different apparatus on identical test material. The reproducibility limits for IG-110 and NBG-18 were found to be 0.29 and 0.46 GPa, respectively.

No graphite standard exists for this measurement, so a bias or accuracy of the measurement cannot be determined.

4.5 Thermal Expansion

Understanding the CTE for graphite components is critical for determining the dimensional changes that occur as a result of temperature cycles. Localized external stresses can be imposed upon mechanically interlocked graphite-core components as the individual pieces experience differential thermal expansion. Internal stresses can occur within larger graphite components if there is a temperature gradient causing differential expansion within the piece (one side has a higher temperature than the other). Finally, the thermal expansion is highly dependent upon the graphite microstructure, such as orientation/anisotropy, pore size and distribution, and crystallinity. Irradiation damage can significantly alter graphite microstructure and thus CTE values. Determining the extent of the changes as a function of irradiation dose and temperature will be a key parameter for reliable calculation of stress states within graphite components, volumetric changes, and irradiation creep rates.

The CTE measured here follows ASTM E228-06. This test method uses a push-rod-type dilatometer to determine the change in length of a graphite specimen relative to that of the holder as a function of temperature. The temperature is varied over the desired range at a slow constant heating or cooling rate. The linear thermal expansion and mean CTE, α, are calculated from the recorded data using:

$$\alpha = \frac{1}{L_0}\frac{\Delta \mathrm{L}}{\Delta \mathrm{T}}$$

where

L_0 = the specimen initial length

ΔL = the change in length

ΔT = the temperature difference between a specified reference temperature and the temperature at which the change in length was measured.

The Netzsch DIL 402 C commercial system (Figure 6) currently used at INL does not have the capability to cool the specimen below ambient temperature. Therefore, the initial length at 20°C is linearly extrapolated from expansion data between 100 and 150°C, and the mean CTE is calculated from a 20°C reference temperature.

The greatest source of experimental error in the dilatometry method described here is the correction made for the expansion of the specimen holder and push rod/linear variable differential transformer (LVDT) mechanism. This differential between the specimen and the apparatus must be accounted for to isolate the specimen expansion only. Studies reported in the precision and bias section of ASTM E228-06 have indicated that this type of dilatometry can be accurate to 4% when calibrations are performed carefully.

4.6 Thermal Diffusivity

The ability to conduct heat through a graphite core is critical to the passive removal of decay heat. Reduction of the thermal conductivity within graphite can have a significant effect on the passive heat removal rate and thus the peak temperature that the core and, subsequently the fuel particles, will experience during off-normal events. Determining changes to the conductivity as a function of irradiation dose and temperature is important for the high-temperature gas-cooled reactor safety analysis. Here, ASTM E1461-07 is followed for the calculation of thermal diffusivity and conductivity. Thermal diffusivity (δ) is measured and defined as the ratio of thermal conductivity to volumetric heat capacity by:

$$\delta = \frac{k}{\rho C_P}$$

where

k = thermal conductivity

ρ = density

C_P = specific heat.

The measurement is performed on small, thin, disk-shaped piggyback specimens. A pulsed laser is used to subject one surface of the specimen to a high-intensity, short-duration energy pulse. The energy of this pulse is absorbed on the front surface of the specimen, and the resulting rise in rear-face temperature is recorded. The thermal diffusivity is calculated from the specimen thickness and the time required for the rear-face temperature to reach 50% of its maximum value. A commercially available laser flash apparatus (LFA), complete with vendor-developed software for instrument control and data acquisition, is used as shown in Figure 8.

Figure 8. Netzch LFA measurement station for determination of thermal diffusivity.

Uncertainty in the measurement of thermal diffusivity comes about from specimen heat loss and temperature measurement error. Specimen temperature measurement is performed with a calibrated type-S thermocouple in the near vicinity of the specimen. Being relatively straight forward, the specimen temperature measurement is typically a small contribution to the overall measurement error or uncertainty.

The main contributor to the measurement uncertainty is heat loss from the specimen. Because this measurement technique depends on the assumption of one-dimensional heat transfer, from the flat face receiving the laser pulse to the flat face radiating to the detector, heat-loss errors are mainly attributed to radiative heat loss from the circumference of the specimen at temperatures above 300°C. Typically, several correction models are provided with the instrument software to account for this heat loss. As the specimen diameter-to-thickness ratio decreases, the heat loss increases to the point that the correction models no longer can account for the error. A study was performed to gain a better understanding of the limits of the models made available with the Netzsch LFA and the dependence of the diameter-to- thickness ratio on measurement error. In this study, the heat-loss models were applied to data taken on specimens with various diameter-to-thickness ratios and at specimen temperatures between 25 and 1000°C. It was determined that the Cowan (Cowan 1963) model along with diameter-to-thickness ratios ≥2 resulted in determination of the diffusivity within ASTM E1461-07 and the manufacturer's specified uncertainties of 4 and 3%, respectively. This was further verified by instrument functional tests performed monthly on a pure iron validation specimen for which the diffusivity was determined to be within 3% of the Touloukian values between 100 and 700°C (Touloukian 1973).

5. DATA ANALYSIS

Data gathered for the characterization of AGC-5 specimens are contained in the appendixes of this report. Appendix A contains plots of the individual data points for each specimen. Shown by the dashed lines in each plot are the upper and lower limits of the interquartile range (IQR). These limits are established by the lesser of either the least or greatest value in the data or by multiplying the IQR by 1.5 and adding or subtracting this value from the third and first quartile. Any data value outside of these limits is a suspected outlier of the established pattern. However, it is important to note that these outlying values are not only subject to measurement variability but also material variability and, therefore, cannot necessarily be discarded. These outlying values are examined in the context of the entire data set and will be evaluated further following irradiation. Other statistical parameters are calculated and presented in the tables of Appendix B. The mean, standard deviation, and coefficient of variance are all calculated for the different measurement data sets and graphite types. Upper and lower limits are presented in the tables of Appendix B, as are the IQR limits described above.

There are many ways to combine and compare the data presented here. In doing so, the validity of the data is exercised and scrutinized. First, the data sets are considered independently using the statistical analysis described above. Additionally, a limited comparison of the absolute property values is performed between different graphite types and grades. The degree of isotropy is also evaluated for the grades by calculating the anisotropy ratio:

$$\text{Anisotropy Ratio} = \frac{\text{Value of the Property in the Against-Grain Direction}}{\text{Value of the Property in the With-Grain Direction}}$$

Note that, in the case of isostatically molded graphite, with grain and against grain indicate specimens taken from orthogonal planes in the billet.

5.1 Mass, Dimensions, and Density Data Analysis

Plots of the measured mass, dimensions, and density for all AGC-5 specimens along with their IQR limits are shown in Appendix A, Figures A-1 through A-20 (creep specimens), and Appendix A, Figures A-56 through A-75 (piggyback specimens). Looking over the dimensional and mass measurements of the creep specimens for combined grain orientations, the data show that the COVs are all below 0.5%, with the exception being the NBG-18 specimens. The NBG-18 specimens' mass measurements differed slightly for the with and the against-grain orientations. Appendix A, Figure A-14, shows a difference of approximately 1% in mass, which in turn led to approximately 1% difference in density, Appendix A, Figure A-19, with no distinguishable difference in the dimensions of with- and against-grain NBG-18 specimens. This difference in mass, and therefore density, is most likely due to material variability in the billet from which the specimens were taken.

One of the most important parameters in the AGC experiment is the dimensional change of the specimens due to irradiation and stress. Therefore, particular care needs to be taken when evaluating the dimensional measurements. The scatter in the dimensional data is reasonable with the combined orientation length measurements for the creep and piggyback specimens having a COV of 0.2% or less and the combined diameter measurements having a COV of 0.12% or less. This is both a function of machining consistency and measurement precision. There are however, some specimens throughout the different grades that fall outside of their respective IQR. This does not necessarily indicate a measurement error. It is possible that the specimen dimensions are simply different than the majority as a result of machining differences.

5.2 Electrical Resistivity

Plots of electrical resistivity are shown in Appendix A, Figures A-41 through A-45, for graphite grades 2114, IG-110, NBG-17, NBG-18, and PCEA. The resistivity measurements were performed on the creep specimens only. The COVs for the combined orientation specimens varies by the grade. Grade 2114 had the lowest COV at 1.56%, and PCEA had the highest at 3.88%. After performing the IQR analysis for each grade, all of the resistivity values fell within the calculated IQR limits.

In Figure 9, the mean resistivity values of all the AGC-5 grades of graphite are plotted for both specimen grain orientations. The anisotropy ratio is displayed above each mean value. NBG-17 exhibited the best isotropy ratio, while PCEA had the largest resistivity difference between the two grain orientations. Grade 2114 specimens were only taken out of the billet in one grain orientation.

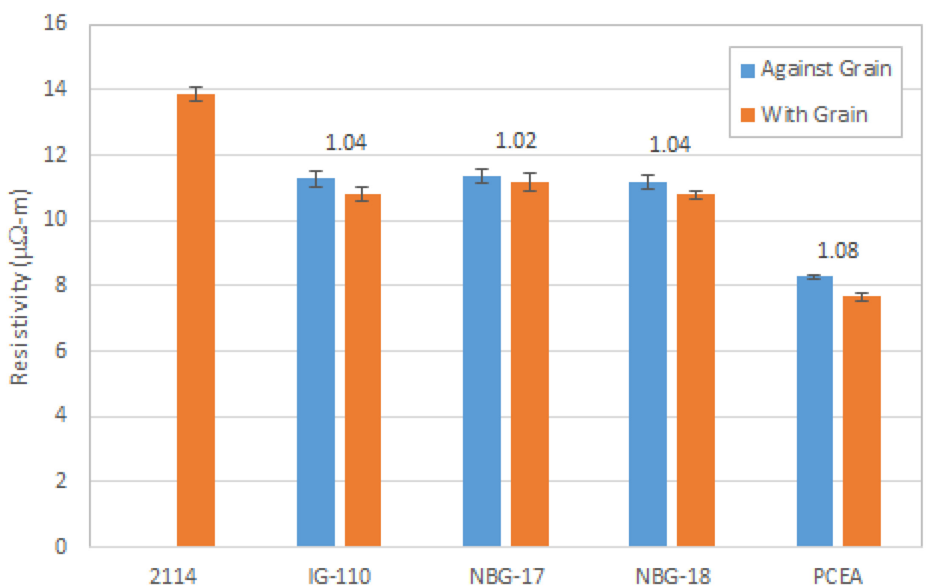

Figure 9. Electrical resistivity for the major graphite grades. The anisotropy ratio is above each set of data bars. The error bars represent ±1 standard deviation.

5.3 Approximation of Elastic Modulus from the Measurement of Sonic Velocity

Appendix A, Figures A-46 through A-55, are plots of Young's and shear modulus that were calculated from the measurement of sonic velocity through the graphite specimens. Young's and shear moduli statistics are shown for each graphite grade in Appendix B, Tables B-10 and B-11, respectively. The IQR analysis showed that there were two Young's modulus outliers and four shear modulus outliers (all were PCEA). The COVs calculated for all of the different graphite grades and grain orientations (maximum of 3.78%) agree with the COV reported in the precision and bias section of ASTM C769 (3.8%).

Figure 10 shows the relationship between Young's modulus measured using the sonic-velocity technique and the density for each graphite grade. In general, as the density of a material increases, so does the modulus of elasticity. Consistent with this, Figure 10 shows that the highest density graphite (NBG-18) had the highest modulus of elasticity. Figure 11 shows Young's modulus by sonic-velocity method for each grade of graphite by grain orientation with the anisotropy ratio. PCEA and IG-110 showed the largest disparity of moduli averages between grain orientations while the NBG-18 specimens showed the least variability with respect to grain orientation.

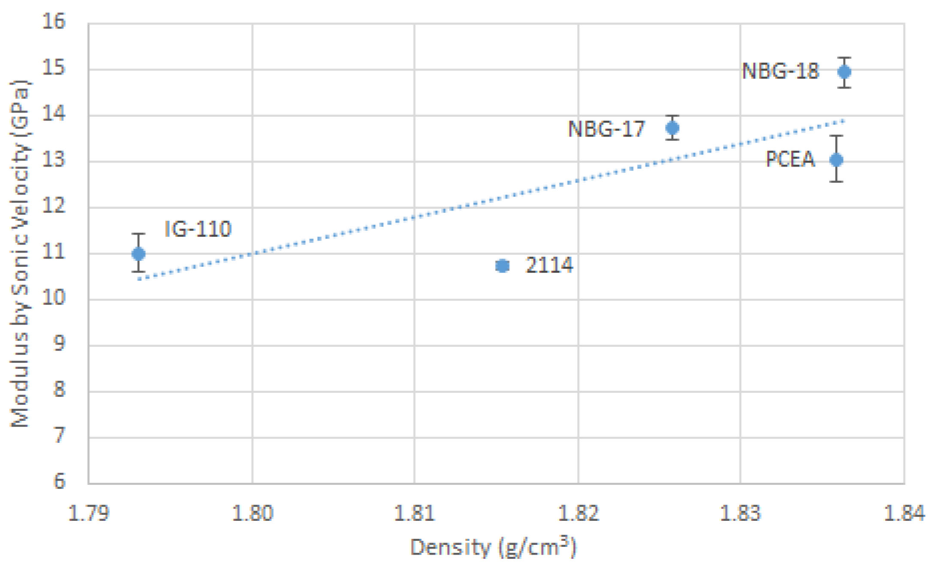

Figure 10. Young's modulus using the sonic-velocity technique versus density for each major graphite grade. The error bars represent ±1 standard deviation.

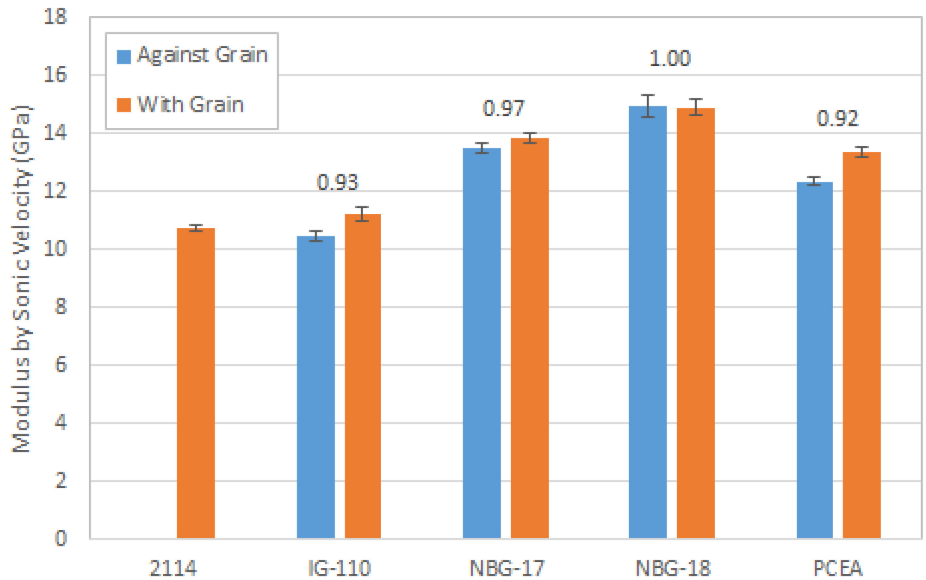

Figure 11. Young's modulus for the major graphite grades. The anisotropy ratio is above each set of data bars. The error bars represent ±1 standard deviation.

5.4 Modulus of Elasticity by Measurement of Fundamental Frequency

Young's modulus of each specimen was also calculated using the fundamental frequency technique. The results are plotted in Appendix A, Figures A-36 through A-40, and the statistical data is contained in Appendix B, Table B-8. Statistically, these data are well-behaved with the IQR analysis showing only one NBG-18 specimen that is outside of the IQR limits (Appendix A, Figure A-39).

It should be noted that, for AGC-5 specimens, the dynamic Young's modulus values determined by sonic-velocity testing techniques are generally 2–3 GPa higher than the measurements obtained by the fundamental-frequency testing technique. This difference can be seen, for example, in the NBG-18 grade, Appendix A, Figures A-39 and A-49. The difference between the two standards has been noted for a number of years and was finally addressed in the latest version of the sonic-velocity standard (ASTM 769-09). In this latest version, the Young's modulus value is calculated from the time-of-flight measurement utilizing a correction factor designated as the Poisson's factor (Cv). This factor is a function of Poisson's ratio and normally has a value between ~0.8 and 0.9. Calculating the modulus using the Poisson's factor effectively lowers the value by 10 to 20%, bringing the Young's modulus values measured by the sonic-velocity technique nearly equal to values arrived at by the fundamental-frequency test method.

Prior AGC specimen testing was performed under the previous ASTM sonic-velocity standard, ASTM 769-98 (re-approved 2005), which does not use Poisson's factor to calculate the modulus values. In order to avoid confusion when comparing AGC-5 data to previous AGC data, it was decided to continue using ASTM 769-98 and, when necessary, applying the correction.

Figure 12 shows a comparison of Young's modulus from the measurement of fundamental frequency for the primary grades of graphite by grain orientation. Again, all of the COVs for the different graphite grades and grain orientations compare favorably with the 3% uncertainty that is reported in the ASTM for this measurement technique with IG-110's COV being slightly high at 3.8%. IG-110 along with PCEA showed the biggest discrepancy between grain orientations. The anisotropy ratio of IG-110 and PCEA was 0.93 and 0.94, respectively. NBG-17 and NBG-18 exhibited very good anisotropy ratios of 0.98 and 0.99.

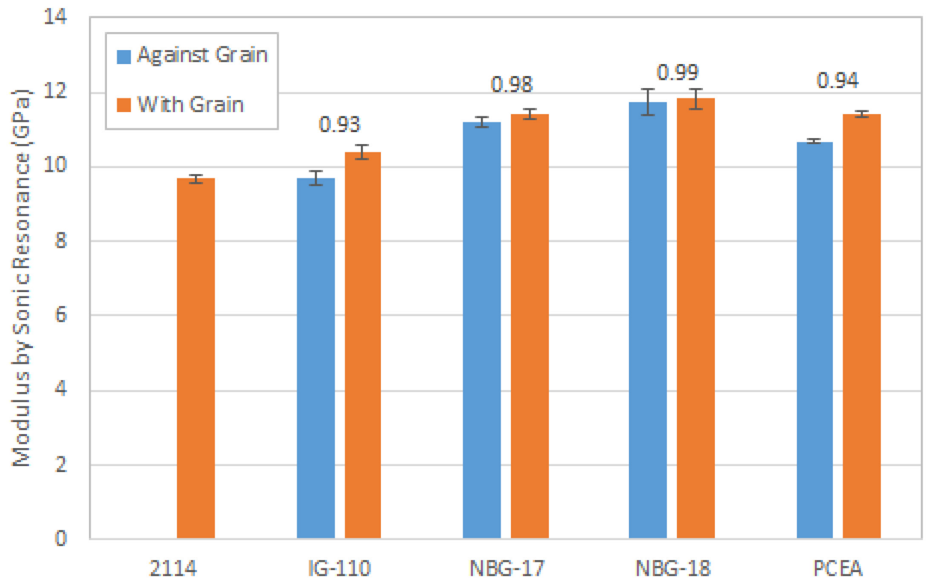

Figure 12. Young's modulus calculated by the fundamental-frequency method for the major graphite grades. The anisotropy ratio is above each set of data bars. The error bars represent ±1 standard deviation.

5.5 Thermal Expansion

Mean CTE data is plotted in Appendix A, Figures A-21 through A-35. A statistical evaluation of the CTE data was performed at three discrete temperatures for each graphite type: 100, 500, and 1000°C. The dashed lines in these plots indicate the upper and lower IQR limits. Appendix B, Tables B-5 through B-7, contain the mean, standard deviation, COV, median, and values of the upper and lower IQR limits for the data evaluated at the discrete temperatures.

Figure 13 shows the CTE COVs for the discrete temperatures listed above by graphite grade and grain orientation. The CTE data is well behaved with almost all of the COVs less than 3%. IG-110 against-grain specimens had the largest COV, almost 5%, at measurement temperature 100°C.

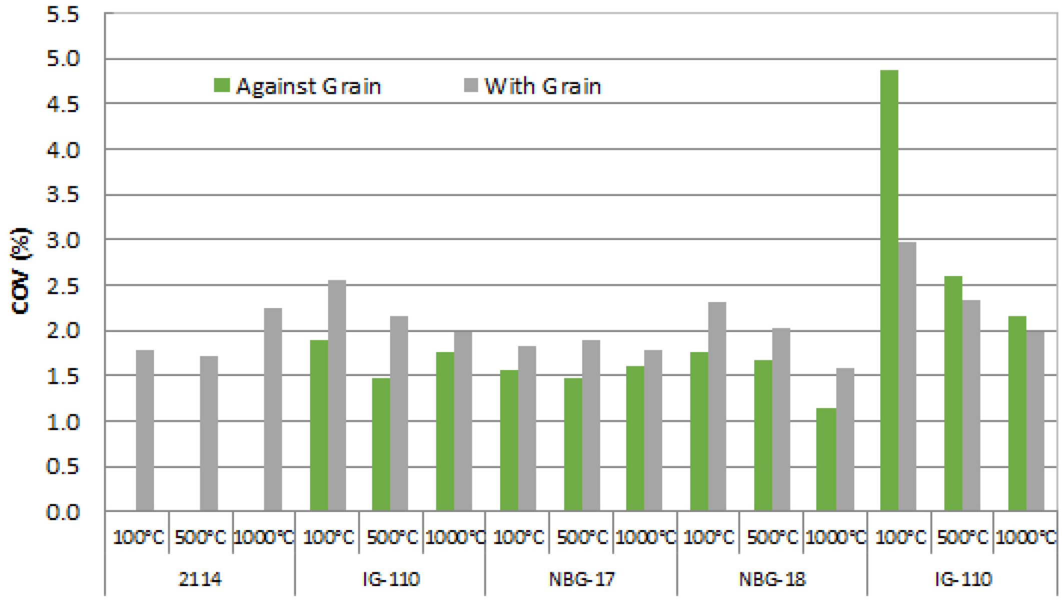

Figure 13. Coefficient of variance for mean CTE at three discrete temperatures for each major graphite grade and grain orientation.

Figure 14 shows the average CTE by grade at each measurement temperature, with error bars indicating ±1 standard deviation. All of the grades show an increase with temperature in a near linear fashion between 300 and 1000°C.

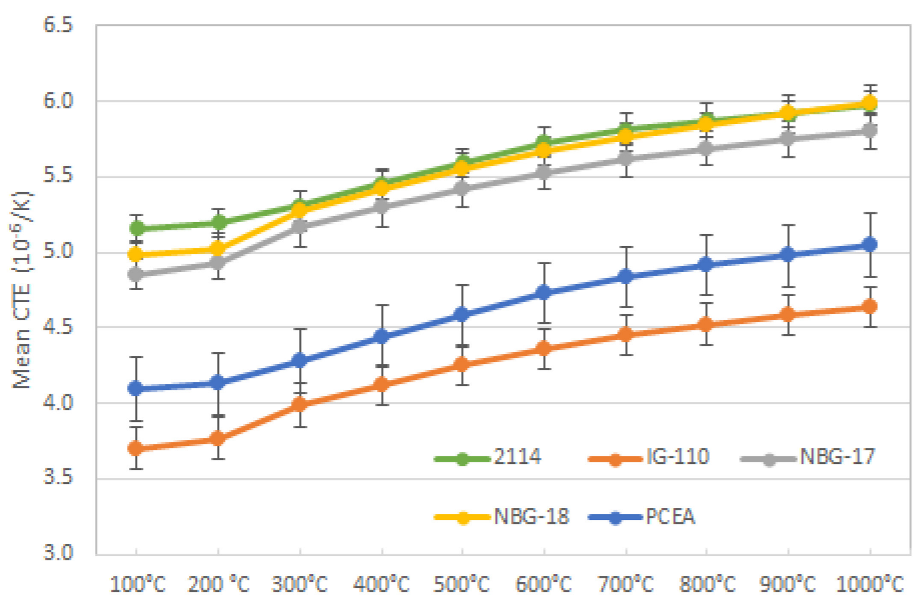

Figure 14. Mean CTE for the major grades of graphite as a function of measurement temperature. The error bars represent ±1 standard deviation.

Measurements of CTE were performed on both with-grain and against-grain specimens. Figure 15 shows the CTE anisotropy ratio for the same primary grades of graphite as a function of temperature. Other than IG-110, the ratios are fairly constant across all measurement temperatures. Grade 2114 is not shown because only specimens in a single-grain orientation were used.

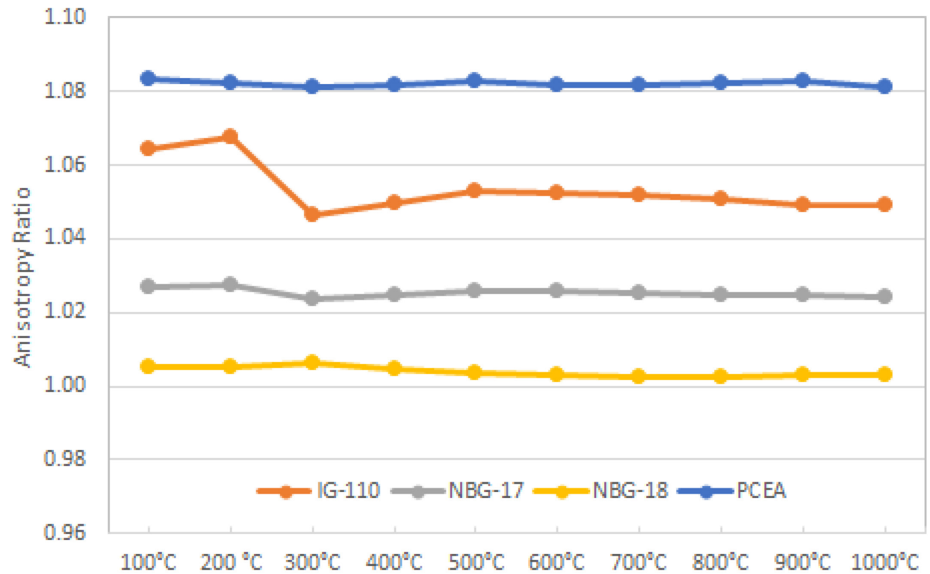

Figure 15. CTE anisotropy ratio for nuclear-grade graphites as a function of temperature.

5.6 Thermal Diffusivity

Plots of thermal diffusivity are shown in Appendix A, Figures A-76 through A-90. As with the CTE data, discrete temperatures of 100, 500, and 1000°C were statistically evaluated. Appendix B, Tables B-16 through B-18, contain values of the mean, standard deviation, COV, median, and lower and upper IQR limits. The COVs for all the graphite grades within specific grain orientations are below 2.5%. Fourteen outliers were found after performing the IQR analysis. The most extreme of the outliers were three 2114 specimens (Appendix A, Figures A-76, A-81, and A-86). For these specimens, the raw data from which the average diffusivity was calculated were examined. The average diffusivity is calculated from three diffusivity measurements. The COV of these three measurements for the above outliers was roughly twice that (about 1.5%) in comparison to the other specimens (0.7%). However, it was decided that this increase did not warrant excluding those specimens.

Figure 16 shows the diffusivity COVs for the discrete temperatures listed above by graphite grade and grain orientation. Here, the scatter in the data for the with-grain specimens of IG-110 is significantly higher than the other grades but still within the estimated measurement precision. Again material variability is thought to be the cause.

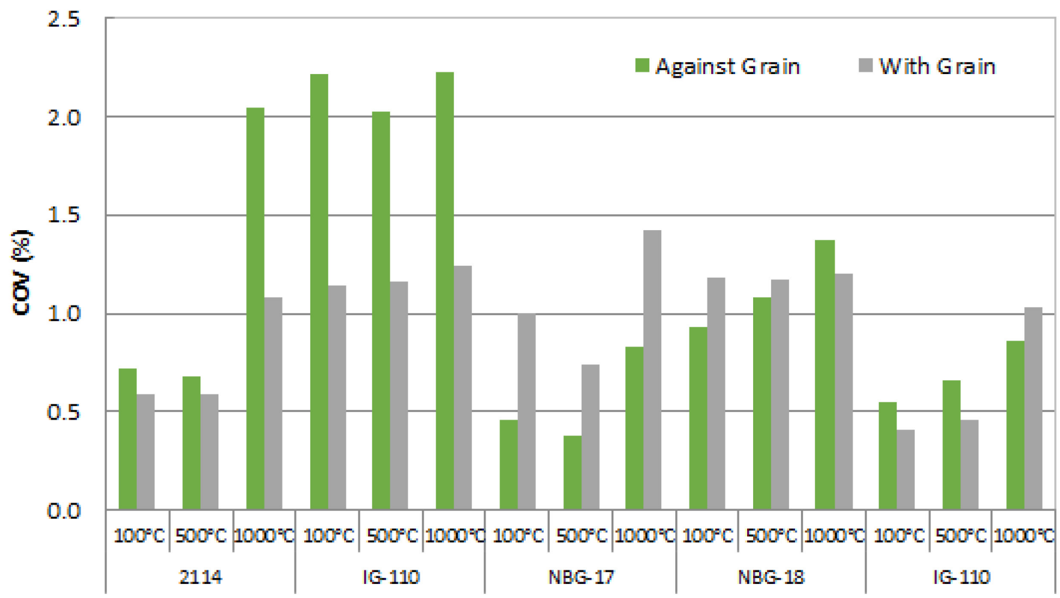

Figure 16. Coefficient of variance for diffusivity at three discrete temperatures for each major graphite grade and grain orientation.

Figure 17 shows the average thermal diffusivity for the five primary graphite grades of interest. Error bars are ±1 standard deviation and in most cases cannot be seen because they are smaller than the plotted symbol. The diffusivity between different grades of graphite varies as much as 40% at room temperature (2114 and PCEA). However, this percentage reduces as the measurement temperature approaches 1000°C. The NBG-17 data in the figure is hidden behind the IG-110 and NBG-18 data.

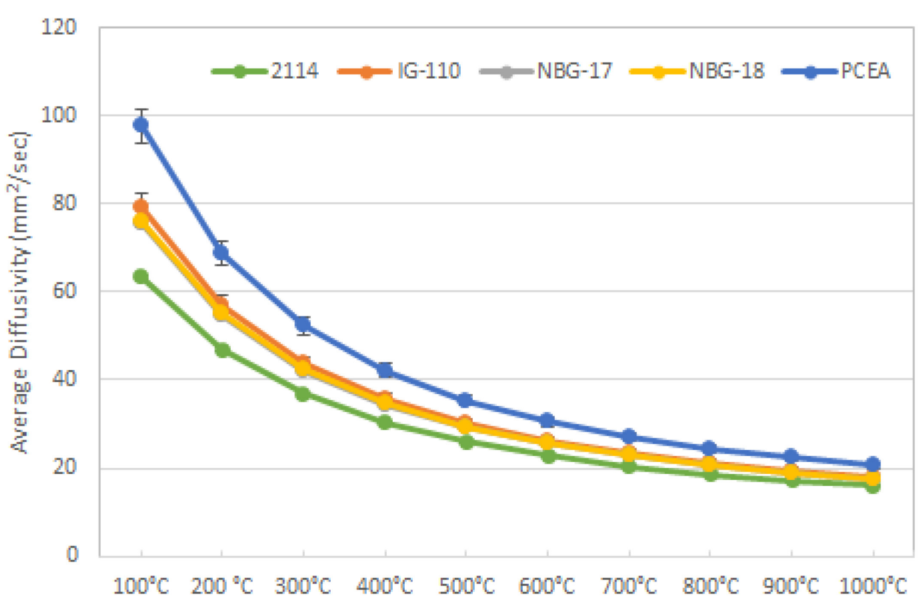

Figure 17. Thermal diffusivity for various graphite types as a function of temperature. Error bars represent ±1 standard deviation.

Figure 18 shows the anisotropy ratio for the same graphite grades. As expected this ratio is constant as a function of temperature for all grades.

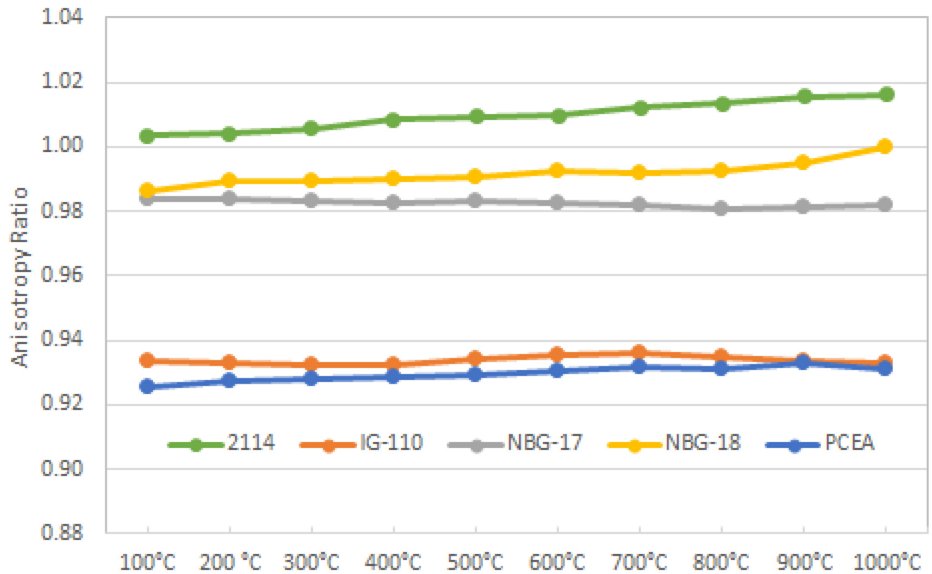

Figure 18. Thermal diffusivity anisotropy ratio for several types of nuclear-grade graphite as a function of temperature.

6. APPENDIXES

Appendix A, AGC-5 Data Plots

Appendix B, Statistical Tables

7. REFERENCES

ASTM C559-90, "Standard Test Method for Bulk Density by Physical Measurements of Manufactured Carbon and Graphite Articles"

ASTM C611-98, "Standard Test Method for Electrical Resistivity of Manufactured Carbon and Graphite Articles at Room Temperature"

ASTM C747-16, "Standard Test Method for Moduli of Elasticity and Fundamental Frequencies of Carbon and Graphite Materials by Sonic Resonance"

ASTM C769-98, "Standard Test Method for Sonic Velocity in Manufactured Carbon and Graphite Materials for Use in Obtaining an Approximate Youngs [*sic*] Modulus"

ASTM E1461-07, "Standard Test Method for Thermal Diffusivity by the Flash Method"

ASTM E228-06, "Standard Guide for Testing the Thermal Properties of Advanced Ceramics"

Burchell, T., R. Bratton, and W. Windes, *NGNP Graphite Selection and Acquisition Strategy*, ORNL/TM-2007/153, Oak Ridge National Laboratory, September 2007.

Bratton, R. L. and T. D. Burchell, *NGNP Graphite Testing and Qualification Specimen Selection Strategy*, INL/EXT-05-00269, Idaho National Laboratory, May 2005.

Cowan, R. D., 1963, "Pulse method of measuring thermal diffusivity at high temperatures," *Journal of Applied Physics*, Vol. 34, No. 4, p. 926.

Dwg. 780577, "ATR Advanced Graphite Capsule (AGC) AGC-5 Graphite Specimen Cutout Diagrams," Idaho National Laboratory, Rev. 2, April 7, 2015.

Form 250.01, "Data Management and Analysis Transmittal"

LWP-12033, "Personnel Qualification and Certification"

LWP-13455, "Control of Measuring and Test Equipment"

LWP-20000-01, "Conduct of Research"

LWP-21220, "Work Management"

MCP-1380, "Research and Development Test Control"

MCP-2875, "Proper Use and Maintenance of Laboratory Notebooks"

NQA-1-2008/1a-2009, "Quality Assurance Requirements for Nuclear Facility Applications"

PLN-2690, "Idaho National Laboratory Advanced Reactor Technologies Technology Development Office Quality Assurance Program Plan"

PLN-4653, "INL Records Management Plan"

PLN-5580, "AGC-5 Graphite Specimen Pre-irradiation Characterization Plan"

Touloukian, Y. S., "Thermophysical Properties of Matter - Thermal Diffusivity," John Wiley & Sons Ltd., May 6, 1973.

Windes, W., T. Burchell, and R. Bratton, PLN-2497, "Graphite Technology Development Plan," Idaho National Laboratory, Rev. 1, October 2010.

8. BIBLIOGRAPHY

Burchell, T., J. Strizak, and M. Williams, *AGC-1 Specimen Pre-irradiation Data Report*, ORNL/TM-2010/285, Oak Ridge National Laboratory, August 2011.

Reed, T., ECAR-1943, "AGC-1 Individual Specimen Fluence, Temperature, and Load Calculation and Tabulation," Idaho National Laboratory, September 2012.

Reed, T., ECAR-1944, "AGC-1 As Run Thermal Results", Idaho National Laboratory, September 2012.

Swank, D., *AGC-2 Graphite Pre-irradiation Data Package*, INL/EXT-10-19588, Idaho National Laboratory, August 2010.

Davenport, M., TFR-875, "AGC-5 Test Train Technical and Functional Requirements," Idaho National Laboratory, July 2014.

Dwg. 604554, "AGC-5 Test Train Facility Assembly," Idaho National Laboratory, July 8, 2014.

Dwg. 603521, "AGC Graphite Specimen Holder Machining Details," Idaho National Laboratory, Rev. 2, June 14, 2012.

Dwg. 604553, "AGC-4 Specimen Stack-up Arrangements," Idaho National Laboratory, Rev. 1, April 21, 2015.

Perry, J. R., TEV-2467, "AGC-5 Dose Rate and Shielding Evaluation," Idaho National Laboratory, June 6, 2015.

Burchell, T. and R. Bratton, *Graphite Irradiation Creep Capsule AGC-1 Experimental Plan*, ORNL/TM-2005/505, Oak Ridge National Laboratory, May 2005.

Burchell, T., *A Revised AGC-1 Creep Capsule Layout, ORNL/TM-2009/009*, Oak Ridge National Laboratory, January 2009.

Windes, William, W. David Swank, David Rohrbaugh, and Joseph Lord, *AGC3 Graphite Pre-irradiation Data Analysis Report*, INL/EXT-13-30297, Idaho National Laboratory, September 2013.

Appendix A

AGC-5 Data Plots

Appendix A

AGC-5 Data Plots

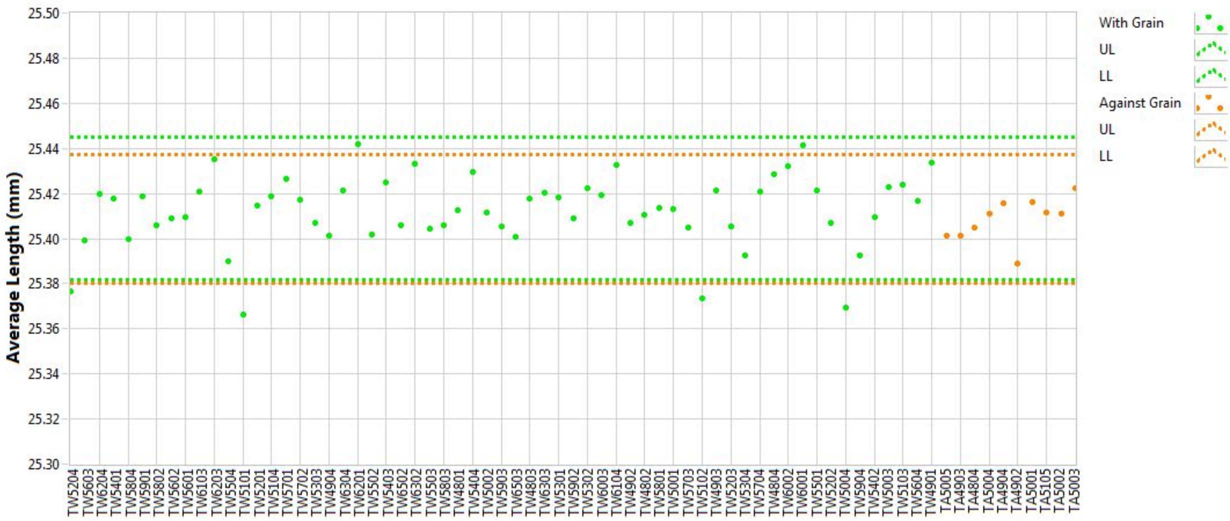

Figure A-1. 2114 creep length.

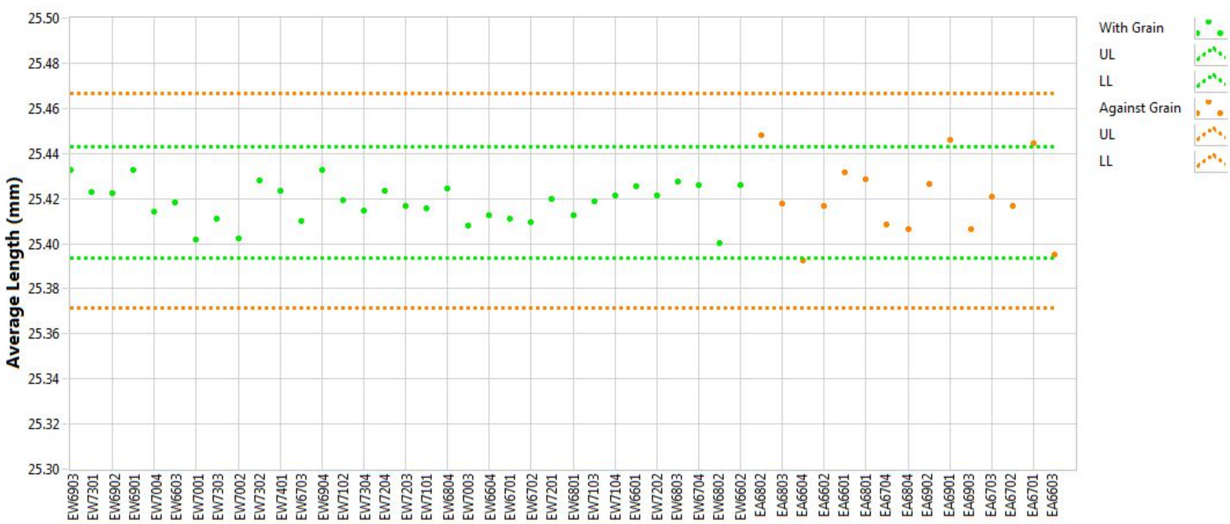

Figure A-2. IG-110 creep length.

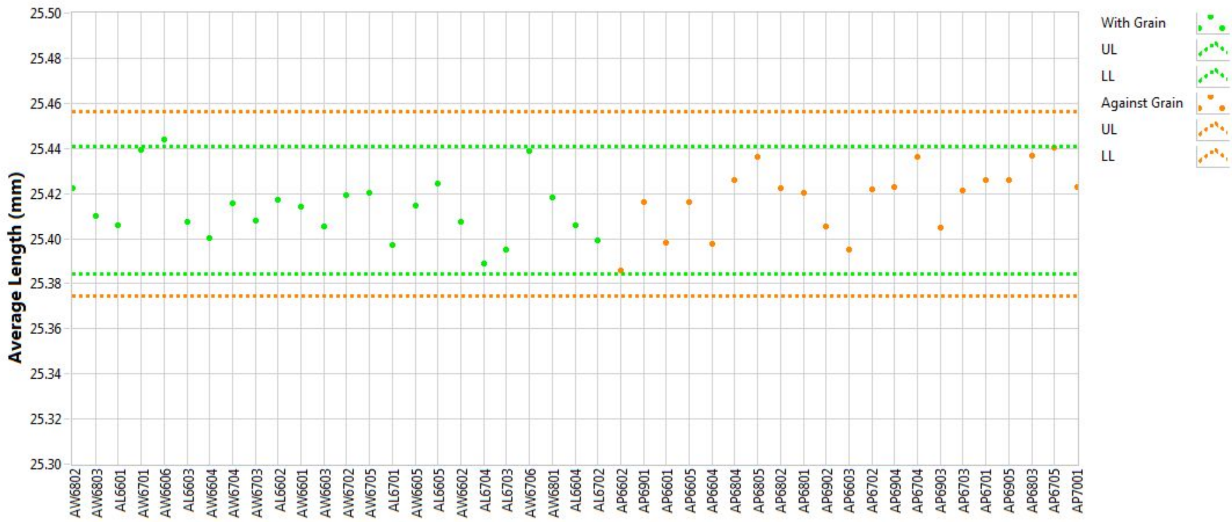

Figure A-3. NBG-17 creep length.

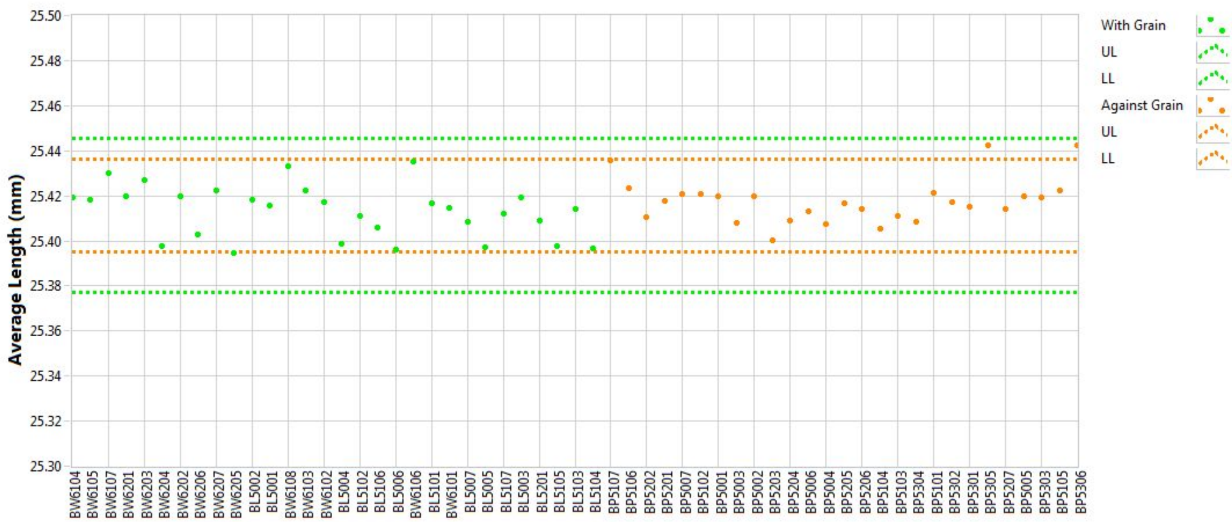

Figure A-4. NBG-18 creep length.

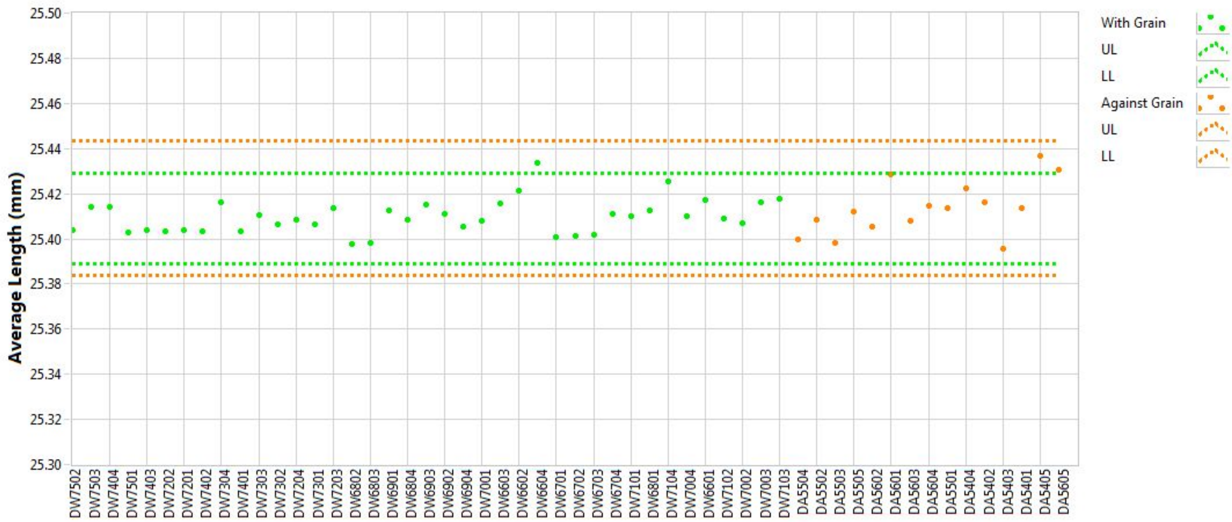

Figure A-5. PCEA creep length.

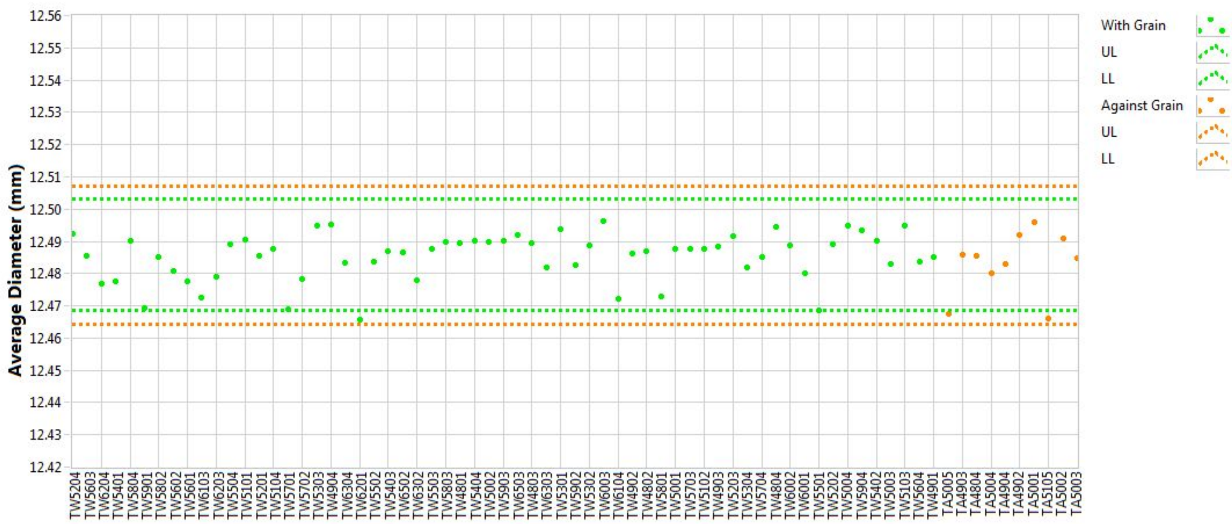

Figure A-6. 2114 creep diameter.

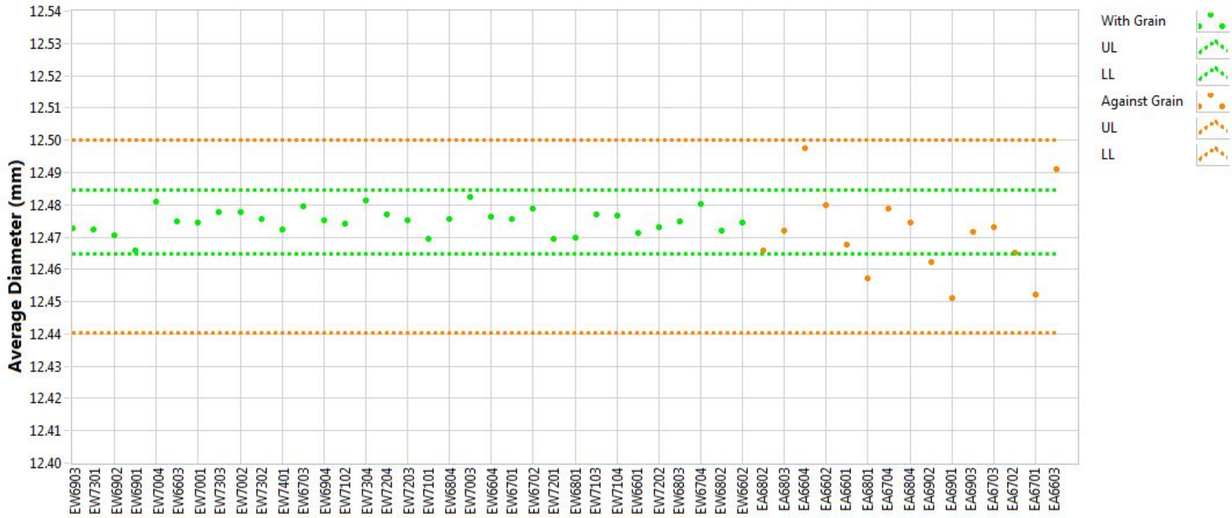

Figure A-7. IG-110 creep diameter.

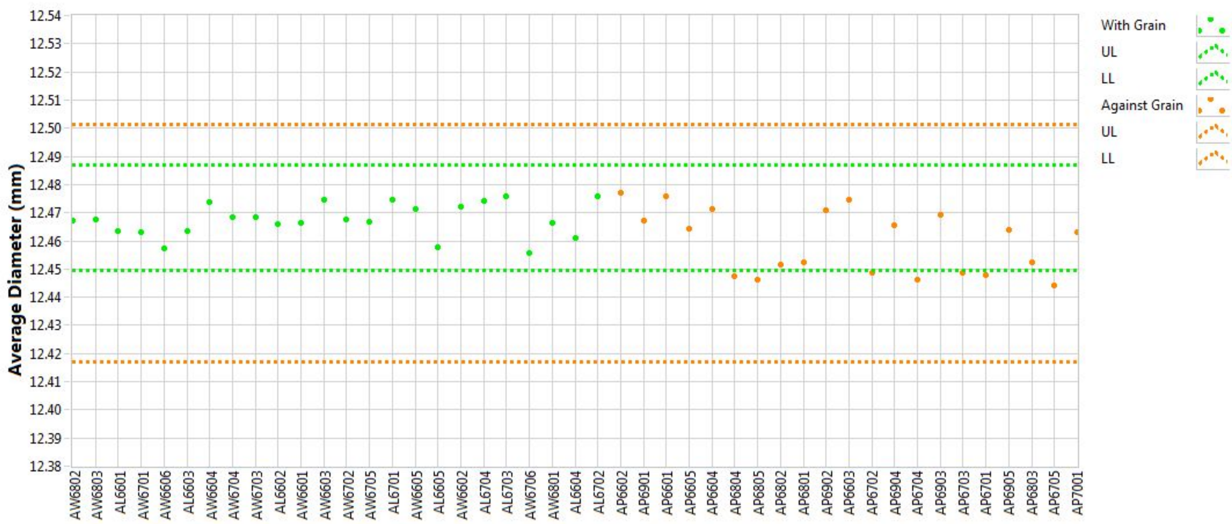

Figure A-8. NBG-17 creep diameter.

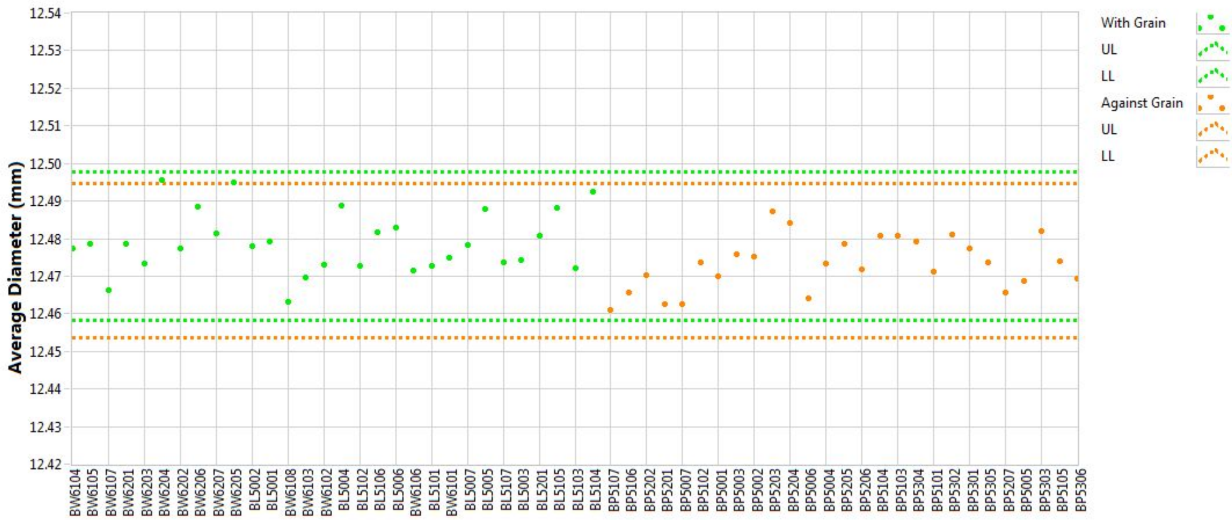

Figure A-9. NBG-18 creep diameter.

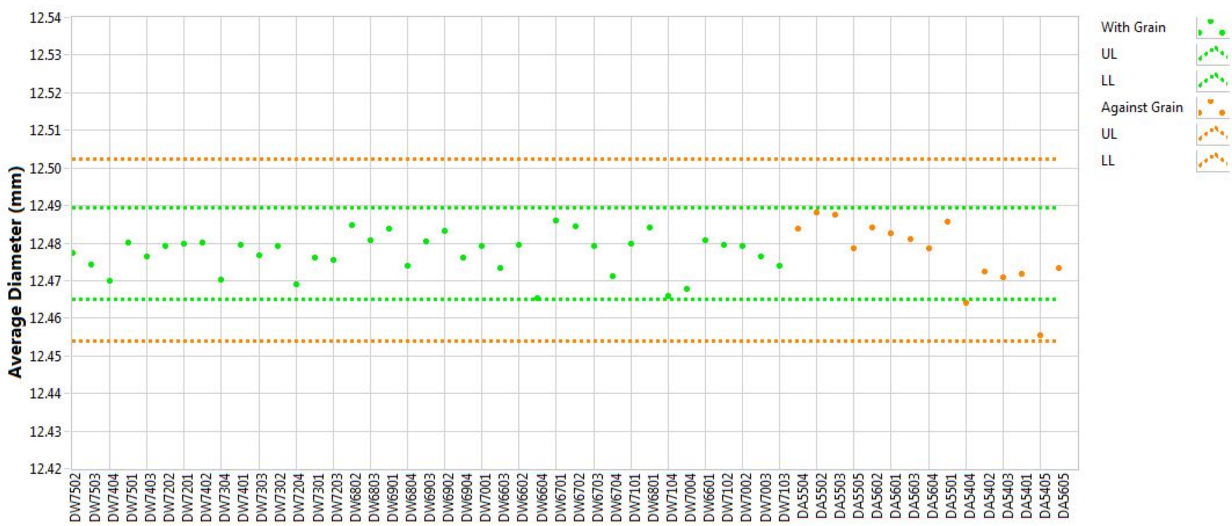

Figure A-10. PCEA creep diameter.

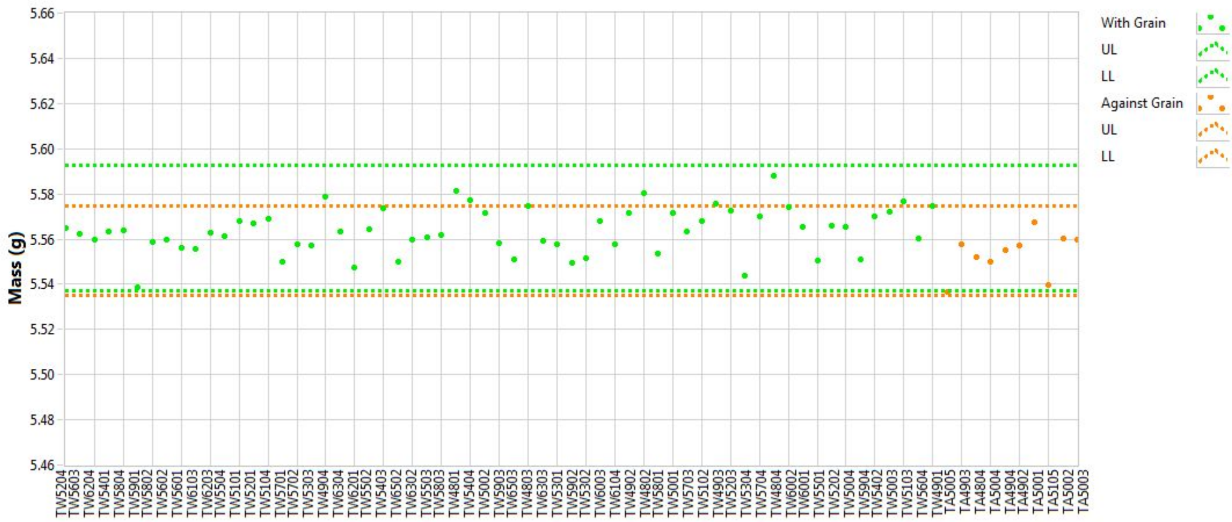

Figure A-11. 2114 creep mass.

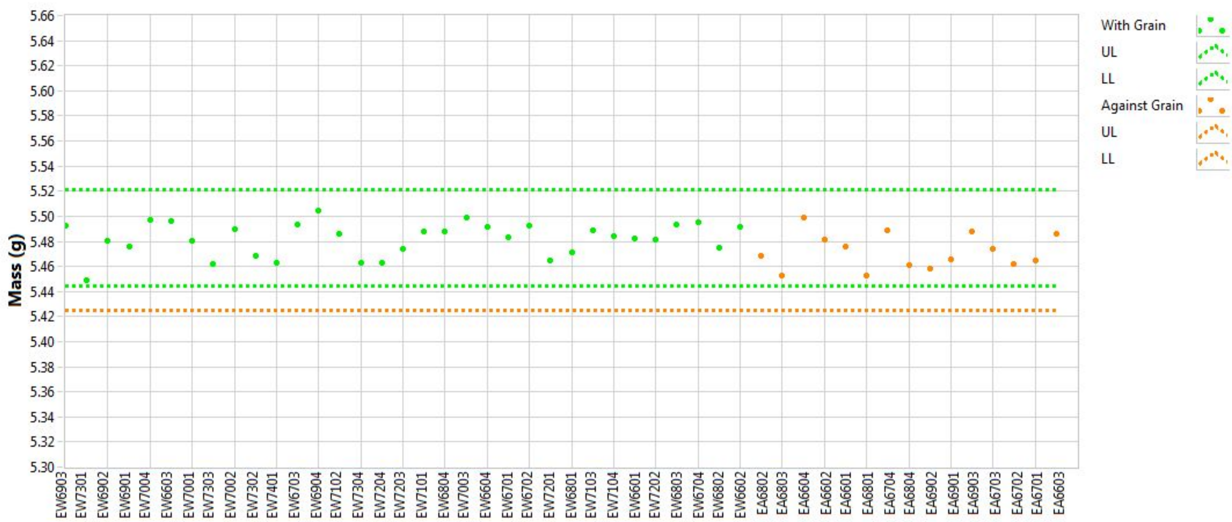

Figure A-12. IG-110 creep mass.

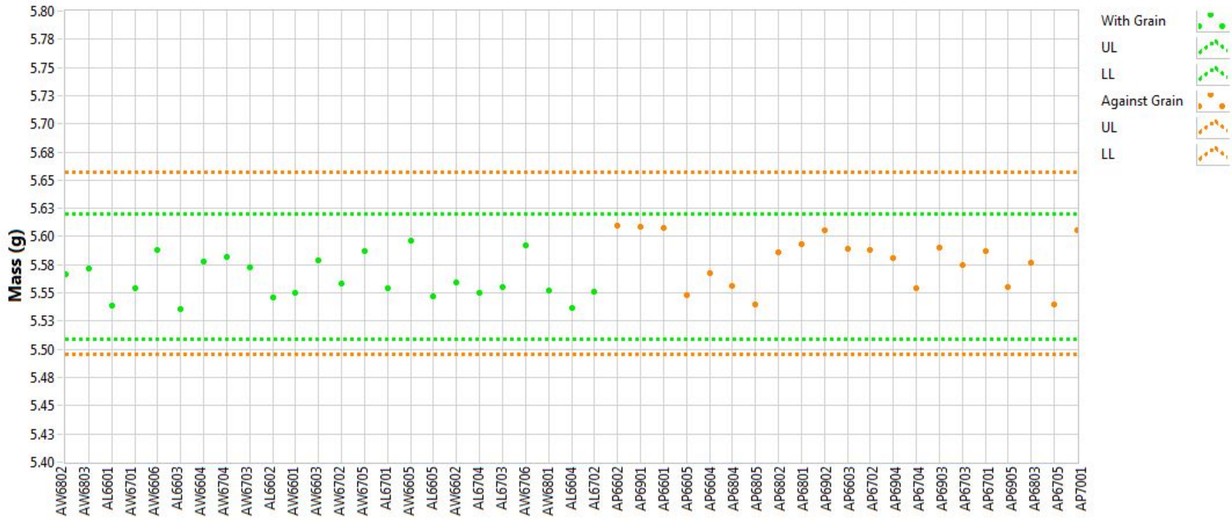

Figure A-13. NBG-17 creep mass.

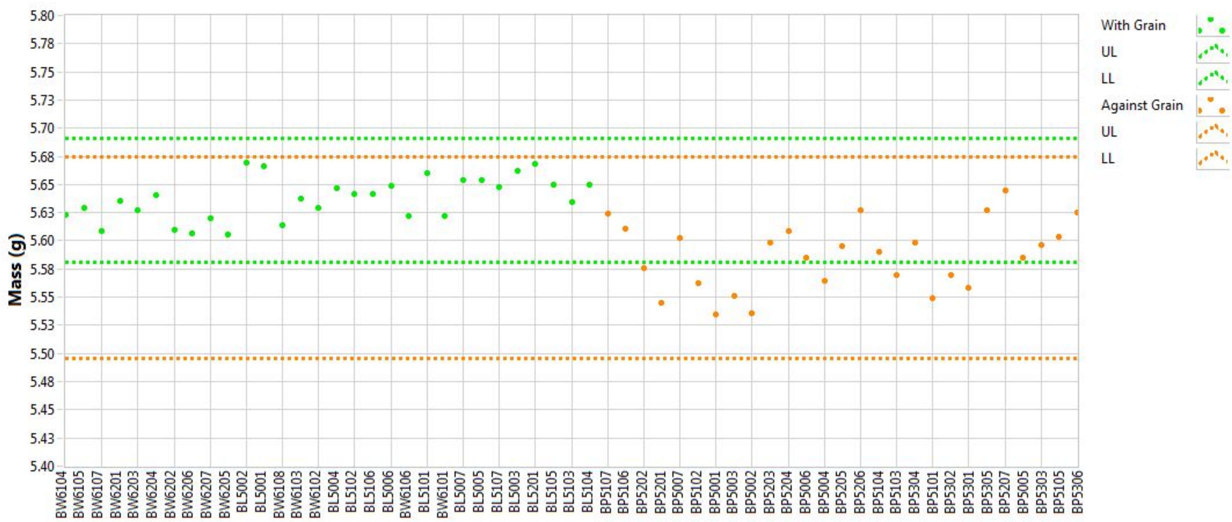

Figure A-14. NBG-18 creep mass.

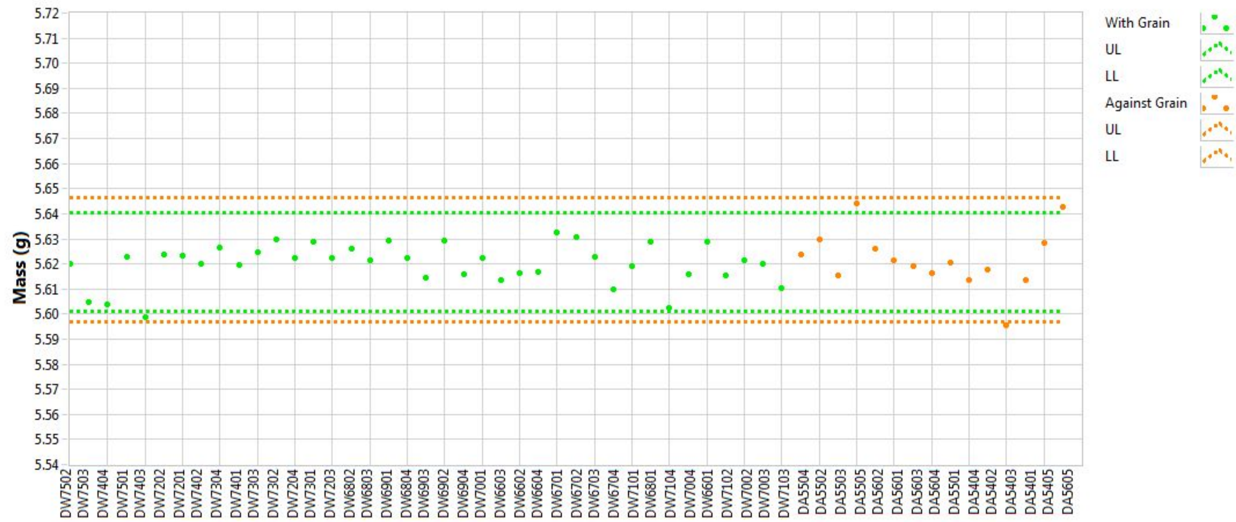

Figure A-15. PCEA creep mass.

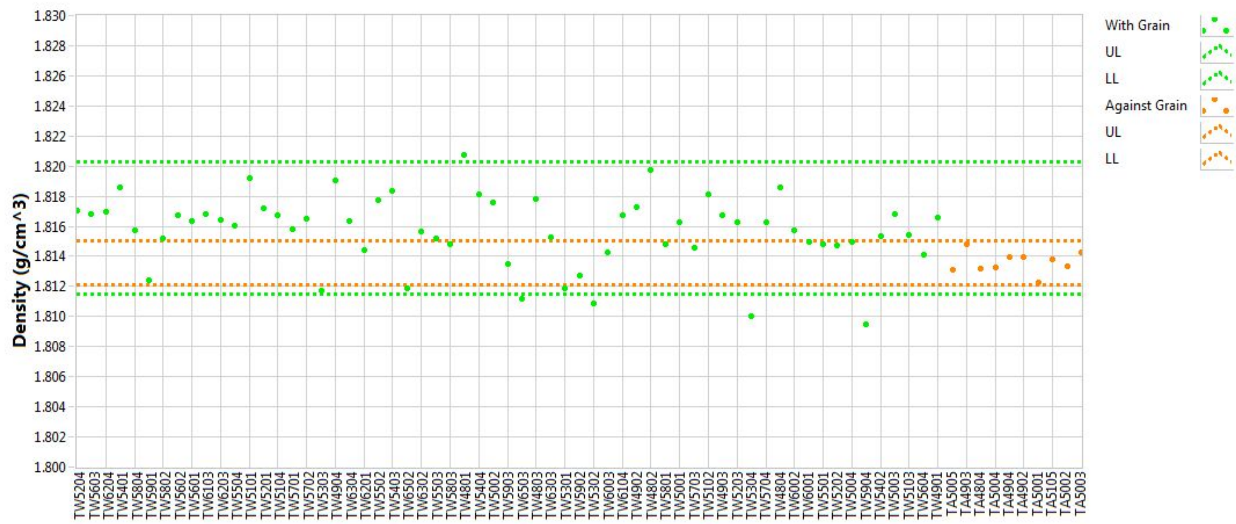

Figure A-16. 2114 creep density.

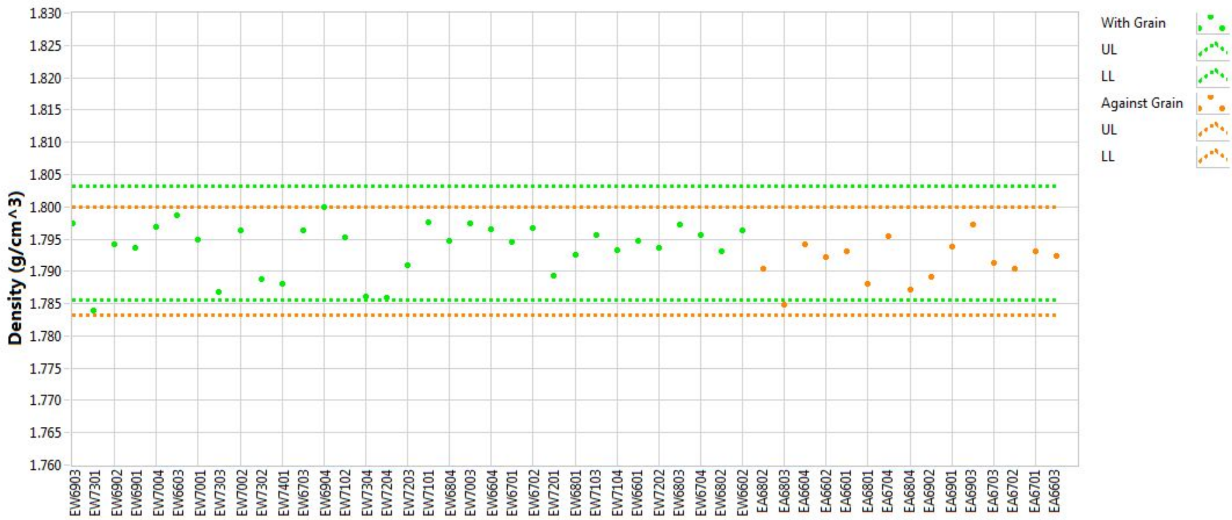

Figure A-17. IG-110 creep density.

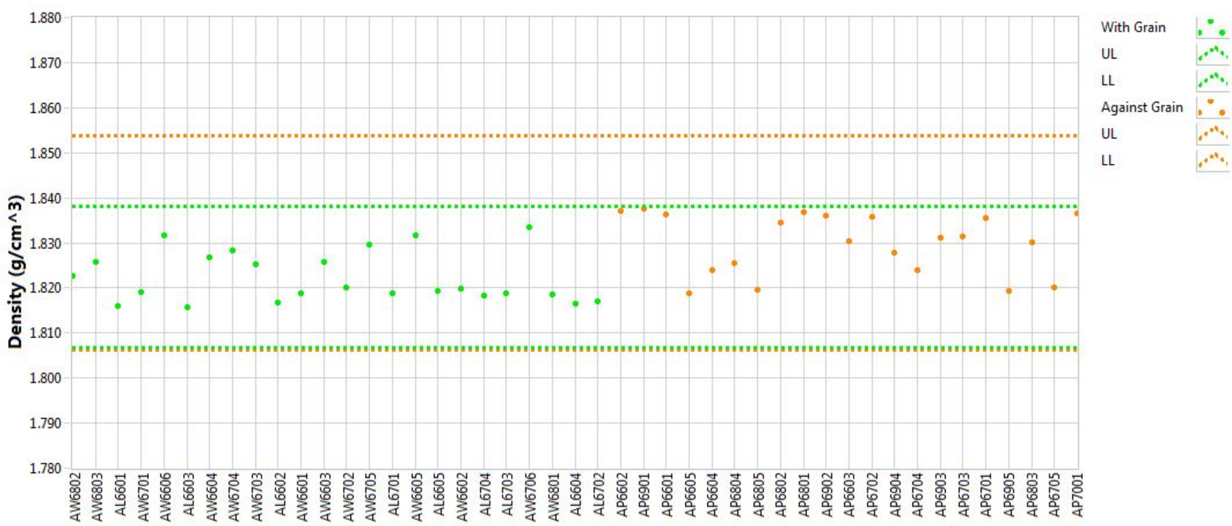

Figure A-18. NBG-17 creep density.

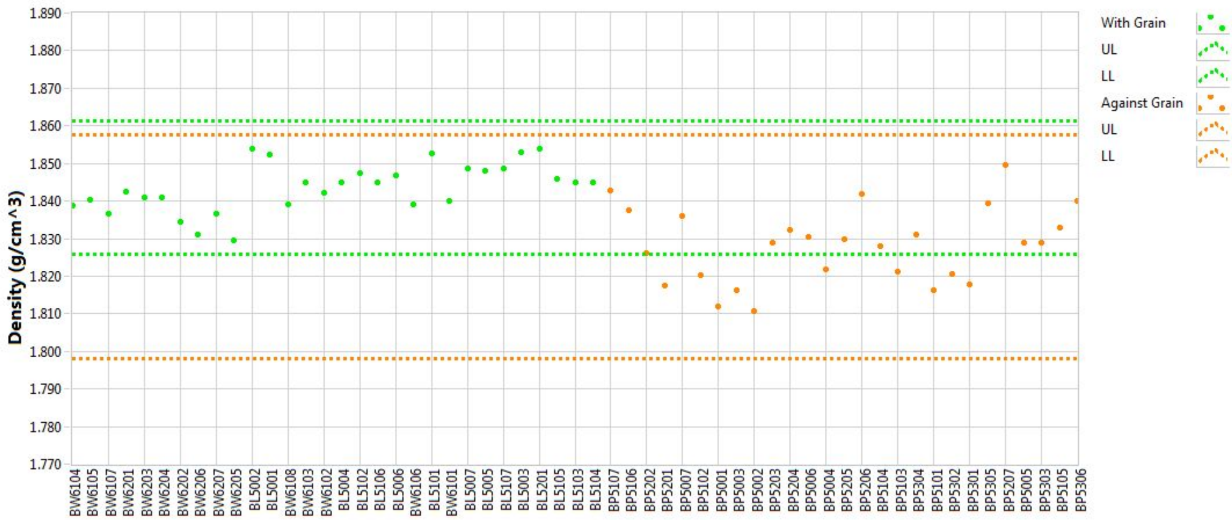

Figure A-19. NBG-18 creep density.

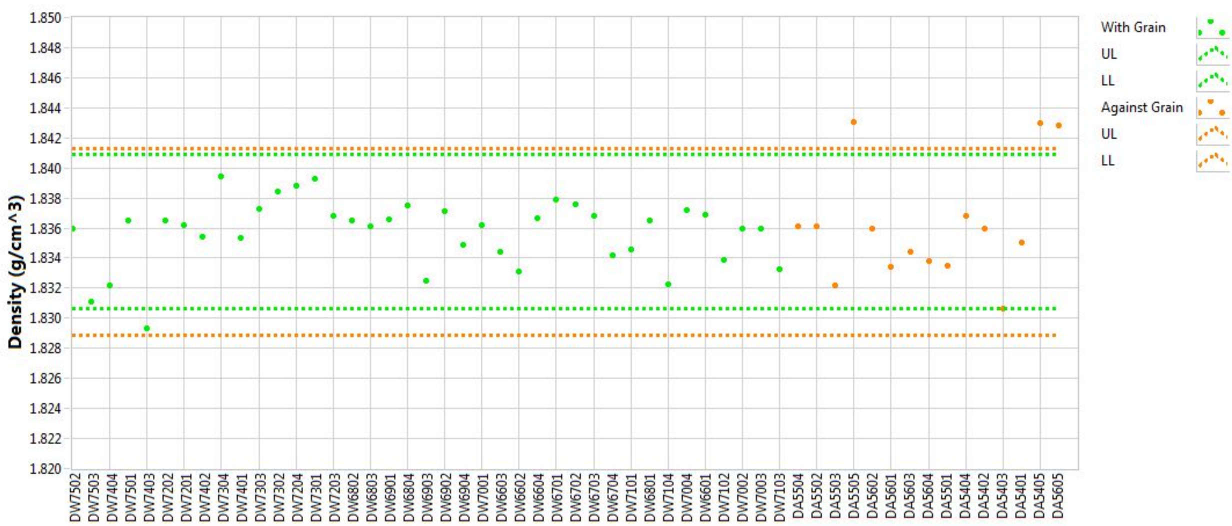

Figure A-20. PCEA creep density.

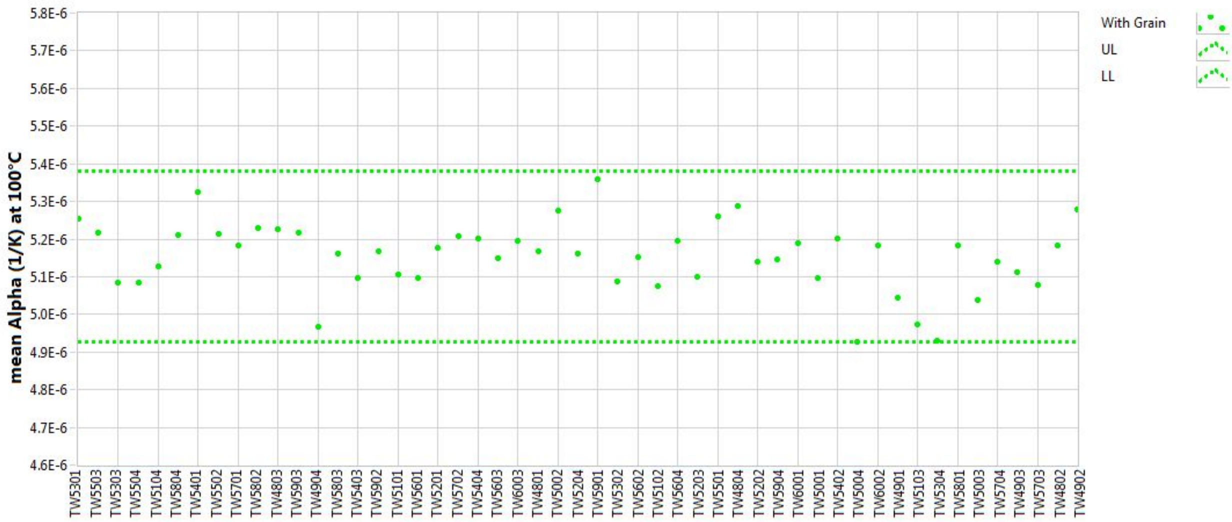

Figure A-21. 2114 creep coefficient of thermal expansion at 100°C.

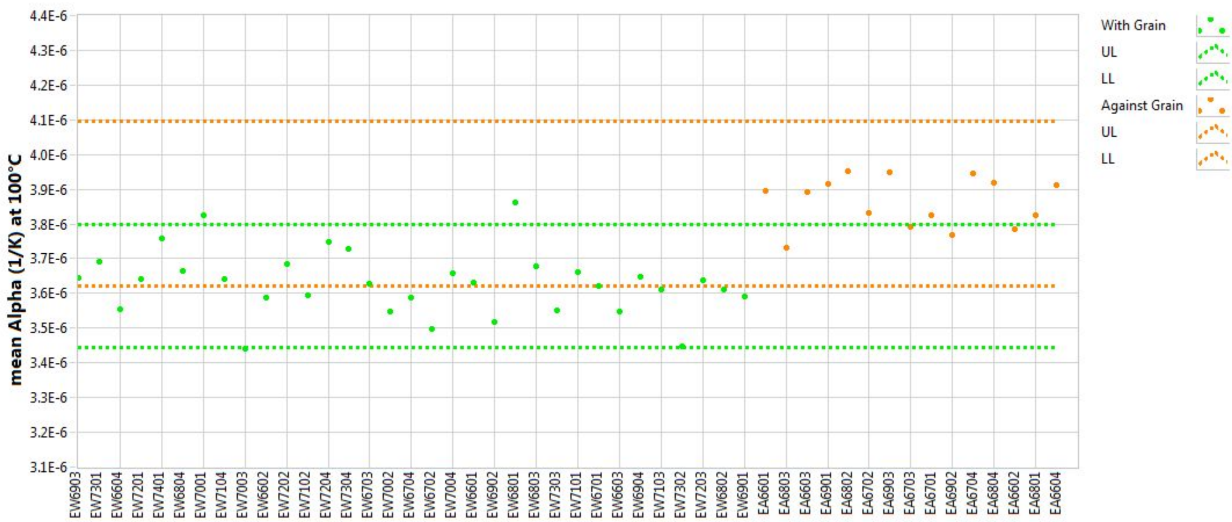

Figure A-22. IG-110 creep coefficient of thermal expansion at 100°C.

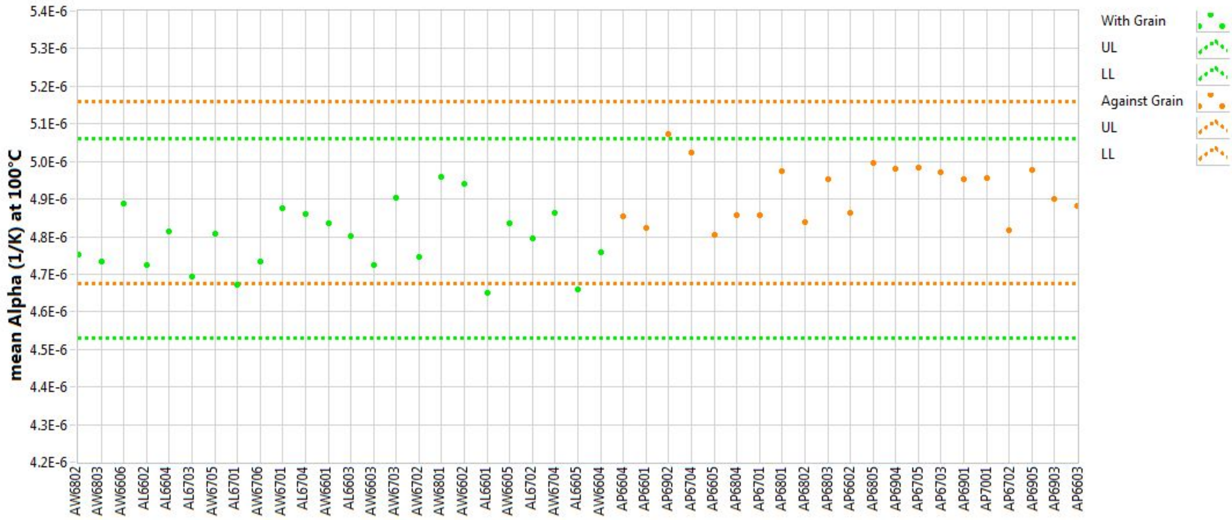

Figure A-23. NBG-17 creep coefficient of thermal expansion at 100°C.

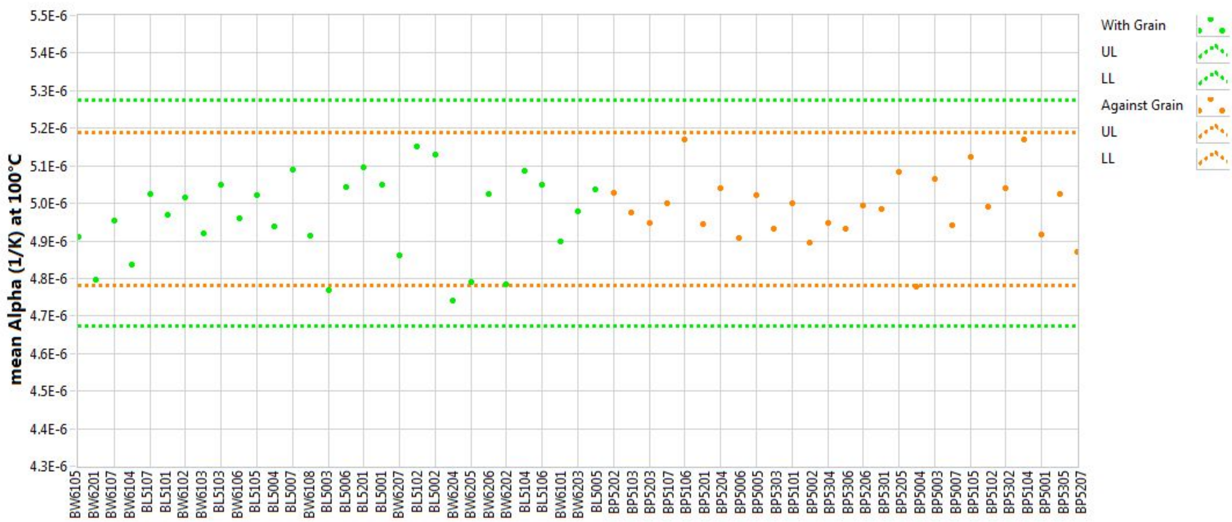

Figure A-24. NBG-18 creep coefficient of thermal expansion at 100°C.

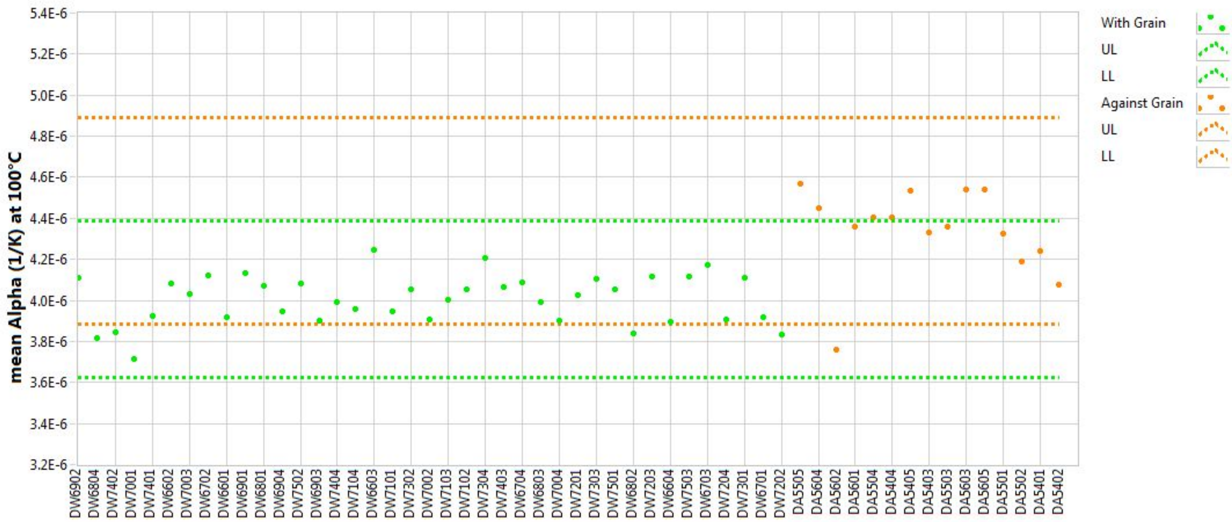

Figure A-25. PCEA creep coefficient of thermal expansion at 100°C.

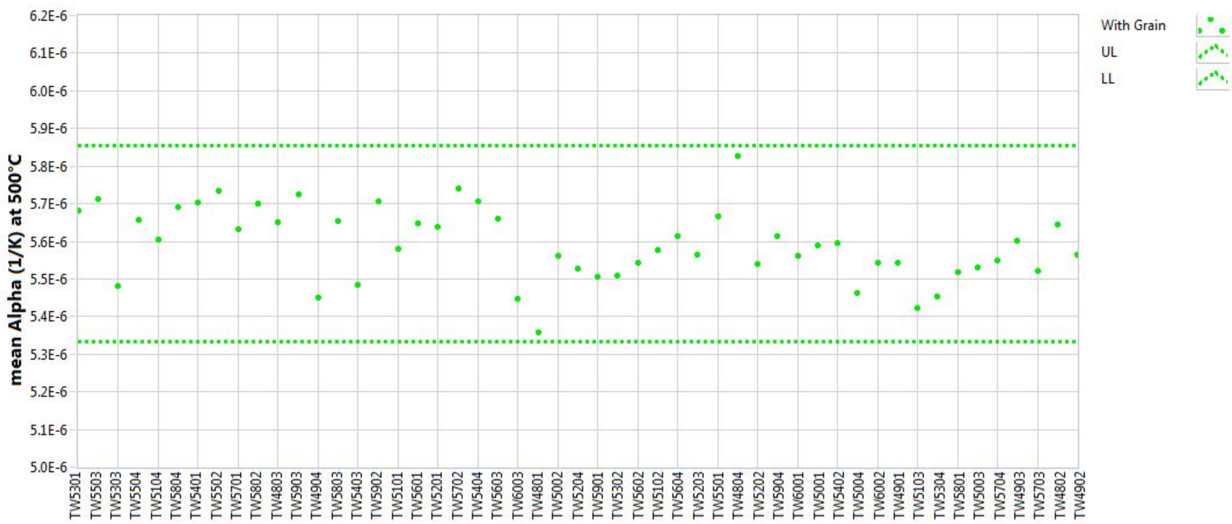

Figure A-26. 2114 creep coefficient of thermal expansion at 500°C.

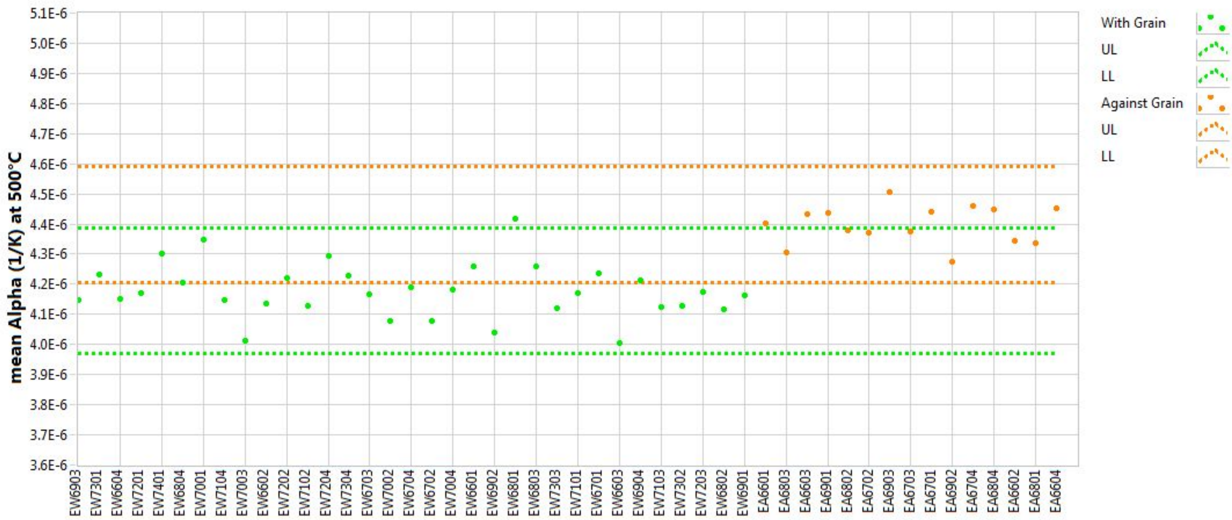

Figure A-27. IG-110 creep coefficient of thermal expansion at 500°C.

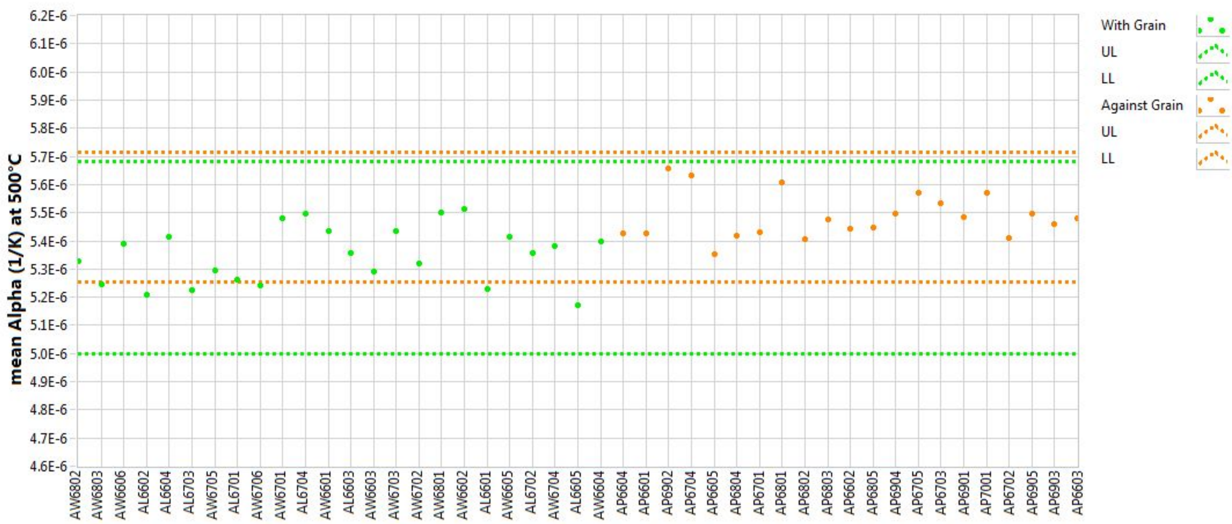

Figure A-28. NBG-17 creep coefficient of thermal expansion at 500°C.

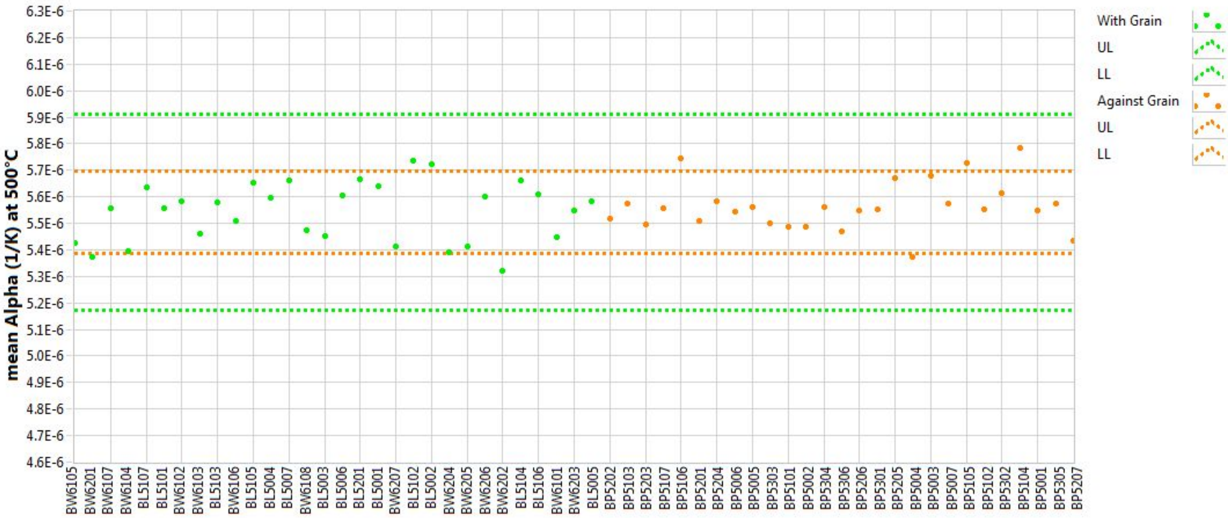

Figure A-29. NBG-18 creep coefficient of thermal expansion at 500°C.

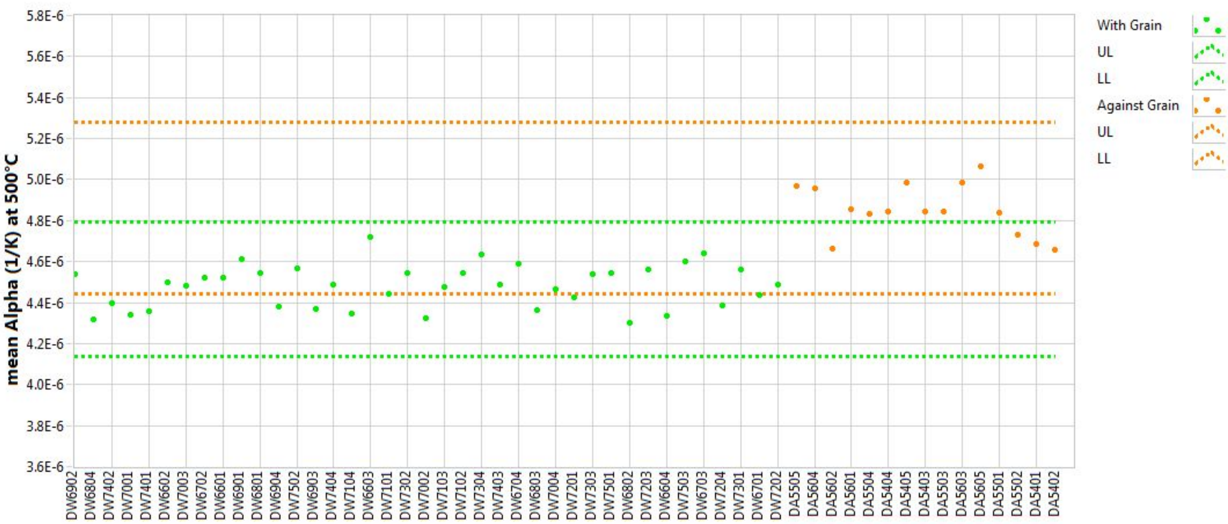

Figure A-30. PCEA creep coefficient of thermal expansion at 500°C.

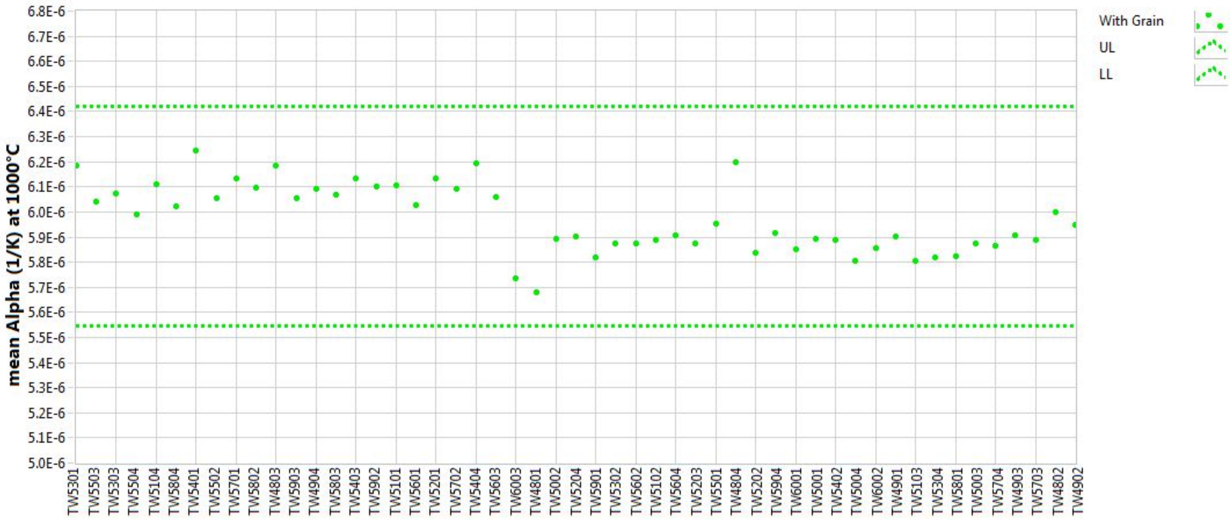

Figure A-31. 2114 creep coefficient of thermal expansion at 1000°C.

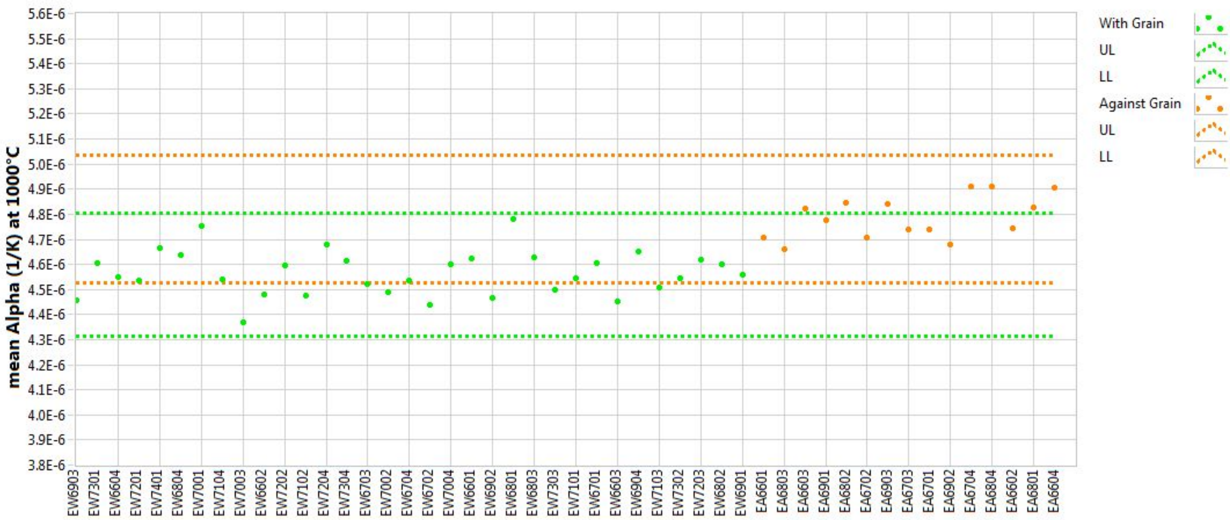

Figure A-32. IG-110 creep coefficient of thermal expansion at 1000°C.

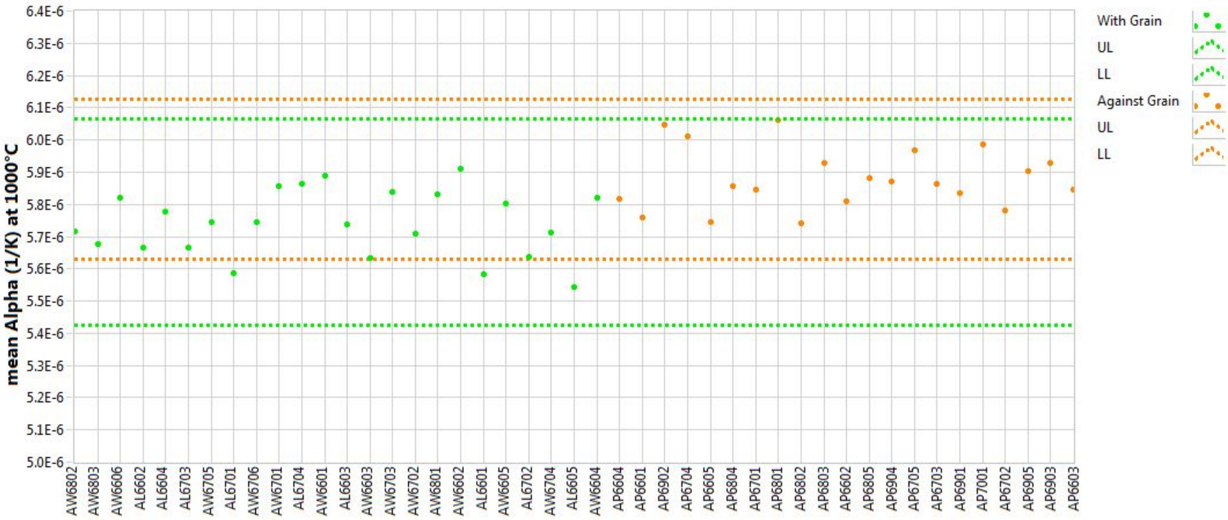

Figure A-33. NBG-17 Creep Coefficient of Thermal Expansion at 1000°C.

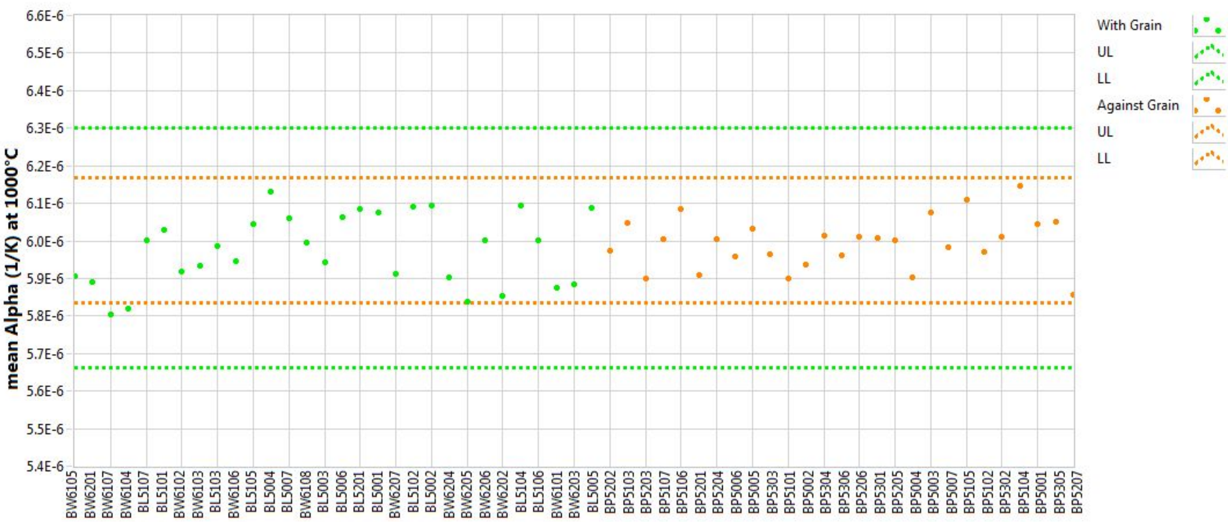

Figure A-34. NBG-18 creep coefficient of thermal expansion at 1000°C.

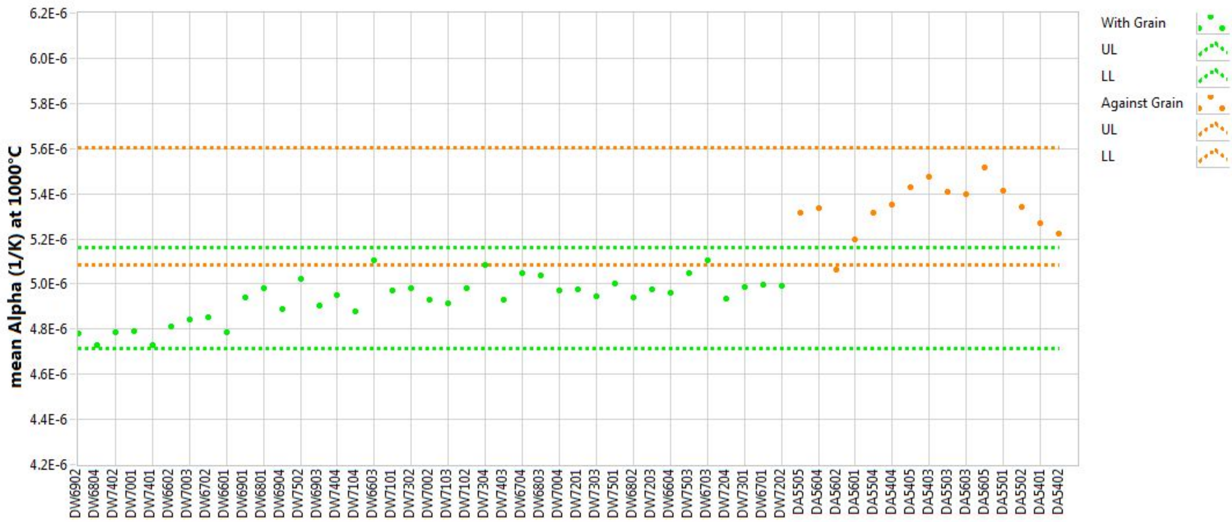

Figure A-35. PCEA creep coefficient of thermal expansion at 1000°C.

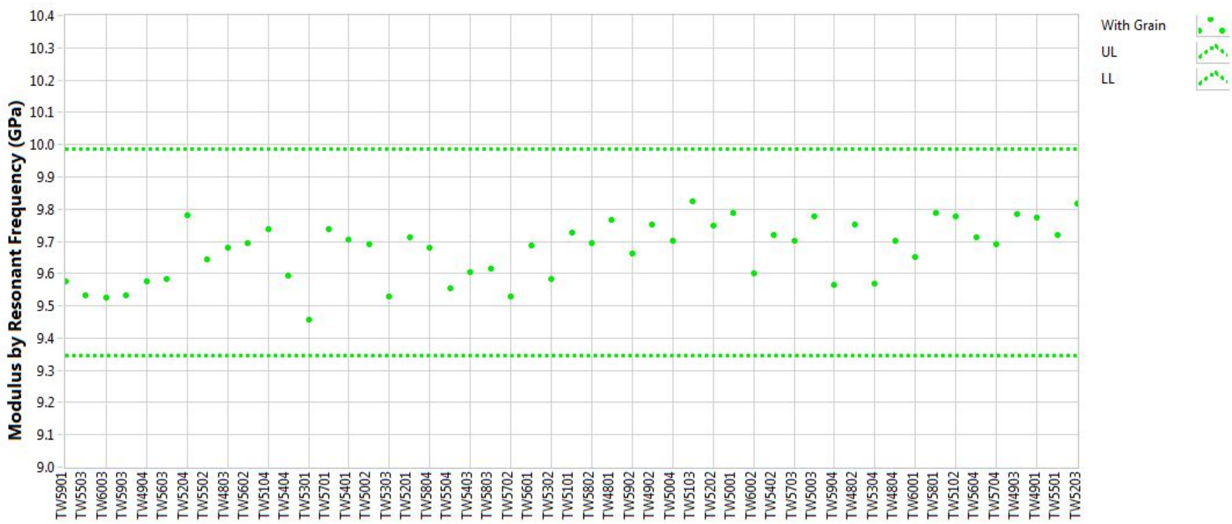

Figure A-36. 2114 creep modulus by resonant frequency.

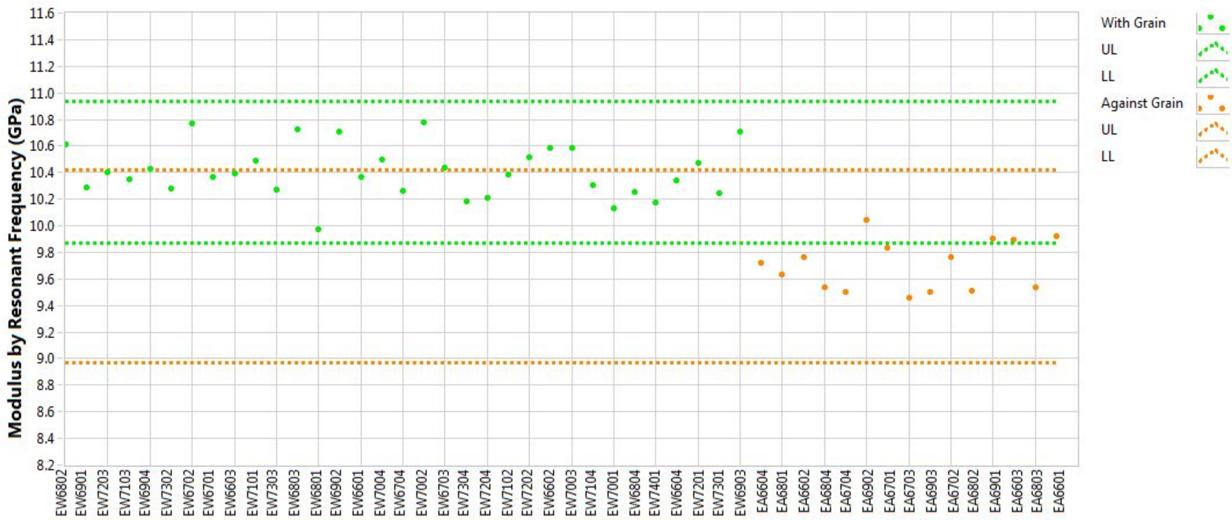

Figure A-37. IG-110 creep modulus by resonant frequency.

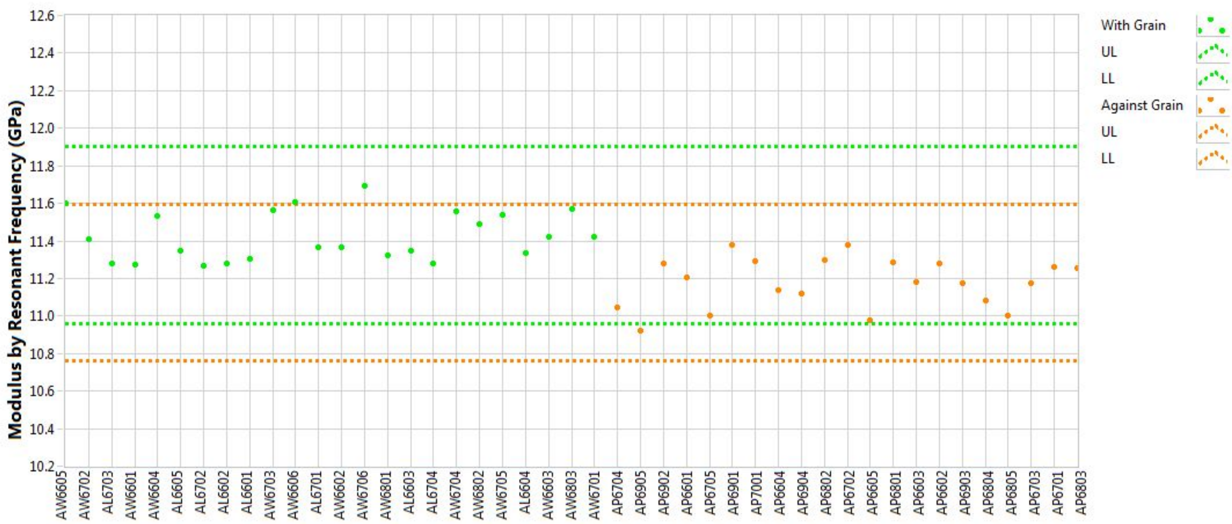

Figure A-38. NBG-17 creep modulus by resonant frequency.

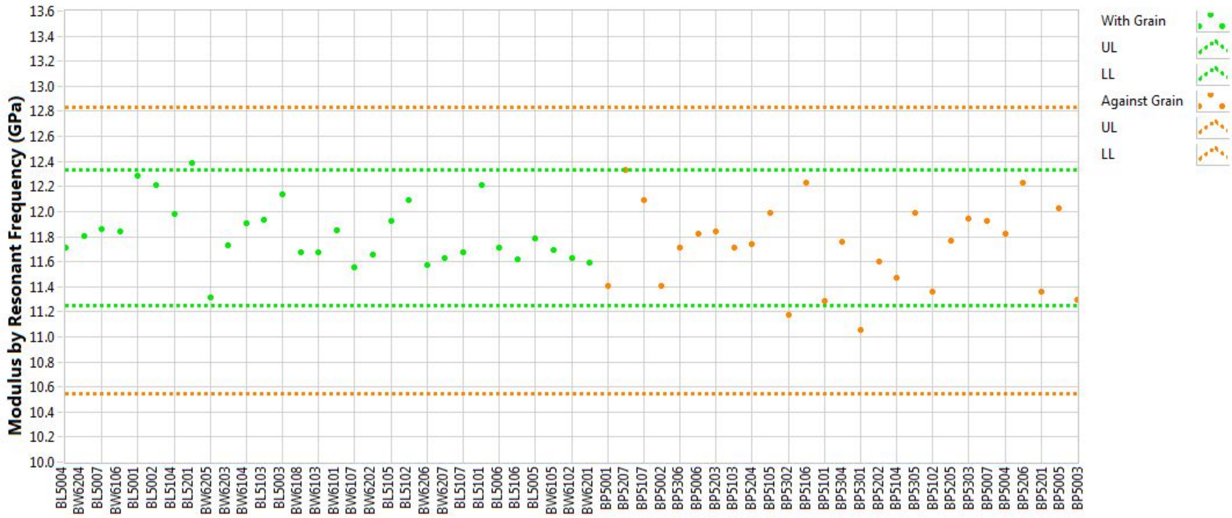

Figure A-39. NBG-18 creep modulus by resonant frequency.

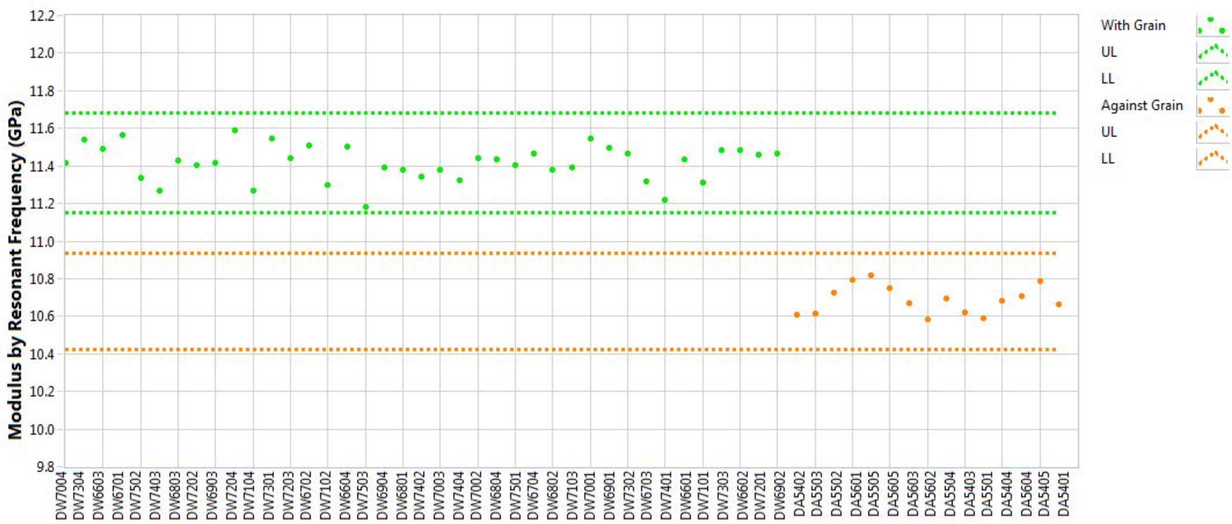

Figure A-40. PCEA creep modulus by resonant frequency.

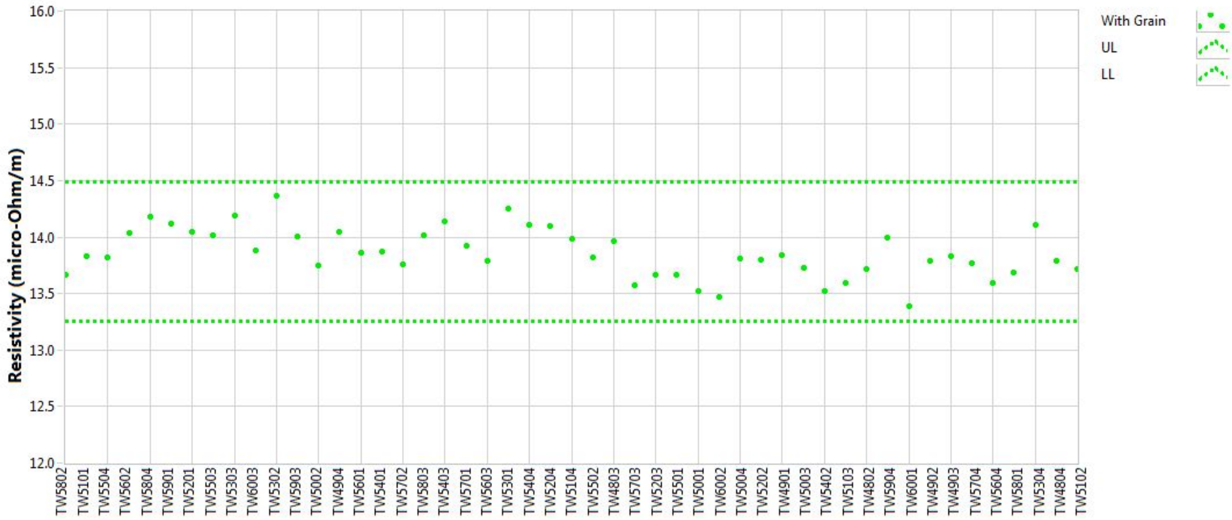

Figure A-41. 2114 creep resistivity.

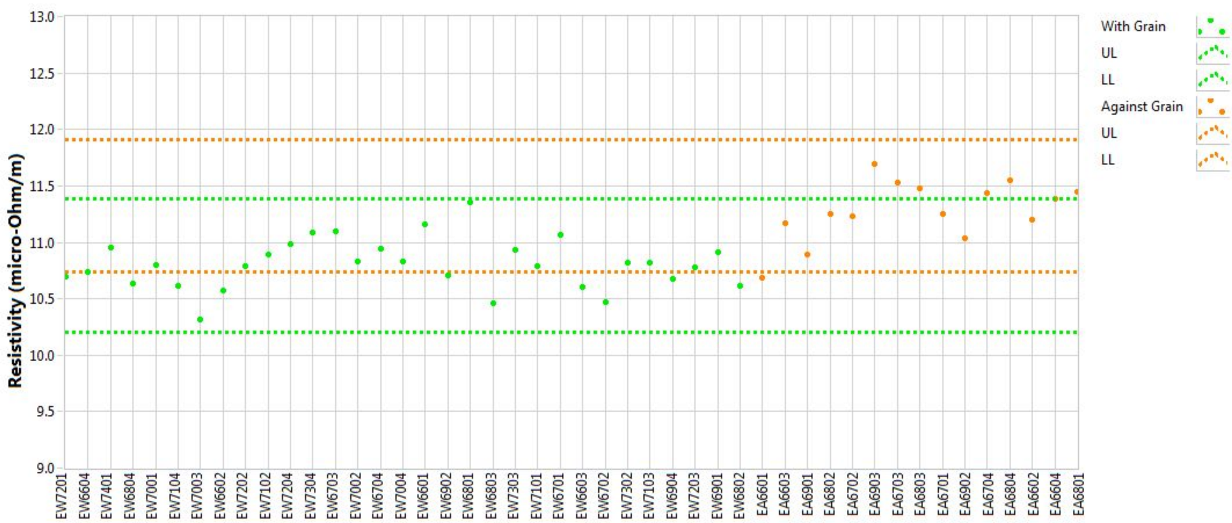

Figure A-42. IG-110 creep resistivity.

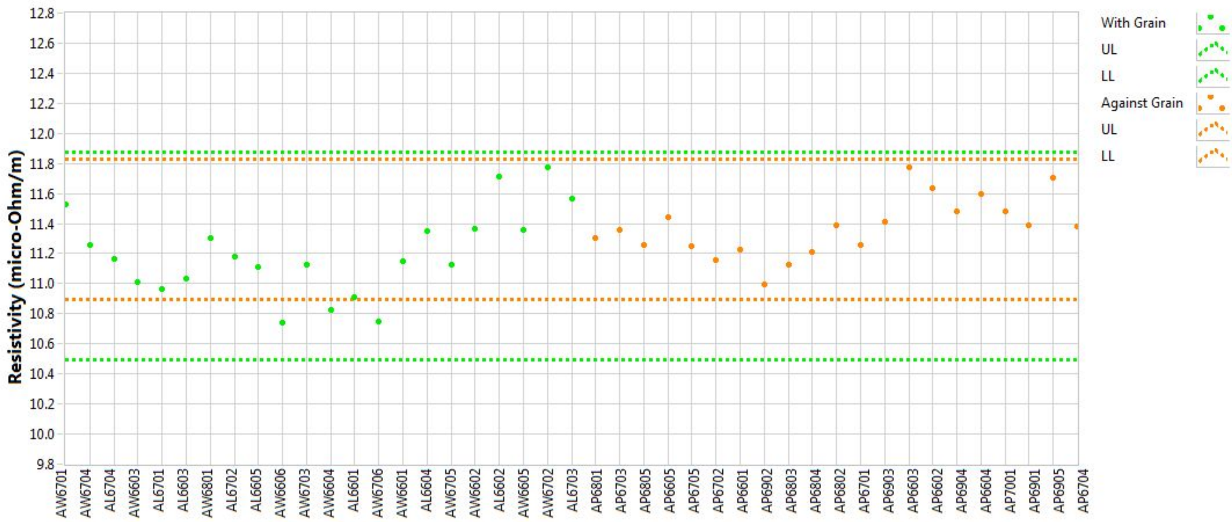

Figure A-43. NBG-17 creep resistivity.

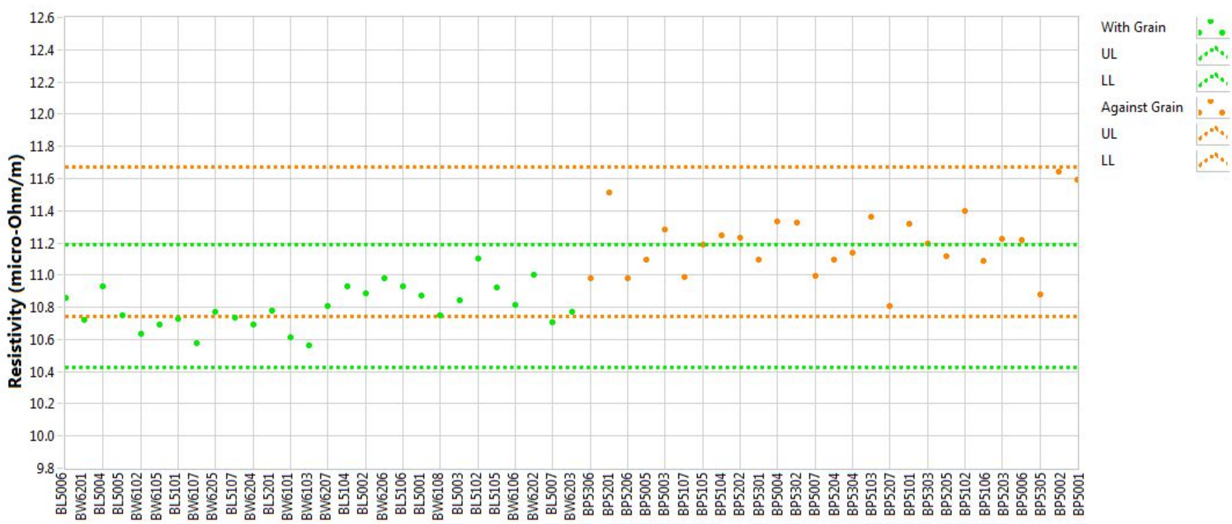

Figure A-44. NBG-18 creep resistivity.

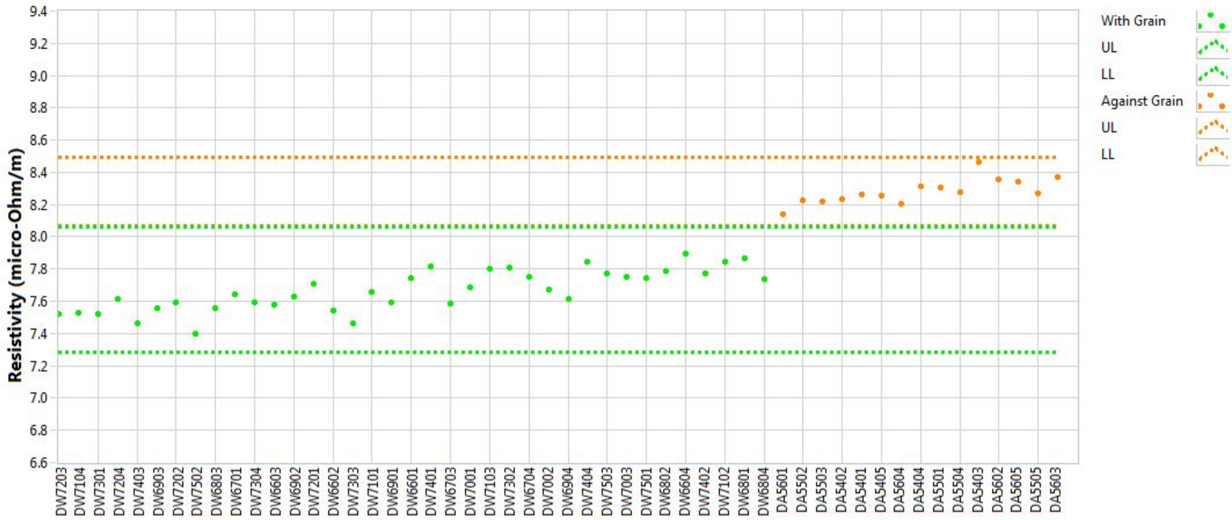

Figure A-45. PCEA creep resistivity.

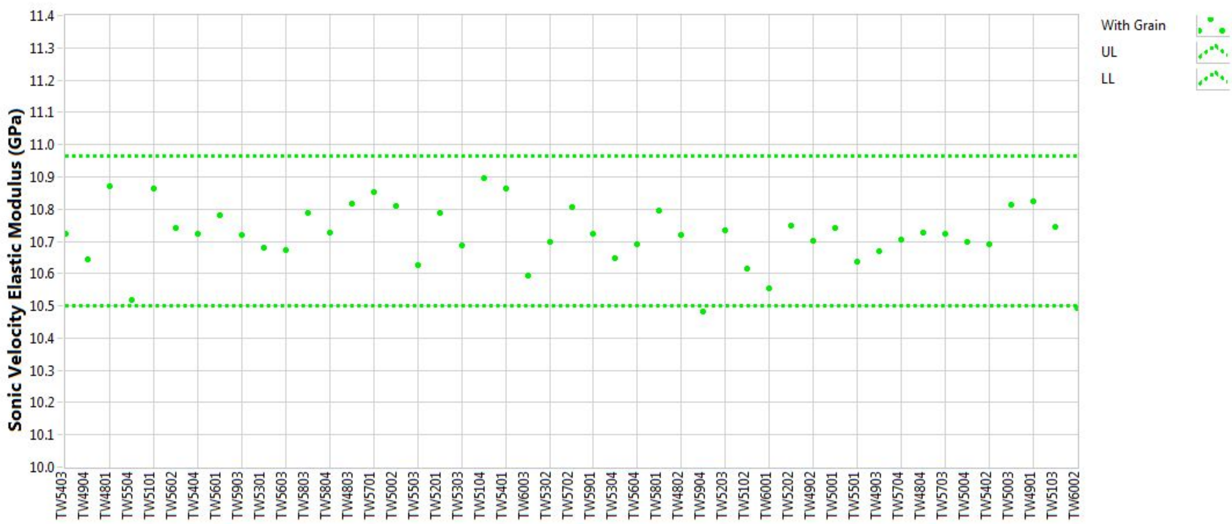

Figure A-46. 2114 creep modulus by sonic velocity.

Figure A-47. IG-110 creep modulus by sonic velocity.

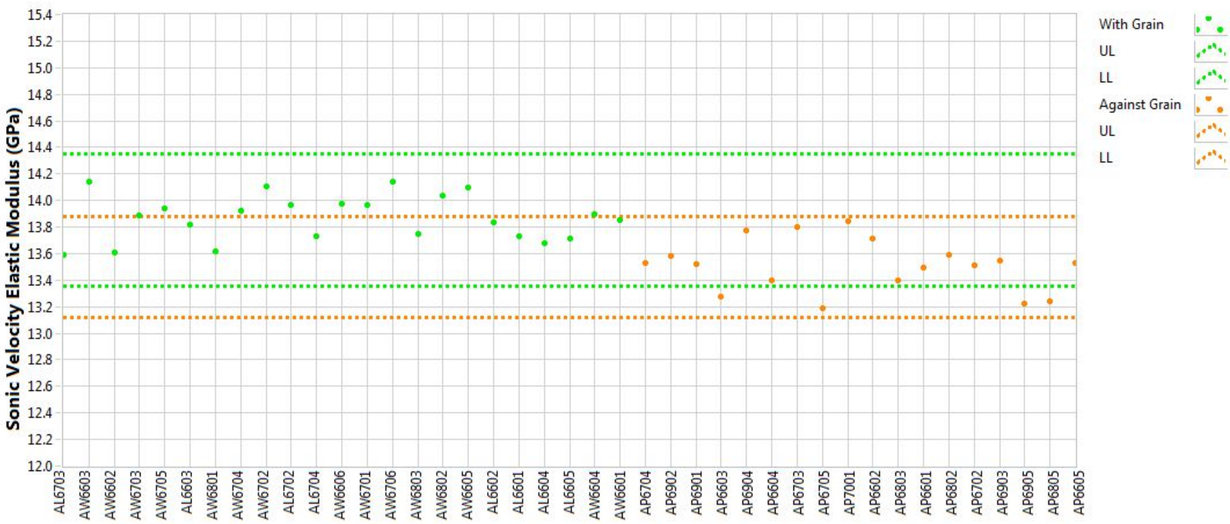

Figure A-48. NBG-17 creep modulus by sonic velocity.

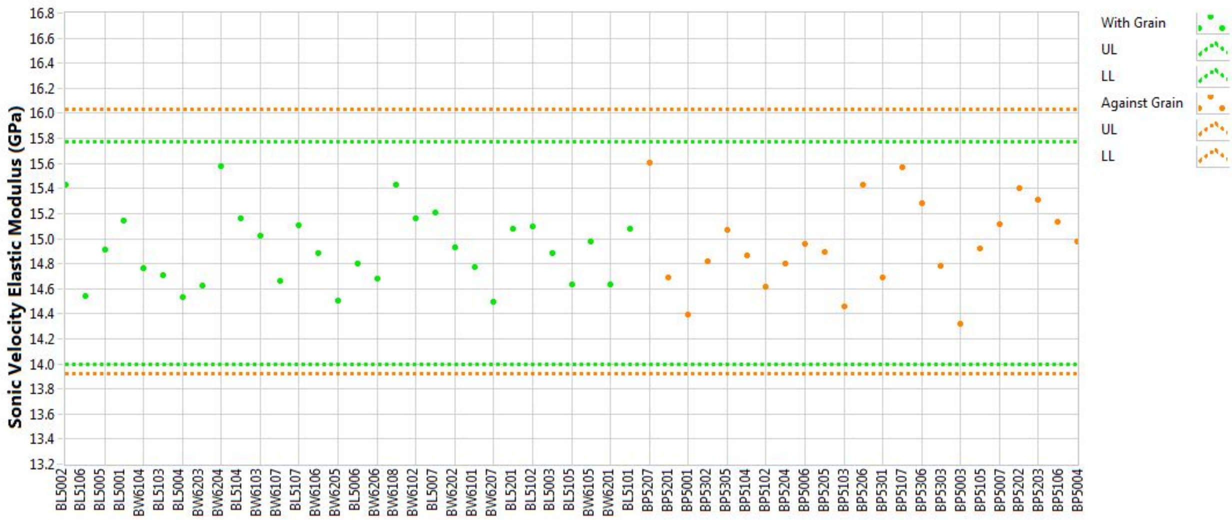

Figure A-49. NBG-18 creep modulus by sonic velocity.

Figure A-50. PCEA creep modulus by sonic velocity.

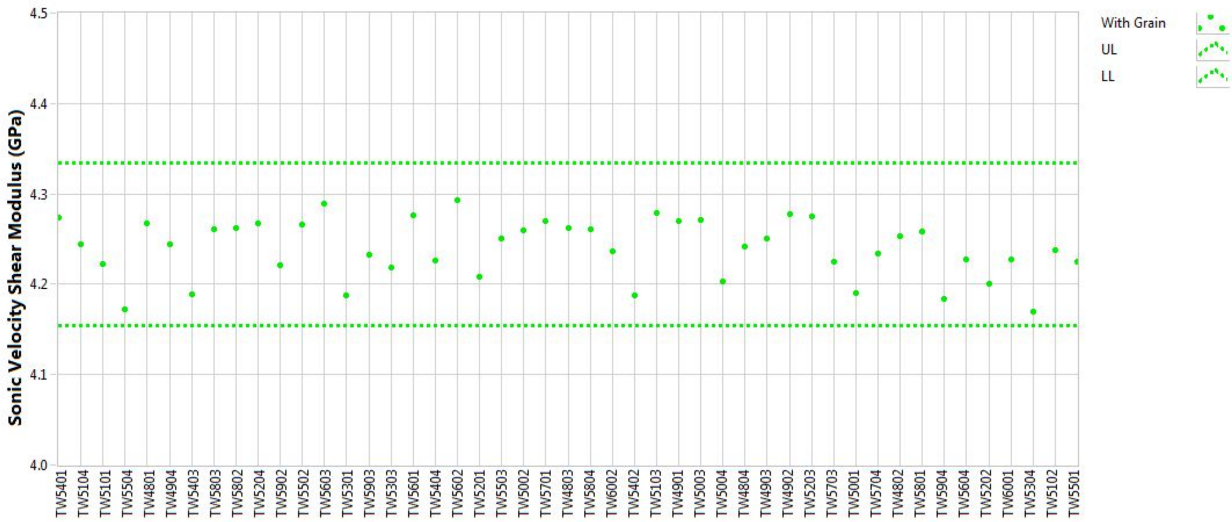

Figure A-51. 2114 creep shear modulus by sonic velocity.

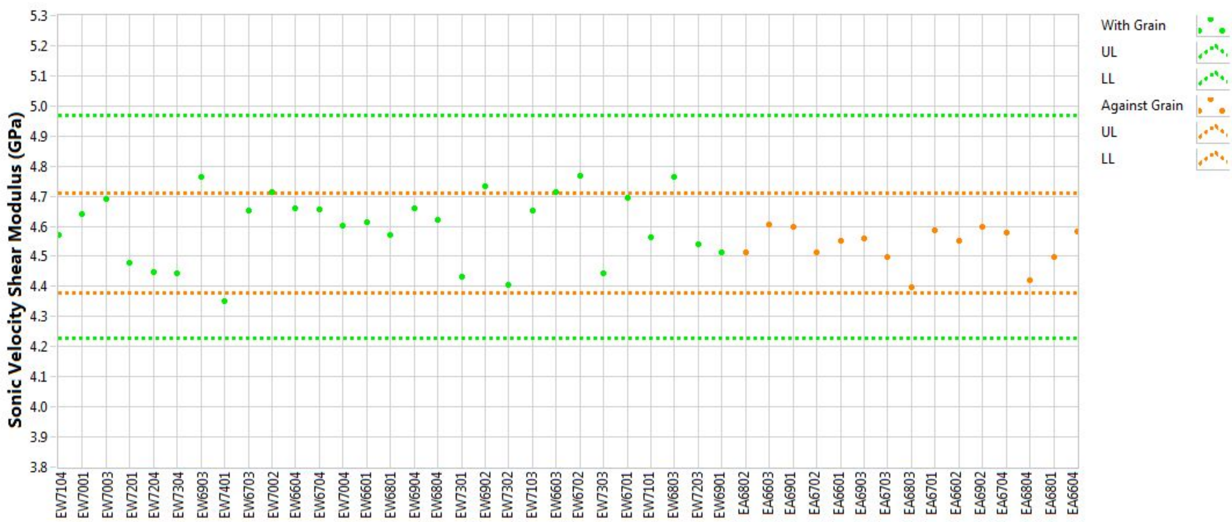

Figure A-52. IG-110 creep shear modulus by sonic velocity.

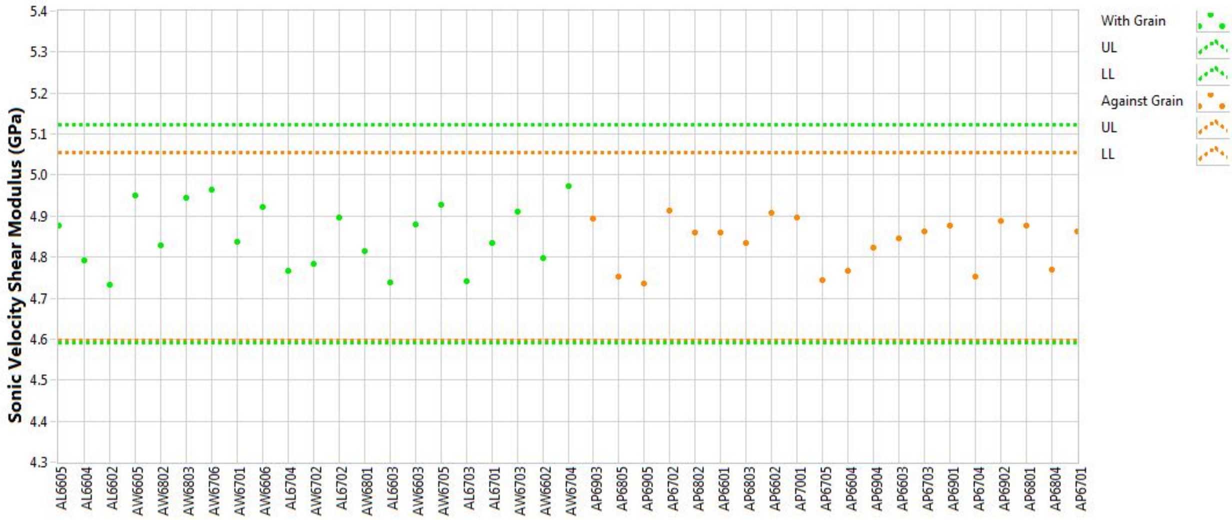

Figure A-53. NBG-17 creep shear modulus by sonic velocity.

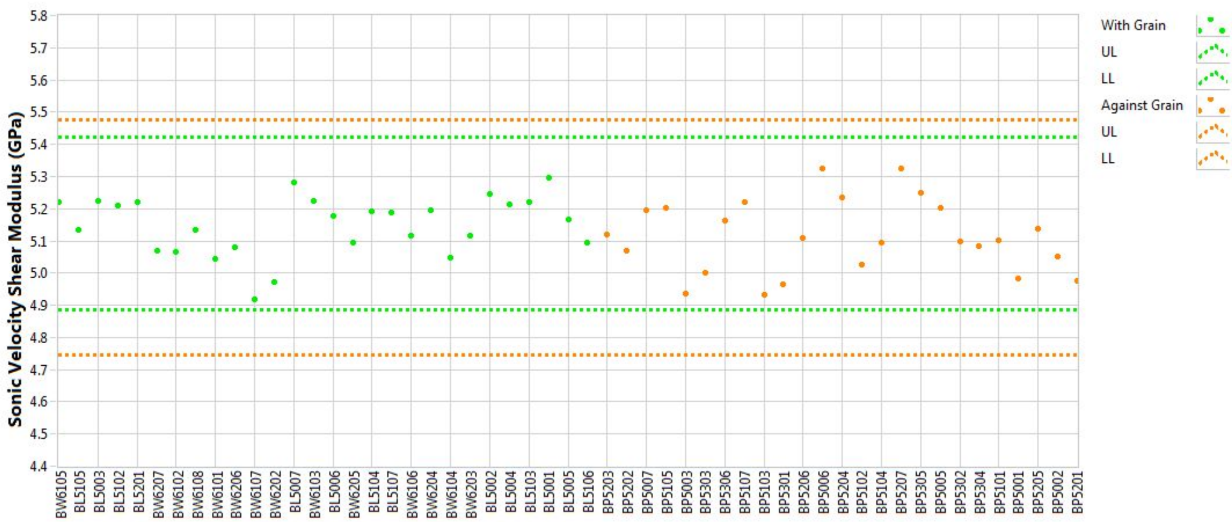

Figure A-54. NBG-18 creep shear modulus by sonic velocity.

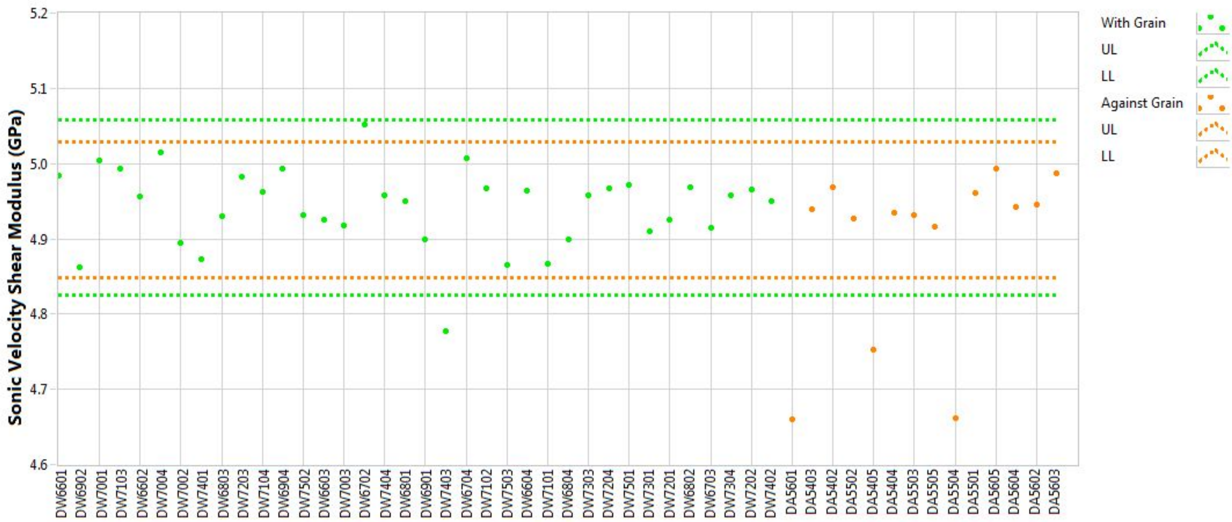

Figure A-55. PCEA creep shear modulus by sonic velocity.

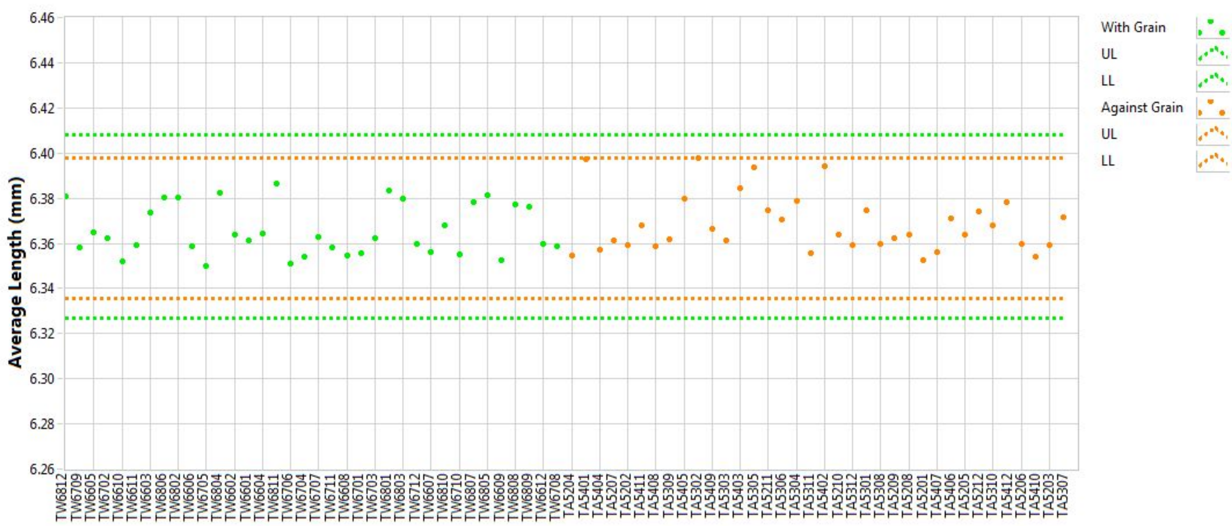

Figure A-56. 2114 piggyback length.

Figure A-57. IG-110 piggyback length.

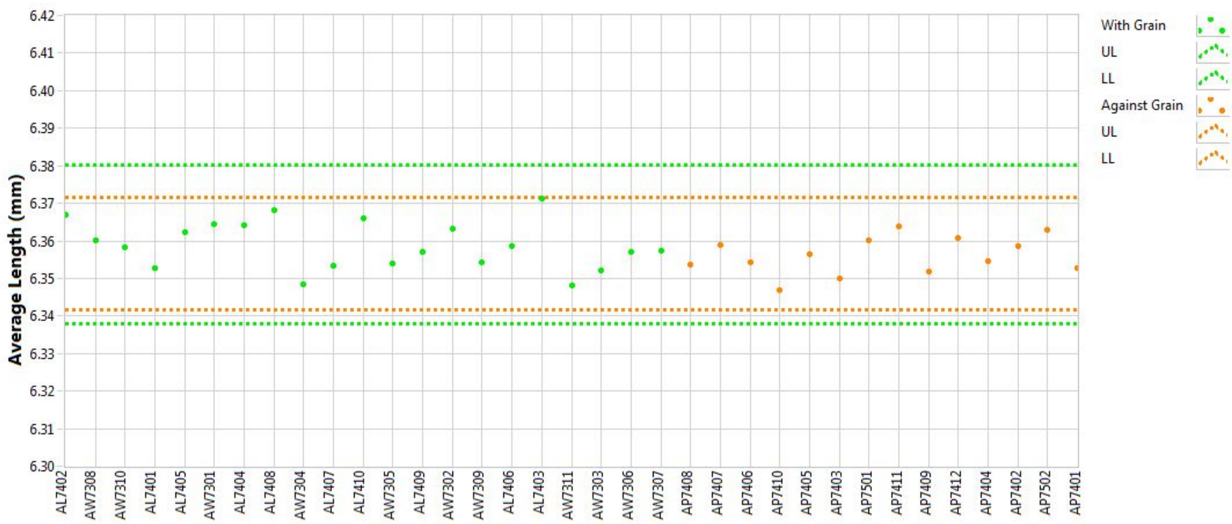

Figure A-58. NBG-17 piggyback length.

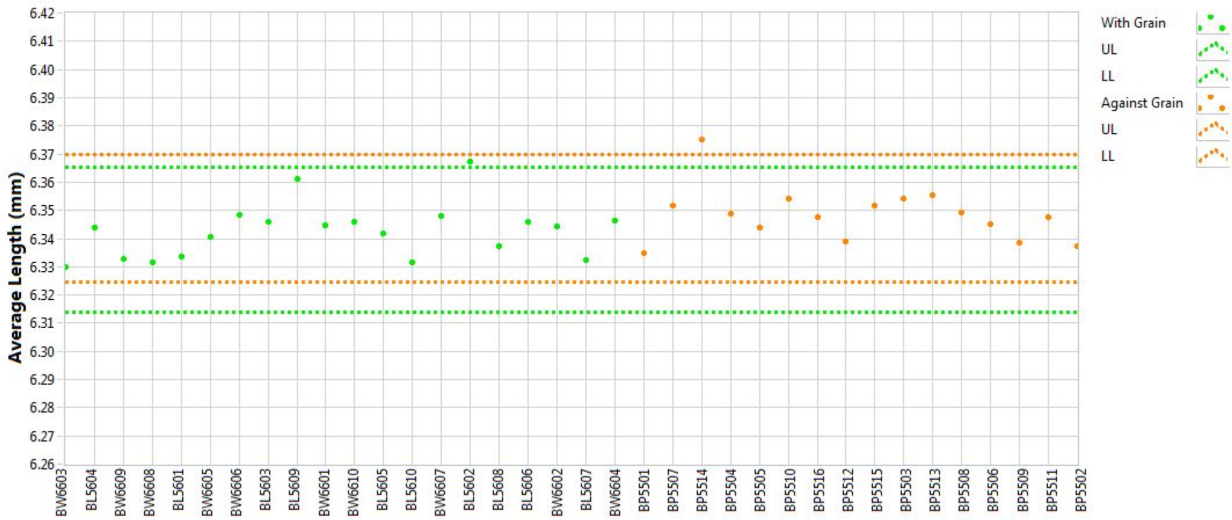

Figure A-59. NBG-18 piggyback length.

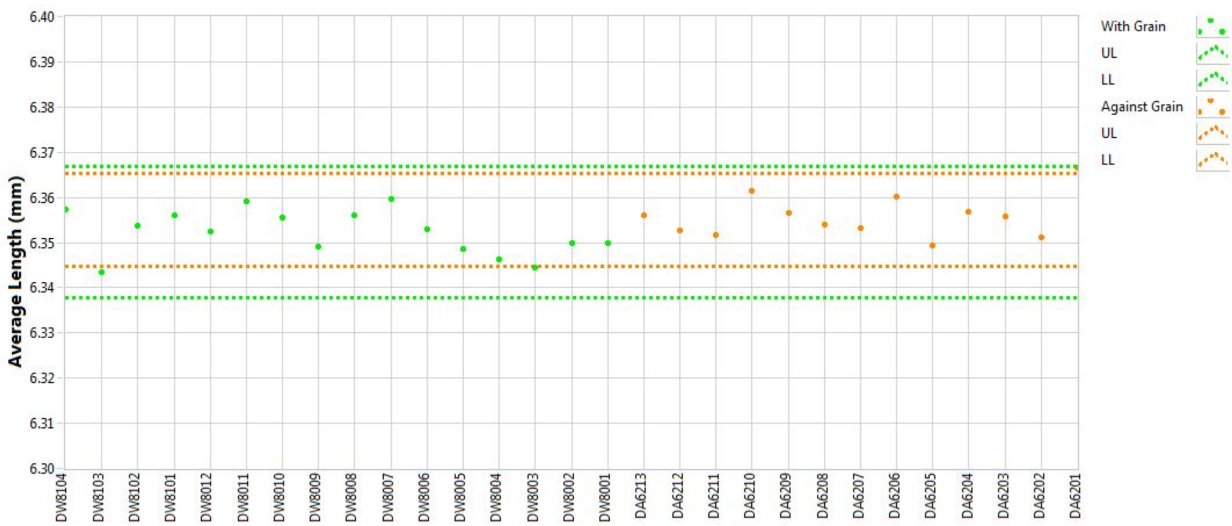

Figure A-60. PCEA piggyback length.

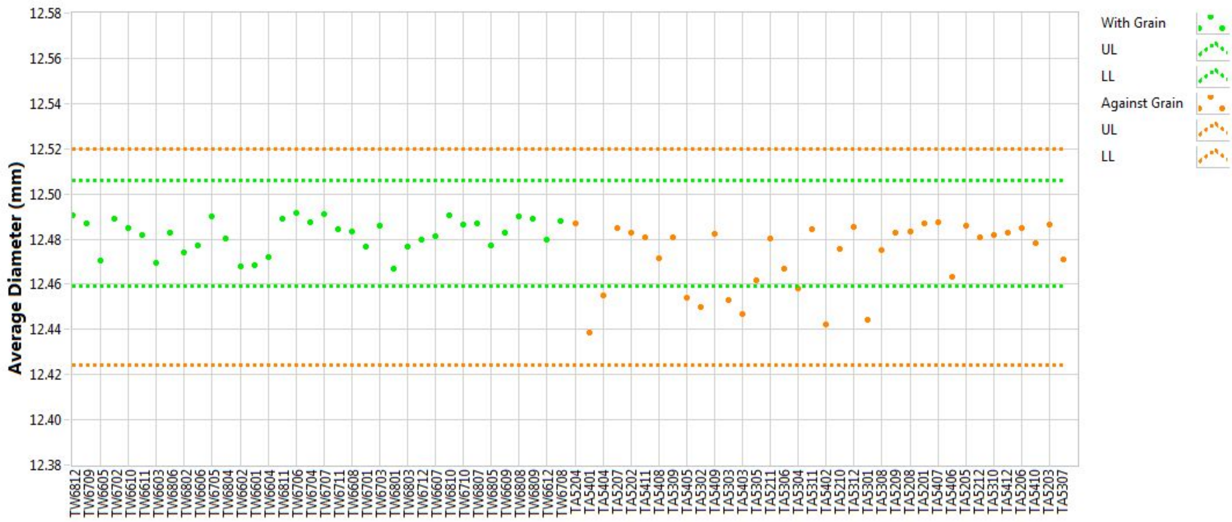

Figure A-61. 2114 piggyback diameter.

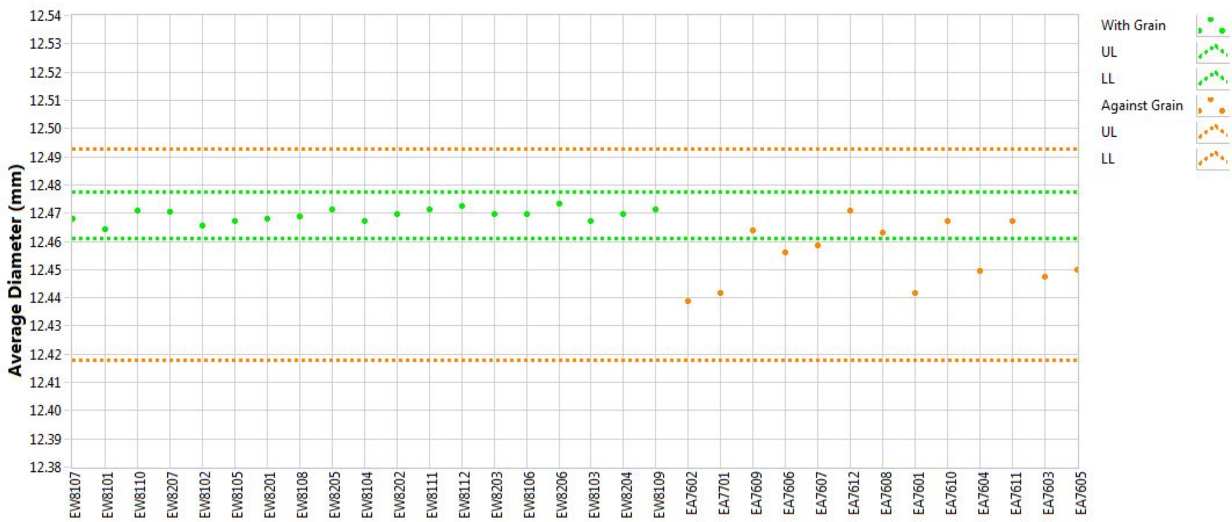

Figure A-62. IG-110 piggyback diameter.

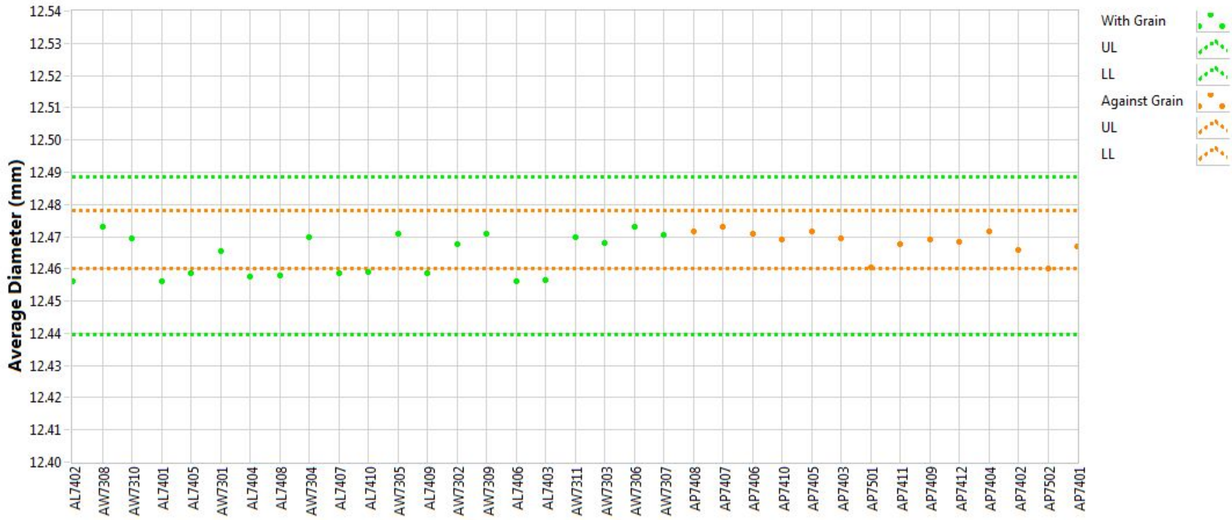

Figure A-63. NBG-17 piggyback diameter.

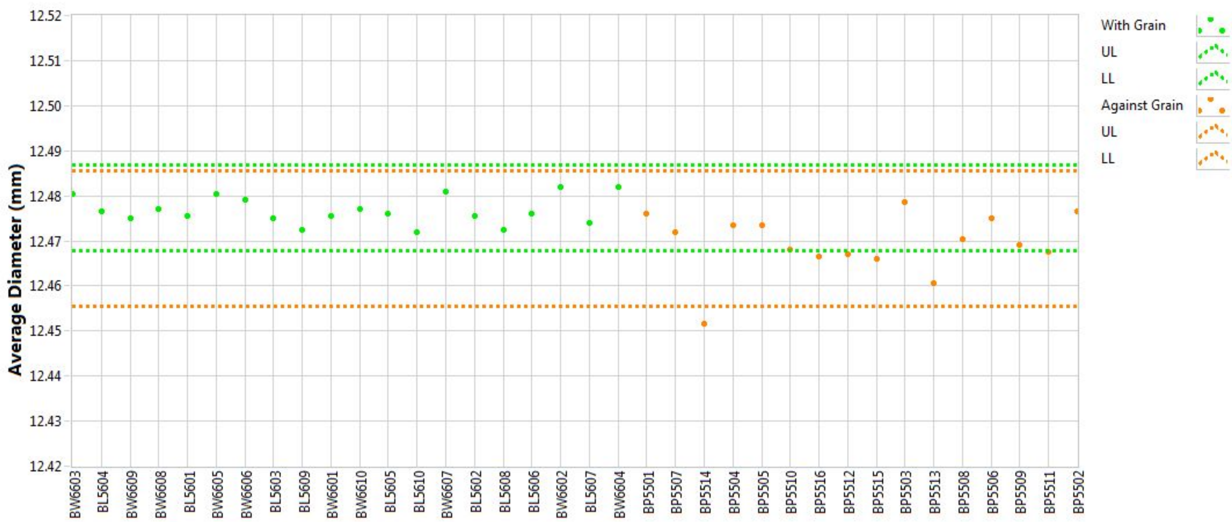

Figure A-64. NBG-18 piggyback diameter.

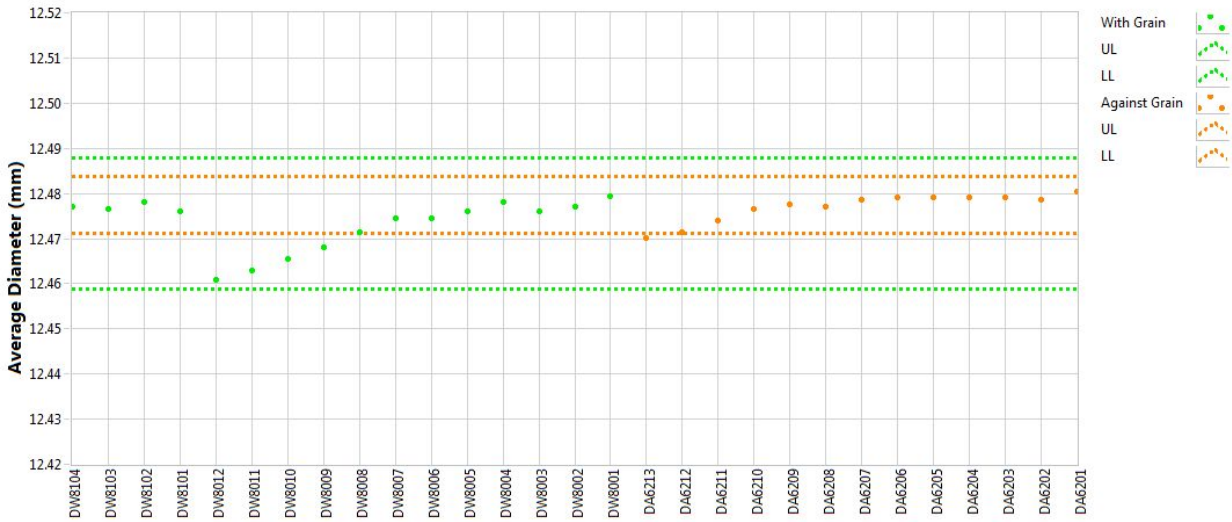

Figure A-65. PCEA piggyback diameter.

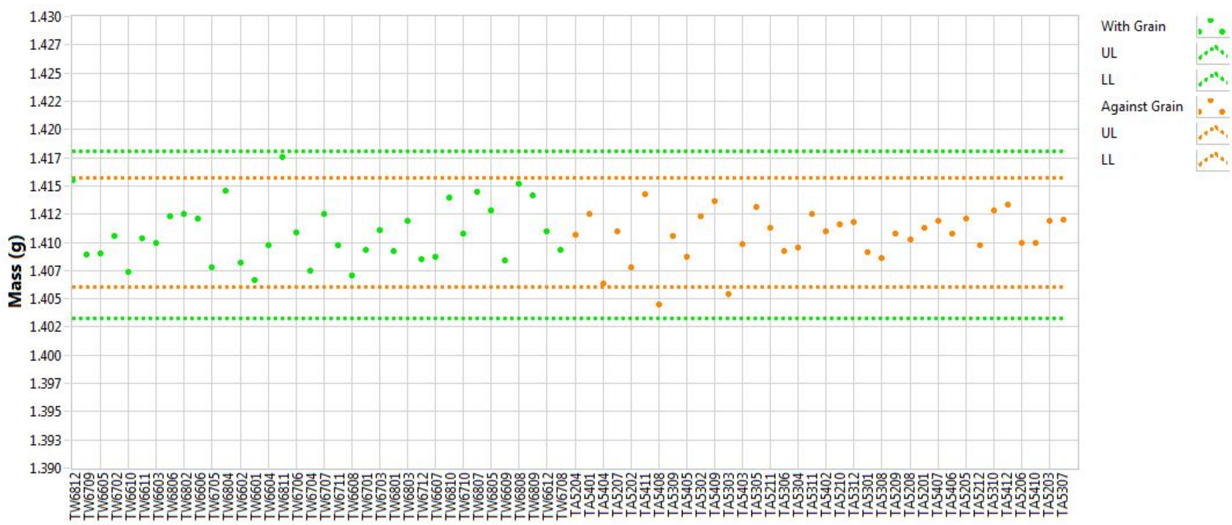

Figure A-66. 2114 piggyback mass.

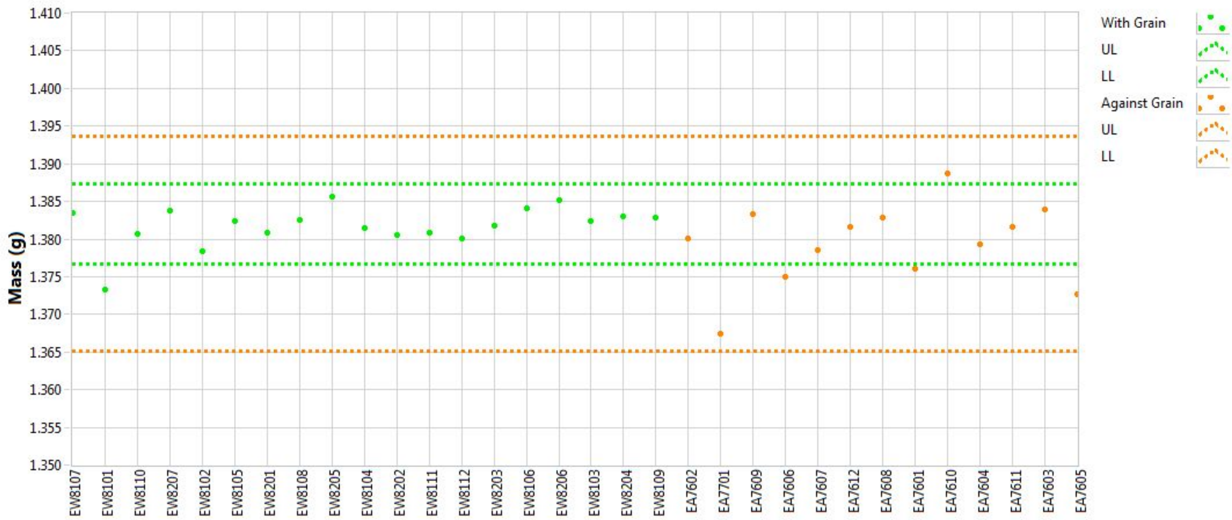

Figure A-67. IG-110 piggyback mass.

Figure A-68. NBG-17 piggyback mass.

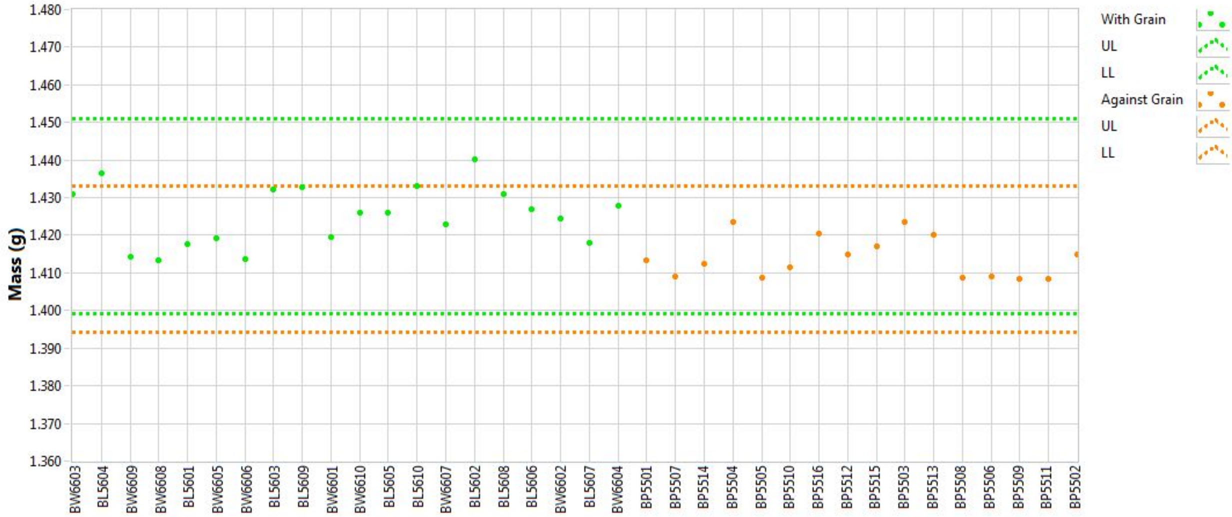

Figure A-69. NBG-18 piggyback mass.

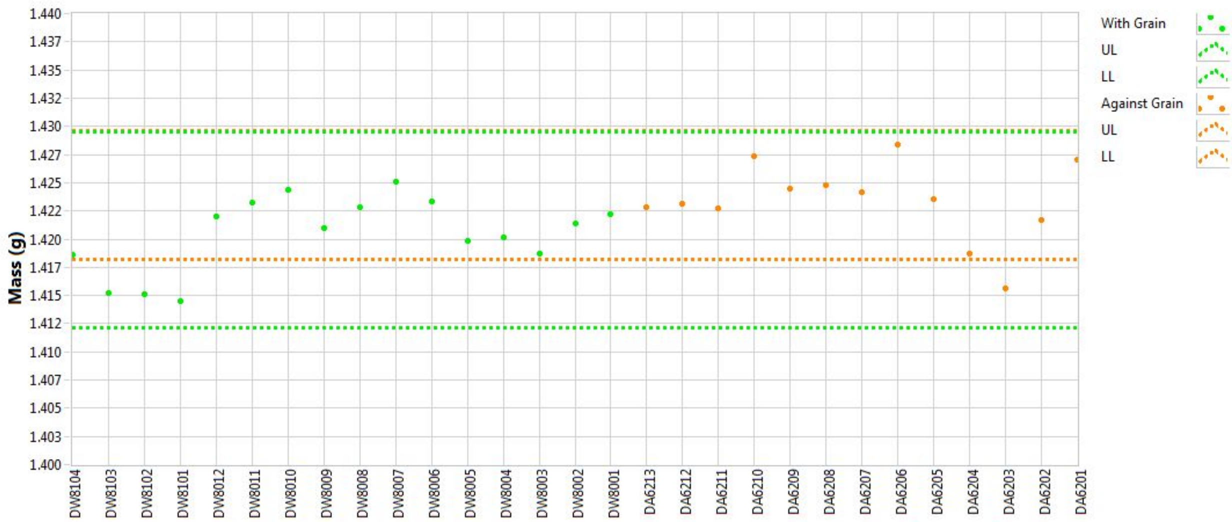

Figure A-70. PCEA piggyback mass.

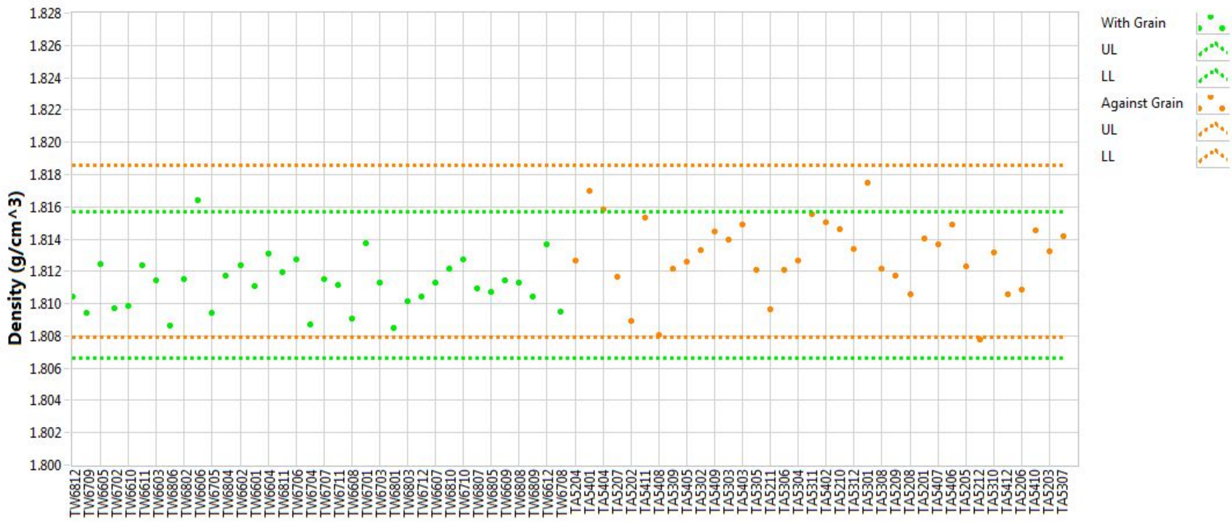

Figure A-71. 2114 piggyback density.

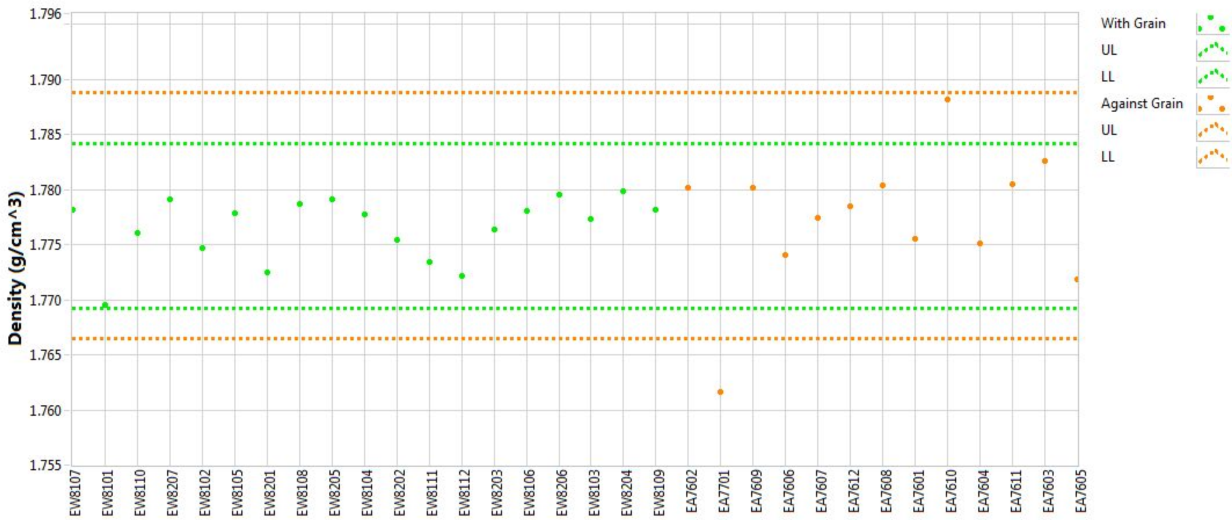

Figure A-72. IG-110 piggyback density.

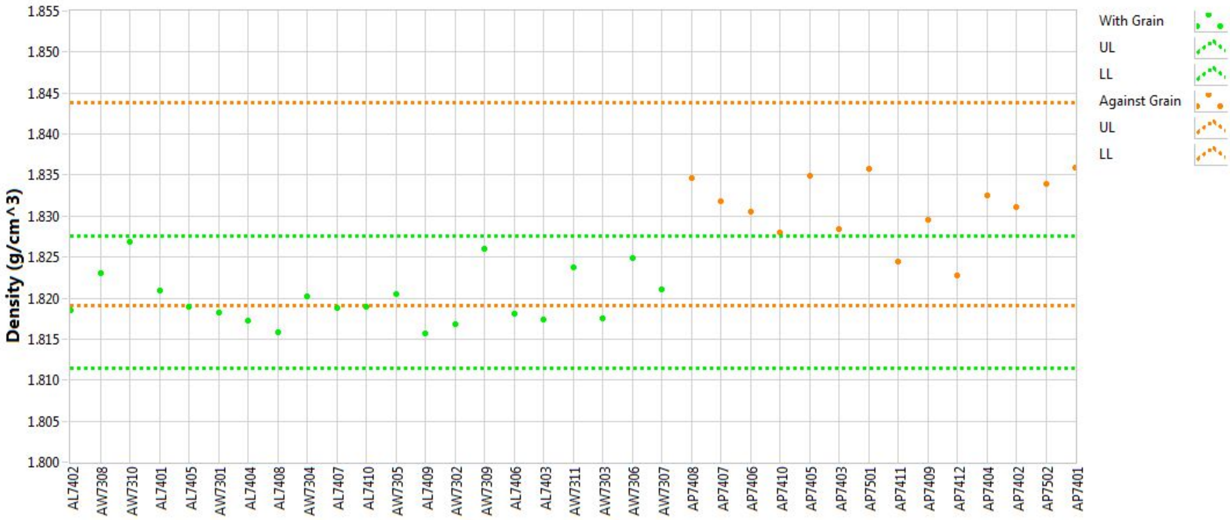

Figure A-73. NBG-17 piggyback density.

Figure A-74. NBG-18 piggyback density.

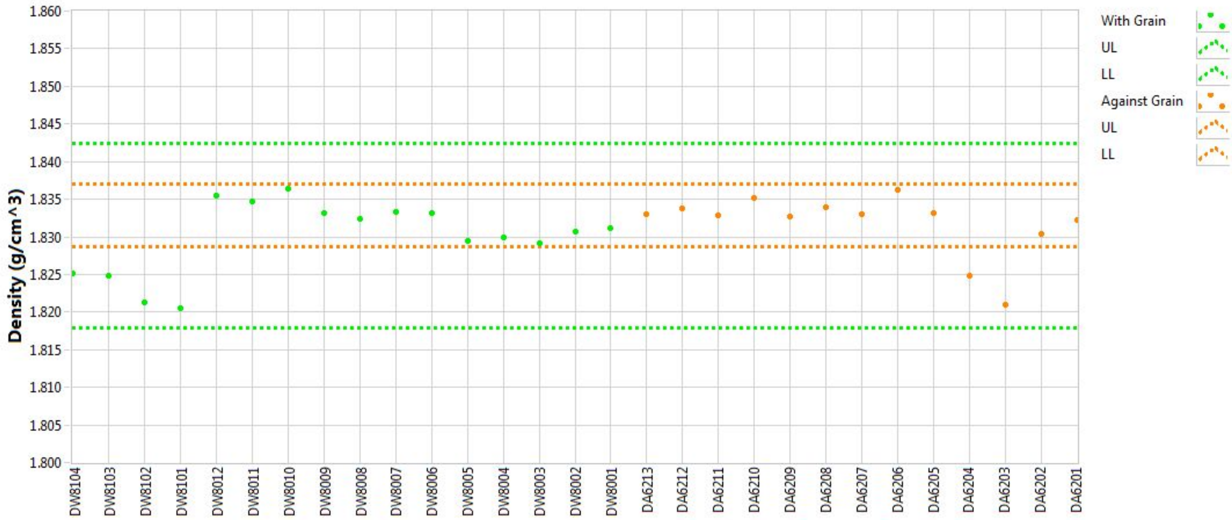

Figure A-75. PCEA piggyback density.

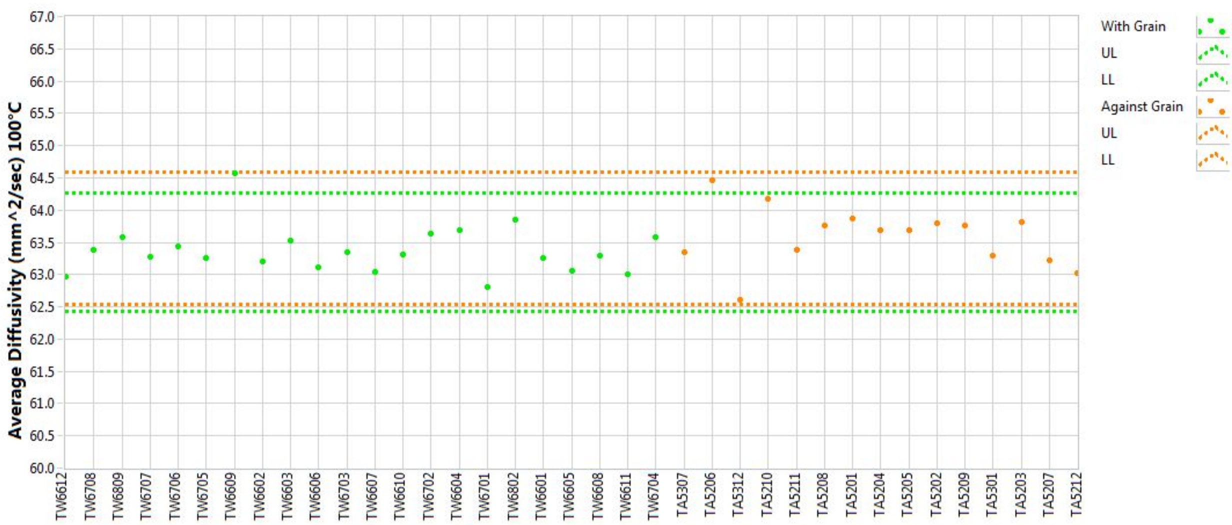

Figure A-76. 2114 piggyback diffusivity at 100°C.

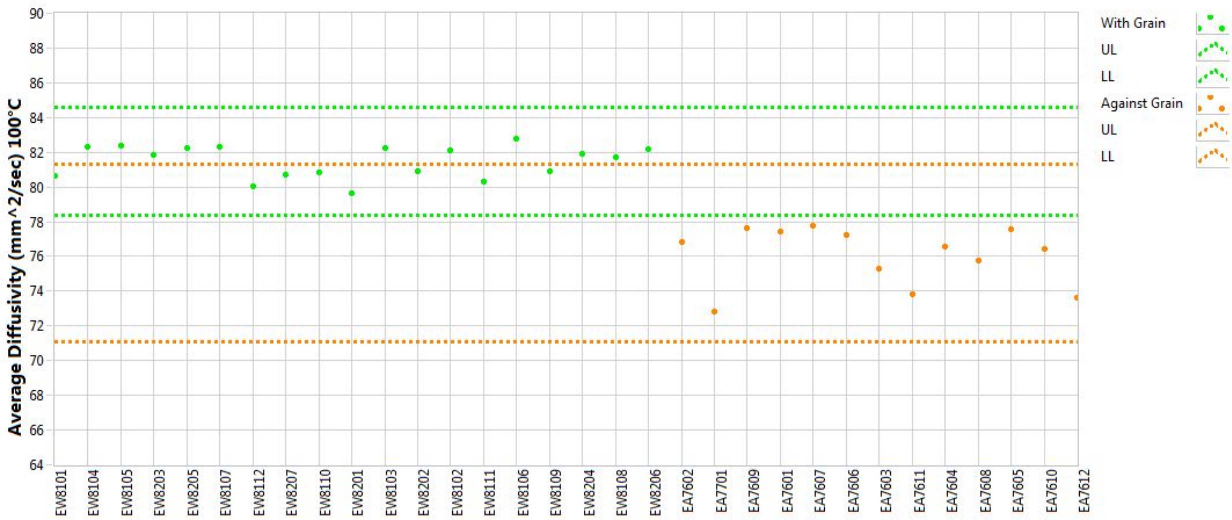

Figure A-77. IG-110 piggyback diffusivity at 100°C.

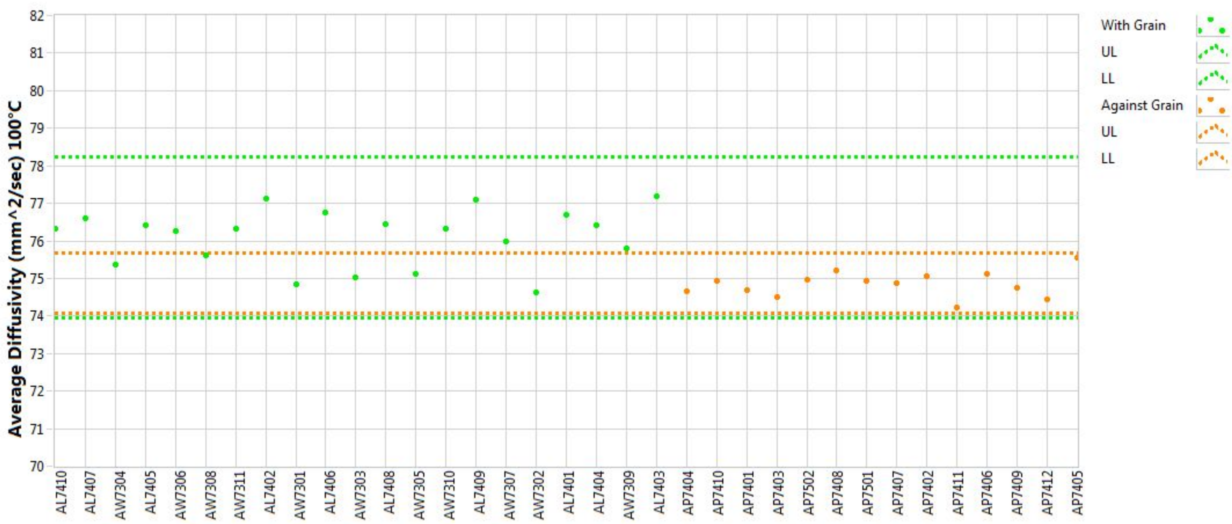

Figure A-78. NBG-17 piggyback diffusivity at 100°C.

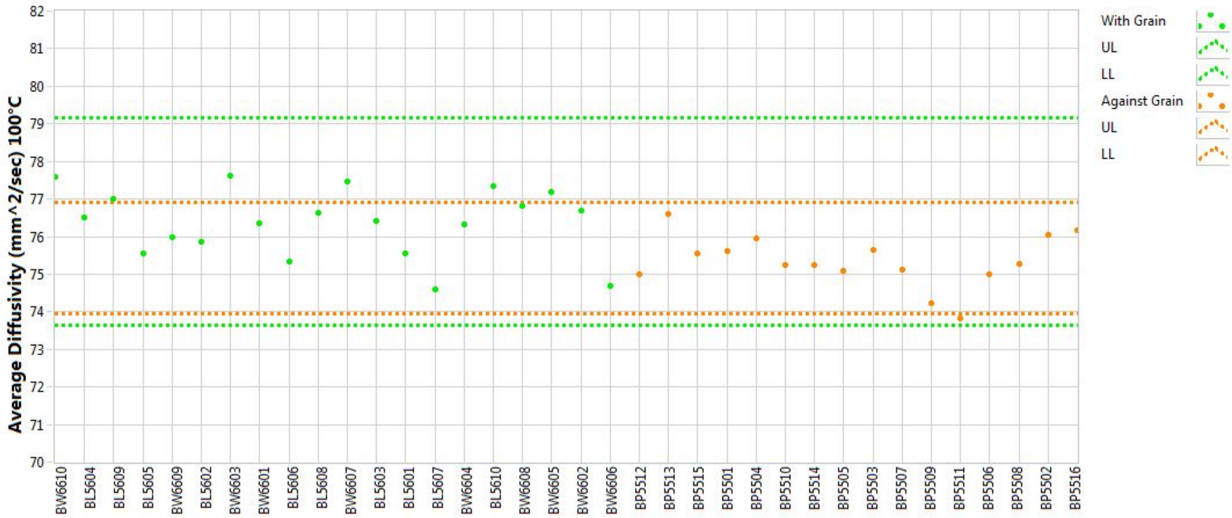

Figure A-79. NBG-18 piggyback diffusivity at 100°C.

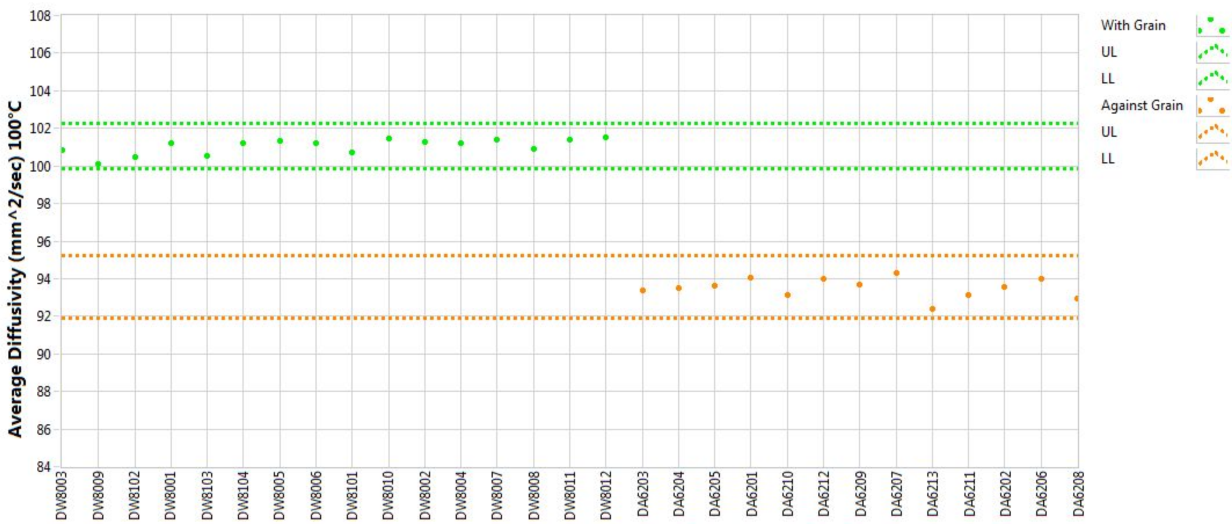

Figure A-80. PCEA piggyback diffusivity at 100°C.

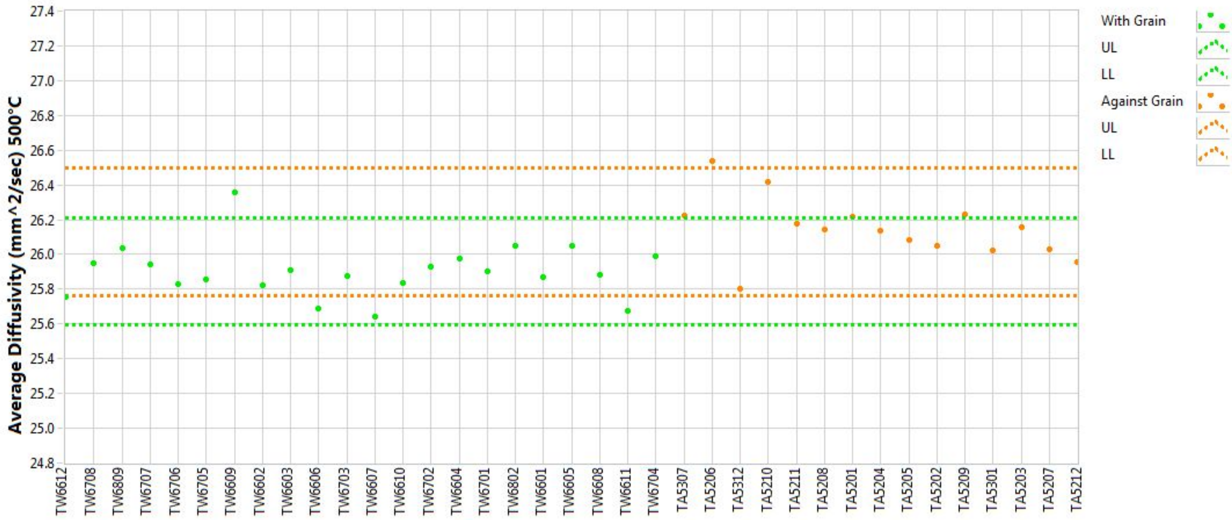

Figure A-81. 2114 piggyback diffusivity at 500°C.

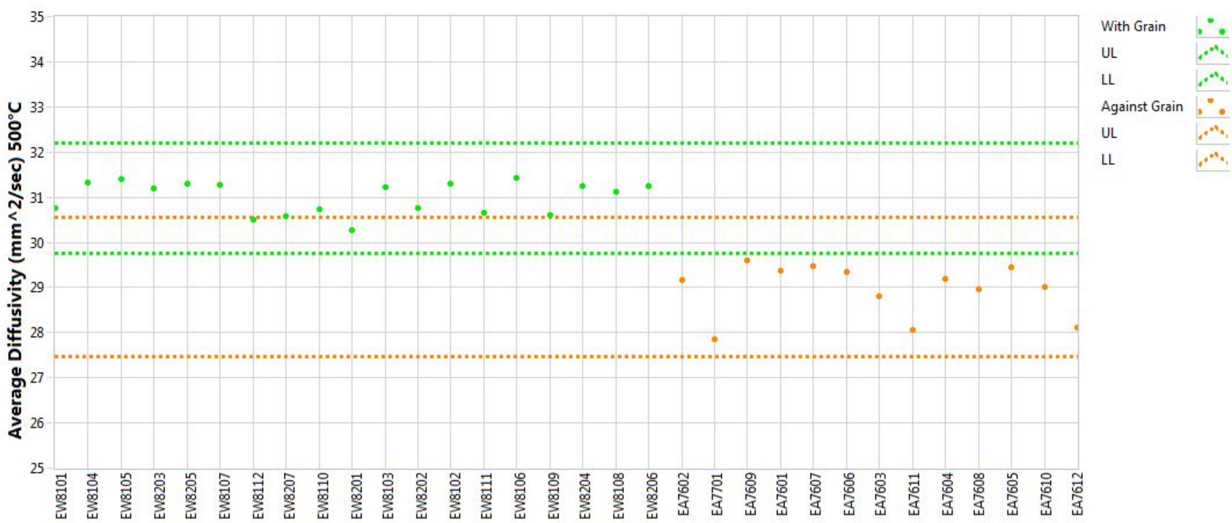

Figure A-82. IG-110 piggyback diffusivity at 500°C.

Figure A-83. NBG-17 piggyback diffusivity at 500°C.

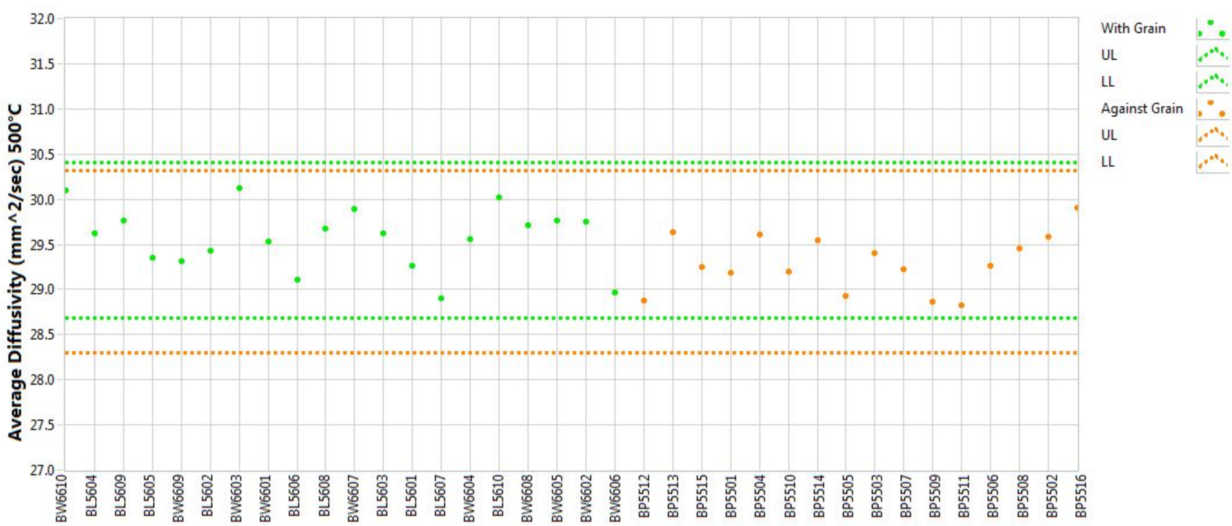

Figure A-84. NBG-18 piggyback diffusivity at 500°C.

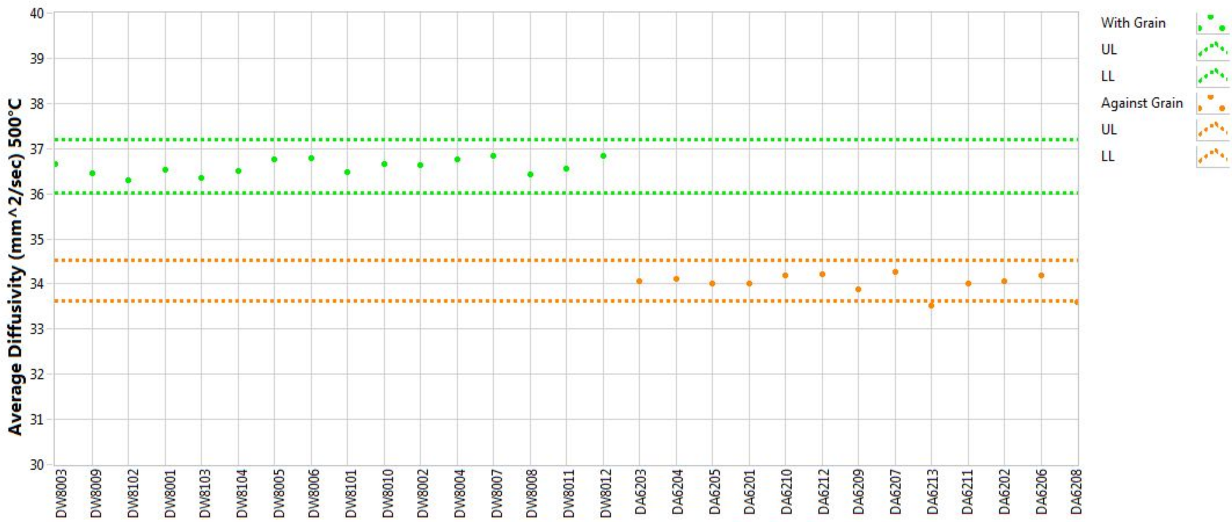

Figure A-85. PCEA piggyback diffusivity at 500°C.

Figure A-86. 2114 piggyback diffusivity at 1000°C.

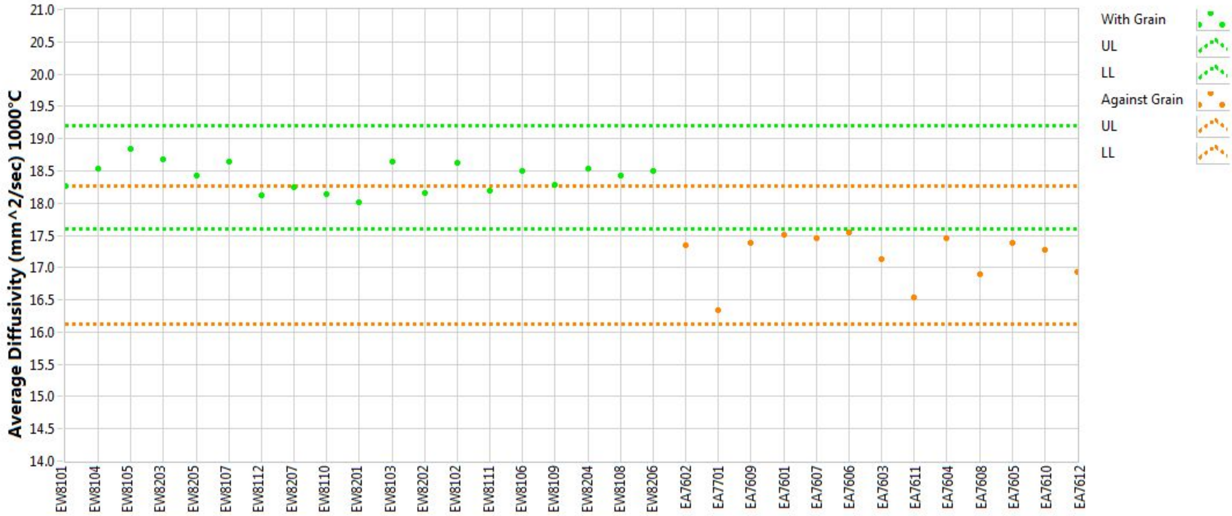

Figure A-87. IG-110 piggyback diffusivity at 1000°C.

Figure A-88. NBG-17 piggyback diffusivity at 1000°C.

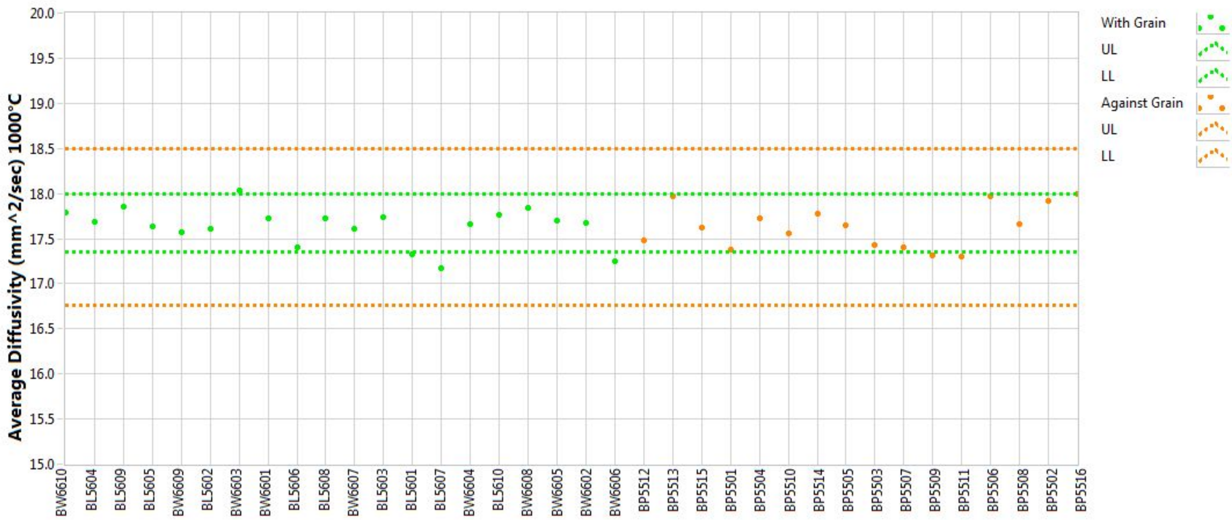

Figure A-89. NBG-18 piggyback diffusivity at 1000°C.

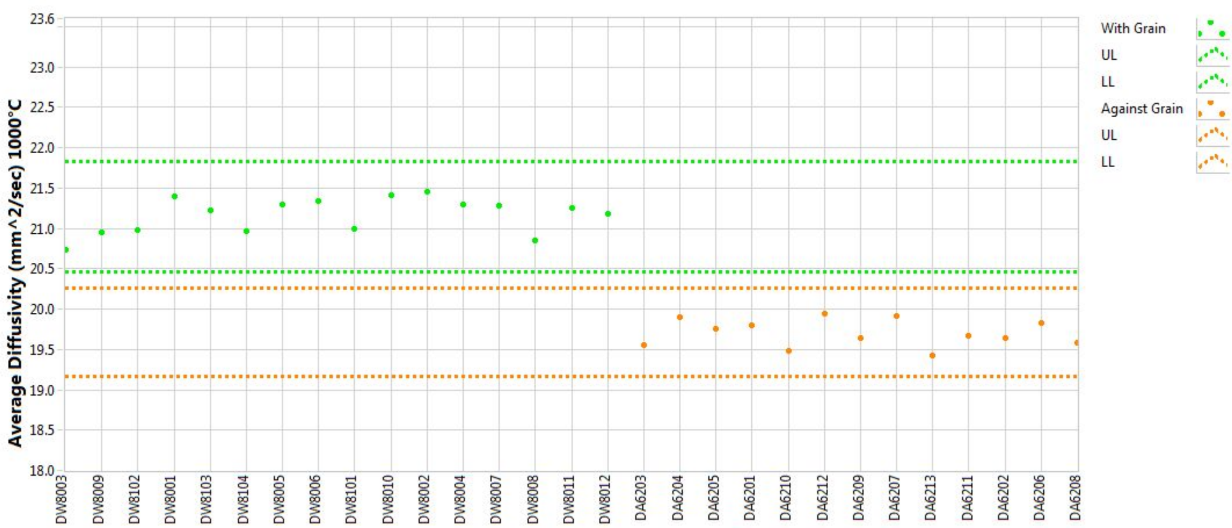

Figure A-90. PCEA piggyback diffusivity at 1000°C.

Appendix B

Statistical Tables

Appendix B

Statistical Tables

Table B-1. Creep specimen length (mm) summary statistics.

Combined Specimens	Mean	Standard Deviation	Coefficient of Variation (%)	Median	Upper Limit	Lower Limit
2114	25.412	0.015	0.06	25.413	25.445	25.381
IG-110	25.419	0.012	0.05	25.419	25.448	25.389
NBG-17	25.415	0.014	0.06	25.416	25.450	25.379
NBG-18	25.415	0.011	0.04	25.417	25.438	25.391
PCEA	25.411	0.009	0.04	25.410	25.432	25.388

Against-Grain Specimens	Mean	Standard Deviation	Coefficient of Variation (%)	Median	Upper Limit	Lower Limit
2114	25.408	0.010	0.04	25.411	25.437	25.380
IG-110	25.420	0.017	0.07	25.418	25.467	25.371
NBG-17	25.418	0.015	0.06	25.422	25.456	25.375
NBG-18	25.418	0.010	0.04	25.417	25.436	25.395
PCEA	25.414	0.012	0.05	25.414	25.443	25.384

With-Grain Specimens	Mean	Standard Deviation	Coefficient of Variation (%)	Median	Upper Limit	Lower Limit
2114	25.412	0.016	0.06	25.414	25.445	25.382
IG-110	25.418	0.009	0.03	25.419	25.443	25.394
NBG-17	25.413	0.014	0.05	25.412	25.441	25.384
NBG-18	25.413	0.012	0.05	25.415	25.445	25.377
PCEA	25.410	0.007	0.03	25.409	25.429	25.389

Table B-2. Creep specimen diameter (mm) summary statistics.

Combined Specimens	Mean	Standard Deviation	Coefficient of Variation (%)	Median	Upper Limit	Lower Limit
2114	12.485	0.008	0.06	12.487	12.504	12.467
IG-110	12.474	0.008	0.06	12.475	12.487	12.461
NBG-17	12.464	0.010	0.08	12.466	12.493	12.435
NBG-18	12.476	0.008	0.06	12.475	12.495	12.457
PCEA	12.477	0.006	0.05	12.479	12.492	12.463

Against-Grain Specimens	Mean	Standard Deviation	Coefficient of Variation (%)	Median	Upper Limit	Lower Limit
2114	12.483	0.010	0.08	12.485	12.507	12.464
IG-110	12.471	0.013	0.10	12.472	12.500	12.440
NBG-17	12.459	0.011	0.09	12.463	12.501	12.417
NBG-18	12.473	0.007	0.06	12.474	12.495	12.454
PCEA	12.477	0.009	0.07	12.479	12.502	12.454

With-Grain Specimens	Mean	Standard Deviation	Coefficient of Variation (%)	Median	Upper Limit	Lower Limit
2114	12.485	0.007	0.06	12.487	12.503	12.469
IG-110	12.475	0.004	0.03	12.475	12.485	12.465
NBG-17	12.467	0.006	0.05	12.467	12.487	12.450
NBG-18	12.479	0.008	0.06	12.478	12.498	12.458
PCEA	12.477	0.005	0.04	12.479	12.489	12.465

Table B-3. Creep specimen mass (g) summary statistics.

Combined Specimens	Mean	Standard Deviation	Coefficient of Variation (%)	Median	Upper Limit	Lower Limit
2114	5.562	0.010	0.19	5.562	5.589	5.537
IG-110	5.479	0.014	0.26	5.481	5.528	5.428
NBG-17	5.570	0.022	0.40	5.572	5.643	5.497
NBG-18	5.613	0.036	0.64	5.622	5.713	5.523
PCEA	5.620	0.009	0.17	5.621	5.642	5.600

Against-Grain Specimens	Mean	Standard Deviation	Coefficient of Variation (%)	Median	Upper Limit	Lower Limit
2114	5.554	0.010	0.17	5.556	5.574	5.535
IG-110	5.472	0.014	0.26	5.469	5.521	5.425
NBG-17	5.579	0.023	0.41	5.586	5.657	5.496
NBG-18	5.587	0.030	0.54	5.590	5.675	5.496
PCEA	5.622	0.012	0.21	5.621	5.647	5.597

With-Grain Specimens	Mean	Standard Deviation	Coefficient of Variation (%)	Median	Upper Limit	Lower Limit
2114	5.564	0.010	0.18	5.564	5.593	5.537
IG-110	5.482	0.013	0.24	5.484	5.521	5.445
NBG-17	5.563	0.018	0.33	5.557	5.620	5.509
NBG-18	5.638	0.019	0.34	5.639	5.691	5.581
PCEA	5.620	0.008	0.15	5.622	5.640	5.601

Table B-4. Creep specimen density (g/cm^3) summary statistics.

Combined Specimens	Mean	Standard Deviation	Coefficient of Variation (%)	Median	Upper Limit	Lower Limit
2114	1.8154	0.0023	0.13	1.8157	1.8210	1.8098
IG-110	1.7931	0.0039	0.22	1.7937	1.8054	1.7815
NBG-17	1.8258	0.0072	0.39	1.8254	1.8504	1.8002
NBG-18	1.8363	0.0114	0.62	1.8391	1.8689	1.8050
PCEA	1.8359	0.0027	0.15	1.8361	1.8410	1.8301

Against-Grain Specimens	Mean	Standard Deviation	Coefficient of Variation (%)	Median	Upper Limit	Lower Limit
2114	1.8136	0.0007	0.04	1.8136	1.8150	1.8121
IG-110	1.7915	0.0033	0.18	1.7923	1.7999	1.7832
NBG-17	1.8299	0.0067	0.37	1.8312	1.8539	1.8062
NBG-18	1.8281	0.0101	0.55	1.8289	1.8576	1.7981
PCEA	1.8362	0.0039	0.21	1.8359	1.8413	1.8289

With-Grain Specimens	Mean	Standard Deviation	Coefficient of Variation (%)	Median	Upper Limit	Lower Limit
2114	1.8157	0.0023	0.13	1.8162	1.8203	1.8115
IG-110	1.7938	0.0041	0.23	1.7947	1.8032	1.7856
NBG-17	1.8223	0.0056	0.30	1.8195	1.8381	1.8066
NBG-18	1.8436	0.0065	0.35	1.8449	1.8614	1.8259
PCEA	1.8357	0.0022	0.12	1.8362	1.8409	1.8306

Table B-5. Creep specimen coefficient of thermal expansion (1/K) at 100°C summary statistics.

Combined Specimens	Mean	Standard Deviation	Coefficient of Variation (%)	Median	Upper Limit	Lower Limit
2114	5.15E-06	9.17E-08	1.78	5.17E-06	5.38E-06	4.93E-06
IG-110	3.70E-06	1.40E-07	3.77	3.66E-06	4.16E-06	3.27E-06
NBG-17	4.85E-06	1.04E-07	2.14	4.86E-06	5.20E-06	4.54E-06
NBG-18	4.98E-06	1.03E-07	2.06	4.98E-06	5.23E-06	4.73E-06
PCEA	4.10E-06	2.11E-07	5.16	4.07E-06	4.64E-06	3.49E-06

Against-Grain Specimens	Mean	Standard Deviation	Coefficient of Variation (%)	Median	Upper Limit	Lower Limit
2114	—	—	—	—	—	—
IG-110	3.86E-06	7.27E-08	1.88	3.89E-06	4.10E-06	3.62E-06
NBG-17	4.92E-06	7.64E-08	1.55	4.95E-06	5.16E-06	4.67E-06
NBG-18	4.99E-06	8.80E-08	1.76	4.99E-06	5.19E-06	4.78E-06
PCEA	4.34E-06	2.12E-07	4.88	4.36E-06	4.89E-06	3.88E-06

With-Grain Specimens	Mean	Standard Deviation	Coefficient of Variation (%)	Median	Upper Limit	Lower Limit
2114	5.15E-06	9.17E-08	1.78	5.17E-06	5.38E-06	4.93E-06
IG-110	3.63E-06	9.30E-08	2.56	3.63E-06	3.80E-06	3.45E-06
NBG-17	4.79E-06	8.72E-08	1.82	4.80E-06	5.06E-06	4.53E-06
NBG-18	4.96E-06	1.14E-07	2.30	4.97E-06	5.27E-06	4.67E-06
PCEA	4.01E-06	1.19E-07	2.97	4.03E-06	4.39E-06	3.62E-06

Table B-6. Creep specimen coefficient of thermal expansion (1/K) at 500°C summary statistics.

Combined Specimens	Mean	Standard Deviation	Coefficient of Variation (%)	Median	Upper Limit	Lower Limit
2114	5.59E-06	9.62E-08	1.72	5.59E-06	5.86E-06	5.33E-06
IG-110	4.25E-06	1.32E-07	3.11	4.23E-06	4.68E-06	3.83E-06
NBG-17	5.41E-06	1.14E-07	2.11	5.43E-06	5.70E-06	5.14E-06
NBG-18	5.55E-06	1.03E-07	1.85	5.56E-06	5.81E-06	5.29E-06
PCEA	4.58E-06	2.00E-07	4.37	4.54E-06	5.06E-06	4.06E-06

Against-Grain Specimens	Mean	Standard Deviation	Coefficient of Variation (%)	Median	Upper Limit	Lower Limit
2114	—	—	—	—	—	—
IG-110	4.40E-06	6.43E-08	1.46	4.40E-06	4.59E-06	4.21E-06
NBG-17	5.49E-06	8.05E-08	1.47	5.47E-06	5.72E-06	5.25E-06
NBG-18	5.56E-06	9.27E-08	1.67	5.55E-06	5.70E-06	5.39E-06
PCEA	4.85E-06	1.26E-07	2.60	4.84E-06	5.28E-06	4.44E-06

With-Grain Specimens	Mean	Standard Deviation	Coefficient of Variation (%)	Median	Upper Limit	Lower Limit
2114	5.59E-06	9.62E-08	1.72	5.59E-06	5.86E-06	5.33E-06
IG-110	4.18E-06	8.98E-08	2.15	4.17E-06	4.39E-06	3.97E-06
NBG-17	5.35E-06	1.01E-07	1.89	5.36E-06	5.68E-06	5.00E-06
NBG-18	5.54E-06	1.12E-07	2.02	5.57E-06	5.91E-06	5.17E-06
PCEA	4.48E-06	1.04E-07	2.33	4.49E-06	4.79E-06	4.14E-06

Table B-7. Creep specimen coefficient of thermal expansion (1/K) at 1000°C summary statistics.

Combined Specimens	Mean	Standard Deviation	Coefficient of Variation (%)	Median	Upper Limit	Lower Limit
2114	5.97E-06	1.35E-07	2.26	5.95E-06	6.42E-06	5.55E-06
IG-110	4.63E-06	1.37E-07	2.95	4.61E-06	5.05E-06	4.23E-06
NBG-17	5.81E-06	1.21E-07	2.08	5.82E-06	6.09E-06	5.52E-06
NBG-18	5.98E-06	8.32E-08	1.39	6.00E-06	6.26E-06	5.70E-06
PCEA	5.05E-06	2.08E-07	4.11	4.98E-06	5.60E-06	4.53E-06

Against- Grain Specimens	Mean	Standard Deviation	Coefficient of Variation (%)	Median	Upper Limit	Lower Limit
2114	—	—	—	—	—	—
IG-110	4.79E-06	8.47E-08	1.77	4.78E-06	5.03E-06	4.53E-06
NBG-17	5.88E-06	9.46E-08	1.61	5.86E-06	6.13E-06	5.63E-06
NBG-18	5.99E-06	6.90E-08	1.15	6.00E-06	6.17E-06	5.83E-06
PCEA	5.34E-06	1.15E-07	2.16	5.34E-06	5.61E-06	5.09E-06

With-Grain Specimens	Mean	Standard Deviation	Coefficient of Variation (%)	Median	Upper Limit	Lower Limit
2114	5.97E-06	1.35E-07	2.26	5.95E-06	6.42E-06	5.55E-06
IG-110	4.56E-06	9.04E-08	1.98	4.55E-06	4.80E-06	4.31E-06
NBG-17	5.74E-06	1.02E-07	1.79	5.74E-06	6.06E-06	5.43E-06
NBG-18	5.98E-06	9.44E-08	1.58	5.99E-06	6.30E-06	5.66E-06
PCEA	4.94E-06	9.78E-08	1.98	4.95E-06	5.16E-06	4.71E-06

Table B-8. Creep specimen modulus (GPa) by sonic resonance summary statistics.

Combined Specimens	Mean	Standard Deviation	Coefficient of Variation (%)	Median	Upper Limit	Lower Limit
2114	9.67	0.09	0.95	9.69	9.99	9.35
IG-110	10.19	0.38	3.77	10.28	11.29	9.06
NBG-17	11.31	0.18	1.59	11.29	11.74	10.87
NBG-18	11.77	0.30	2.53	11.76	12.46	11.11
PCEA	11.21	0.34	3.04	11.38	12.47	9.78

Against-Grain Specimens	Mean	Standard Deviation	Coefficient of Variation (%)	Median	Upper Limit	Lower Limit
2114	—	—	—	—	—	—
IG-110	9.70	0.19	1.95	9.72	10.42	8.97
NBG-17	11.18	0.13	1.19	11.18	11.60	10.76
NBG-18	11.72	0.34	2.92	11.76	12.83	10.55
PCEA	10.69	0.08	0.71	10.68	10.94	10.42

With-Grain Specimens	Mean	Standard Deviation	Coefficient of Variation (%)	Median	Upper Limit	Lower Limit
2114	9.67	0.09	0.95	9.69	9.99	9.35
IG-110	10.41	0.20	1.89	10.38	10.93	9.87
NBG-17	11.42	0.13	1.14	11.39	11.90	10.96
NBG-18	11.82	0.25	2.09	11.76	12.34	11.25
PCEA	11.42	0.10	0.84	11.43	11.68	11.15

Table B-9. Creep specimen resistivity (μΩ-m) summary statistics.

Combined Specimens	Mean	Standard Deviation	Coefficient of Variation (%)	Median	Upper Limit	Lower Limit
2114	13.86	0.22	1.56	13.83	14.48	13.25
IG-110	10.96	0.33	2.98	10.90	11.94	9.97
NBG-17	11.28	0.26	2.29	11.26	11.90	10.66
NBG-18	10.99	0.26	2.39	10.98	11.82	10.14
PCEA	7.84	0.30	3.88	7.75	9.14	6.67

Against-Grain Specimens	Mean	Standard Deviation	Coefficient of Variation (%)	Median	Upper Limit	Lower Limit
2114	—	—	—	—	—	—
IG-110	11.28	0.27	2.36	11.25	11.91	10.74
NBG-17	11.37	0.20	1.72	11.38	11.83	10.89
NBG-18	11.20	0.20	1.81	11.19	11.67	10.75
PCEA	8.28	0.08	0.96	8.27	8.50	8.07

With-Grain Specimens	Mean	Standard Deviation	Coefficient of Variation (%)	Median	Upper Limit	Lower Limit
2114	13.86	0.22	1.56	13.83	14.48	13.25
IG-110	10.81	0.22	2.06	10.80	11.39	10.20
NBG-17	11.20	0.28	2.54	11.16	11.88	10.49
NBG-18	10.80	0.13	1.22	10.77	11.19	10.43
PCEA	7.67	0.13	1.65	7.66	8.06	7.29

Table B-10. Creep specimen Young's modulus (GPa) by sonic velocity.

Combined Specimens	Mean	Standard Deviation	Coefficient of Variation (%)	Median	Upper Limit	Lower Limit
2114	10.72	0.10	0.89	10.72	10.96	10.50
IG-110	11.00	0.42	3.78	11.10	12.27	9.70
NBG-17	13.71	0.26	1.87	13.73	14.46	12.97
NBG-18	14.93	0.32	2.14	14.91	15.80	14.02
PCEA	13.05	0.49	3.77	13.29	14.75	11.14

Against-Grain Specimens	Mean	Standard Deviation	Coefficient of Variation (%)	Median	Upper Limit	Lower Limit
2114	—	—	—	—	—	—
IG-110	10.48	0.16	1.57	10.50	11.11	9.89
NBG-17	13.51	0.20	1.46	13.52	13.88	13.12
NBG-18	14.96	0.36	2.40	14.92	16.03	13.93
PCEA	12.34	0.14	1.11	12.33	12.63	12.05

With-Grain Specimens	Mean	Standard Deviation	Coefficient of Variation (%)	Median	Upper Limit	Lower Limit
2114	10.72	0.10	0.89	10.72	10.96	10.50
IG-110	11.24	0.24	2.10	11.21	11.79	10.66
NBG-17	13.87	0.17	1.24	13.89	14.35	13.35
NBG-18	14.91	0.29	1.95	14.90	15.77	14.00
PCEA	13.36	0.15	1.11	13.36	13.69	13.01

Table B-11. Creep specimen shear modulus (GPa) by sonic velocity.

Combined Specimens	Mean	Standard Deviation	Coefficient of Variation (%)	Median	Upper Limit	Lower Limit
2114	4.24	0.03	0.77	4.24	4.33	4.15
IG-110	4.58	0.11	2.31	4.58	4.88	4.28
NBG-17	4.84	0.07	1.45	4.86	5.07	4.60
NBG-18	5.13	0.10	2.00	5.13	5.43	4.85
PCEA	4.93	0.08	1.56	4.95	5.05	4.83

Against-Grain Specimens	Mean	Standard Deviation	Coefficient of Variation (%)	Median	Upper Limit	Lower Limit
2114	--	0.00	--	0.00	0.00	0.00
IG-110	4.54	0.06	1.39	4.55	4.71	4.38
NBG-17	4.84	0.06	1.25	4.86	5.06	4.60
NBG-18	5.11	0.11	2.22	5.10	5.48	4.74
PCEA	4.89	0.11	2.33	4.94	5.03	4.85

With-Grain Specimens	Mean	Standard Deviation	Coefficient of Variation (%)	Median	Upper Limit	Lower Limit
2114	4.24	0.03	0.77	4.24	4.33	4.15
IG-110	4.60	0.12	2.56	4.62	4.97	4.23
NBG-17	4.85	0.08	1.62	4.84	5.12	4.59
NBG-18	5.15	0.09	1.76	5.17	5.42	4.89
PCEA	4.94	0.05	1.07	4.96	5.06	4.82

Table B-12. Piggyback specimen length (mm) summary statistics.

Combined Specimens	Mean	Standard Deviation	Coefficient of Variation (%)	Median	Upper Limit	Lower Limit
2114	6.367	0.012	0.19	6.363	6.404	6.332
IG-110	6.369	0.007	0.12	6.368	6.390	6.349
NBG-17	6.358	0.006	0.09	6.358	6.377	6.339
NBG-18	6.345	0.010	0.16	6.346	6.366	6.321
PCEA	6.354	0.005	0.08	6.354	6.367	6.340

Against-Grain Specimens	Mean	Standard Deviation	Coefficient of Variation (%)	Median	Upper Limit	Lower Limit
2114	6.369	0.013	0.20	6.364	6.398	6.336
IG-110	6.369	0.010	0.16	6.367	6.407	6.334
NBG-17	6.356	0.005	0.08	6.356	6.372	6.342
NBG-18	6.348	0.010	0.15	6.348	6.370	6.324
PCEA	6.356	0.005	0.07	6.356	6.365	6.345

With-Grain Specimens	Mean	Standard Deviation	Coefficient of Variation (%)	Median	Upper Limit	Lower Limit
2114	6.366	0.011	0.18	6.362	6.408	6.327
IG-110	6.369	0.005	0.08	6.369	6.386	6.353
NBG-17	6.359	0.006	0.10	6.358	6.380	6.338
NBG-18	6.343	0.010	0.15	6.344	6.365	6.314
PCEA	6.352	0.005	0.08	6.353	6.367	6.338

Table B-13. Piggyback specimen diameter (mm) summary statistics.

Combined Specimens	Mean	Standard Deviation	Coefficient of Variation (%)	Median	Upper Limit	Lower Limit
2114	12.477	0.013	0.10	12.482	12.509	12.449
IG-110	12.463	0.010	0.08	12.467	12.484	12.447
NBG-17	12.466	0.006	0.05	12.468	12.489	12.440
NBG-18	12.474	0.006	0.05	12.475	12.485	12.463
PCEA	12.475	0.005	0.04	12.477	12.486	12.466

Against-Grain Specimens	Mean	Standard Deviation	Coefficient of Variation (%)	Median	Upper Limit	Lower Limit
2114	12.472	0.015	0.12	12.481	12.520	12.424
IG-110	12.455	0.011	0.09	12.456	12.493	12.418
NBG-17	12.468	0.004	0.03	12.469	12.478	12.460
NBG-18	12.469	0.007	0.05	12.470	12.486	12.456
PCEA	12.477	0.003	0.03	12.479	12.484	12.471

With-Grain Specimens	Mean	Standard Deviation	Coefficient of Variation (%)	Median	Upper Limit	Lower Limit
2114	12.482	0.007	0.06	12.483	12.506	12.459
IG-110	12.469	0.002	0.02	12.470	12.478	12.461
NBG-17	12.464	0.007	0.05	12.466	12.489	12.440
NBG-18	12.477	0.003	0.02	12.476	12.487	12.468
PCEA	12.473	0.006	0.05	12.476	12.488	12.459

Table B-14. Piggyback specimen mass (g) summary statistics.

Combined Specimens	Mean	Standard Deviation	Coefficient of Variation (%)	Median	Upper Limit	Lower Limit
2114	1.411	0.002	0.17	1.411	1.417	1.405
IG-110	1.381	0.004	0.30	1.382	1.388	1.375
NBG-17	1.416	0.005	0.38	1.416	1.434	1.397
NBG-18	1.420	0.009	0.62	1.419	1.446	1.394
PCEA	1.422	0.004	0.26	1.423	1.431	1.413

Against-Grain Specimens	Mean	Standard Deviation	Coefficient of Variation (%)	Median	Upper Limit	Lower Limit
2114	1.411	0.002	0.16	1.411	1.416	1.406
IG-110	1.379	0.006	0.40	1.380	1.394	1.365
NBG-17	1.421	0.003	0.22	1.422	1.433	1.409
NBG-18	1.414	0.005	0.39	1.413	1.433	1.394
PCEA	1.423	0.003	0.24	1.424	1.430	1.418

With-Grain Specimens	Mean	Standard Deviation	Coefficient of Variation (%)	Median	Upper Limit	Lower Limit
2114	1.411	0.003	0.19	1.410	1.418	1.403
IG-110	1.382	0.003	0.20	1.382	1.387	1.377
NBG-17	1.412	0.003	0.23	1.411	1.421	1.403
NBG-18	1.425	0.008	0.55	1.426	1.451	1.399
PCEA	1.420	0.003	0.23	1.421	1.430	1.412

Table B-15. Piggyback specimen density (g/cm^3) summary statistics.

Combined Specimens	Mean	Standard Deviation	Coefficient of Variation (%)	Median	Upper Limit	Lower Limit
2114	1.8121	0.0022	0.12	1.8121	1.8180	1.8061
IG-110	1.7769	0.0045	0.25	1.7778	1.7860	1.7683
NBG-17	1.8244	0.0065	0.36	1.8230	1.8478	1.8011
NBG-18	1.8318	0.0109	0.59	1.8315	1.8634	1.7983
PCEA	1.8308	0.0046	0.25	1.8326	1.8396	1.8233

Against-Grain Specimens	Mean	Standard Deviation	Coefficient of Variation (%)	Median	Upper Limit	Lower Limit
2114	1.8130	0.0023	0.13	1.8132	1.8186	1.8079
IG-110	1.7774	0.0063	0.36	1.7785	1.7888	1.7665
NBG-17	1.8310	0.0041	0.22	1.8315	1.8439	1.8191
NBG-18	1.8239	0.0068	0.37	1.8224	1.8492	1.7984
PCEA	1.8317	0.0042	0.23	1.8330	1.8370	1.8286

With-Grain Specimens	Mean	Standard Deviation	Coefficient of Variation (%)	Median	Upper Limit	Lower Limit
2114	1.8112	0.0017	0.09	1.8113	1.8157	1.8066
IG-110	1.7765	0.0029	0.16	1.7777	1.7842	1.7693
NBG-17	1.8200	0.0033	0.18	1.8189	1.8276	1.8114
NBG-18	1.8380	0.0094	0.51	1.8383	1.8715	1.8062
PCEA	1.8301	0.0048	0.26	1.8310	1.8425	1.8180

Table B-16. Piggyback specimen diffusivity (mm^2/sec) at 100°C summary statistics.

Combined Specimens	Mean	Standard Deviation	Coefficient of Variation (%)	Median	Upper Limit	Lower Limit
2114	63.46	0.42	0.66	63.38	64.44	62.48
IG-110	79.28	2.99	3.77	80.48	89.49	69.56
NBG-17	75.61	0.88	1.16	75.36	78.63	72.64
NBG-18	75.92	0.96	1.26	75.91	78.67	73.19
PCEA	97.68	3.84	3.93	100.47	112.63	82.23

Against-Grain Specimens	Mean	Standard Deviation	Coefficient of Variation (%)	Median	Upper Limit	Lower Limit
2114	63.59	0.46	0.72	63.69	64.58	62.54
IG-110	76.06	1.68	2.21	76.53	81.32	71.08
NBG-17	74.85	0.34	0.46	74.91	75.67	74.06
NBG-18	75.35	0.70	0.93	75.25	76.91	73.95
PCEA	93.52	0.52	0.55	93.56	95.21	91.92

With-Grain Specimens	Mean	Standard Deviation	Coefficient of Variation (%)	Median	Upper Limit	Lower Limit
2114	63.37	0.37	0.59	63.30	64.27	62.42
IG-110	81.48	0.93	1.14	81.88	84.62	78.37
NBG-17	76.11	0.76	1.00	76.33	78.23	73.96
NBG-18	76.38	0.90	1.18	76.46	79.17	73.63
PCEA	101.05	0.42	0.41	101.23	102.27	99.87

Table B-17. Piggyback specimen diffusivity (mm^2/sec) at 500°C summary statistics.

Combined Specimens	Mean	Standard Deviation	Coefficient of Variation (%)	Median	Upper Limit	Lower Limit
2114	26.00	0.20	0.78	25.98	26.54	25.46
IG-110	30.17	1.12	3.70	30.59	34.18	26.32
NBG-17	29.29	0.30	1.04	29.28	30.45	28.10
NBG-18	29.45	0.36	1.21	29.49	30.42	28.48
PCEA	35.44	1.32	3.74	36.36	40.48	30.21

Against-Grain Specimens	Mean	Standard Deviation	Coefficient of Variation (%)	Median	Upper Limit	Lower Limit
2114	26.15	0.18	0.68	26.14	26.50	25.76
IG-110	28.95	0.59	2.02	29.16	30.56	27.46
NBG-17	28.99	0.11	0.37	28.97	29.06	28.88
NBG-18	29.30	0.32	1.08	29.26	30.32	28.30
PCEA	34.01	0.22	0.66	34.06	34.52	33.64

With-Grain Specimens	Mean	Standard Deviation	Coefficient of Variation (%)	Median	Upper Limit	Lower Limit
2114	25.90	0.15	0.59	25.90	26.21	25.60
IG-110	31.00	0.36	1.16	31.19	32.20	29.75
NBG-17	29.48	0.22	0.74	29.52	30.06	28.97
NBG-18	29.57	0.35	1.17	29.62	30.41	28.69
PCEA	36.60	0.17	0.46	36.59	37.19	36.03

Table B-18. Piggyback specimen diffusivity (mm^2/sec) at 1000°C summary statistics.

Combined Specimens	Mean	Standard Deviation	Coefficient of Variation (%)	Median	Upper Limit	Lower Limit
2114	15.96	0.27	1.72	15.90	16.32	15.50
IG-110	17.91	0.68	3.82	18.15	20.16	15.71
NBG-17	17.54	0.26	1.50	17.52	18.36	16.75
NBG-18	17.64	0.22	1.26	17.67	18.23	16.99
PCEA	20.51	0.76	3.72	20.85	23.55	17.45

Against-Grain Specimens	Mean	Standard Deviation	Coefficient of Variation (%)	Median	Upper Limit	Lower Limit
2114	16.11	0.33	2.04	16.01	16.42	15.62
IG-110	17.17	0.38	2.23	17.34	18.26	16.12
NBG-17	17.35	0.14	0.83	17.34	17.72	16.93
NBG-18	17.63	0.24	1.37	17.64	18.49	16.77
PCEA	19.70	0.17	0.86	19.68	20.26	19.16

With-Grain Specimens	Mean	Standard Deviation	Coefficient of Variation (%)	Median	Upper Limit	Lower Limit
2114	15.85	0.17	1.08	15.83	16.19	15.44
IG-110	18.41	0.23	1.24	18.43	19.20	17.61
NBG-17	17.66	0.25	1.42	17.71	18.29	17.05
NBG-18	17.64	0.21	1.20	17.68	17.99	17.35
PCEA	21.16	0.22	1.03	21.24	21.83	20.46